HYDROLOGIC INVESTIGATIONS OF WASTE ROCK TEST PILES IN A PERMAFROST ENVIRONMENT

by

Jordan Zak

B.Sc., Carleton University, 2013

A THESIS SUBMITTED IN PARTIAL FULFILLMENT OF

THE REQUIREMENTS FOR THE DEGREE OF

MASTER OF SCIENCE

in

THE FACULTY OF GRADUATE AND POSTDOCTORAL STUDIES

(Geological Sciences)

THE UNIVERSITY OF BRITISH COLUMBIA

(Vancouver)

April 2017

Abstract

Three 14 m tall waste rock test piles were constructed at the Diavik Diamond Mine, NWT, located in a region of continuous permafrost. Since 2006, instrumentation in the piles has been used to develop datasets characterizing the long-term geochemical, hydrologic, and thermal evolution of the waste rock. This thesis focuses on the hydrologic behaviour of two of the waste rock test piles; the Type III pile, considered as PAG material, and the Type I pile which was deconstructed in 2014, considered as NAG material. Complexity in the dataset is added by freeze-thaw processes occurring in this climate.

The distribution of ice was mapped during the deconstruction of the Type I pile. Ice was found primarily in the batter regions, the cause of this was related to the infiltration profile across the crest and batters. Wind redistribution of snow results in a substantial snowpack on the batters with little on the crest. Infiltration through the crest occurs from rainfall alone, which is often low frequency and low magnitude. Snowmelt infiltration to the batters of the Type III pile was determined using an isotopic mass balance (δD and δ^{18}O)- an estimated 77 mm/year representing a significant component of the water budget, about 74% of the annual outflow. Evidence of ice formation in this pile was provided by evaluating the storage of rainwater and trends in deuterium excess.

A bromide tracer test on the Type III pile exhibited a breakthrough curve with a long tail and 46% mass recovery after ten years. The average pore water velocity was estimated to be 2-3 cm/day. Hypotheses were examined to explain low recovery of the tracer and the observed tailing, including the possibility of multirate mass transfer which assumes tailing is related to diffusion. Comparison of late time bromide behaviour to the migration of conservative blasting residuals suggests that tailing may also be influenced by low velocity flow paths.

Concentration/mass loading histories from the two basal drains and basal collection lysimeters were highly variable, suggesting the solute transport system in the heterogeneous waste rock pile is complex and is potentially influenced by the presence of ice.

Preface

This thesis presents original unpublished research in chapters 2, 3, 4, and 5. Chapters 2, 3, and 4 are formatted as papers intended for publication. Unless indicated otherwise, all work in this thesis was completed by myself, including calculations and interpretations. All of the work has been reviewed and edited by my thesis supervisor, Leslie Smith.

The Diavik Waste Rock Project is a research program involving the collaboration from professors, graduate students, and coop students from the University of British Columbia, the University of Waterloo, the University of Alberta, and Carleton University. Long-term monitoring experiments were designed and constructed under the guidance of professors from these universities, prior to my involvement as a graduate student. Measurements of water chemistry were completed at the University of Waterloo by lab technicians.

My involvement in the research program included the on-going sample collection and instrument maintenance at the field site. Hydrology datasets were updated to maintain continuity of the experiments; including infiltration calculations, climate data, outflow calculations, and moisture contents from TDR. Earlier updates to these datasets were completed by Matt Neuner (2006-2009), Steve Momeyer (2007-2009), Nathan Fretz (2009-2012), and Andrew Krentz (2012-2014).

Table of Contents

List of Tables

List of Figures

Acknowledgements

This small section cannot come close to expressing my whole hearted gratitude towards all of the individuals who were involved in the completion of this work. I thoroughly enjoyed myself while involved with this project and have a great deal of respect for all of the Test Piles team members.

Thank you Leslie Smith, for sharing your knowledge and providing an incredible amount of support and patience throughout the process of writing this thesis.

Dave Blowes, Rich Amos, Dave Sego, and Nick Beier. Thank you for your collective support, sarcasm, and continually testing my composure too "go back a slide".

Thank you to my fellow graduate students, David Wilson, Colleen Atherton, David Barsi, Laurier Collette. Jeff Bain, I aspire to your all around handiness and ability to fix things. Steve Holland, keep laughing buddy. I wish you all the best in your futures.

Thank you to the Diavik Environment Department, David, Darcy, Sean, Justin, Kayla. All of you provide a tremendous amount of support to the test piles project.

Thank you to the faculty at UBC, Leslie, Roger, and Uli, for the work that you put into making the hydrogeology group such a success.

Thank you Daniele for your feedback and humor. I hope that your new job has given you the financial means to purchase a watch, you seem to be late for everything.

My time spent at UBC would have certainly been less enjoyable if it were not for my lab mates, especially those of you in 229 (the cool lab). I am happy to call all you my friends.

I've had many professors through university, but only one brofessor, thank you Andrew Krentz for helping me to get started on this project.

I would like to thank my parents, Debbie and Ted, as well as my brother Taylor for your continued support.

Samantha Martin (and Clem and Goose), you are deserving of an enormous thanks. I am excited for our future…

Chapter 1 Introduction

1.1 Problem description

Mining activities are generally associated with the stockpiling of large volumes of rock at the surface, referred to as waste rock piles, during the removal of ore. Waste rock piles can be hundreds of meters in height and several kilometers in length, some containing on the order of 500 million m^3 of material (McCarter, 1990), and in some cases behaving as large reservoirs for potential contaminants. Chemical weathering of minerals due to the presence of water and oxygen in the unsaturated zone of waste rock piles has the potential to generate a variety of contaminants, such as acidity, dissolved metals, and elevated TDS (Blowes et al., 2003). The transport of contaminants in waste rock piles and possible release to the environment is controlled largely by hydrological processes (Amos et al., 2014). Uncertainty in the processes governing transport can lead to problematic predictions of solute behaviour at an active or legacy mines, or during mine closure (Smith et al., 1995).

Characterizing the movement of water through a waste rock pile is challenging due to the heterogeneous nature of the material. Further complexity may be introduced to the characterization process for stockpiles located in cold climates. Below 0ºC, freezing results in the immobilization of water and a decrease in the hydraulic conductivity of the material. The effects of permafrost formation in stockpiles have been mostly undocumented in scientific literature. The influence of ice on internal flow fields in waste rock piles is of particular importance to interpreting solute loading trends and developing effective long-term monitoring strategies (Sinclair et al., 2015).

Reliable infiltration estimates are critical to characterizing the solute transport system in a waste rock pile. Poor recharge estimates can lead to misleading water balances, improper interpretation of patterns of internal moisture contents, and incorrect predictions of solute concentrations/loadings from a pile. Several techniques to estimate infiltration to waste rock piles have been considered successful in the past: Rainfall infiltration to the crests waste rock test piles at Diavik was calculated by Fretz (2013) using a modified Penman Monteith (1948) method. A limitation of this method is that it does not account for infiltration to batter regions or evaporation driven by internal air flow, which may be relevant to the water balance of the stockpile (Sracek et al., 2004; Amos et al., 2009). Water fluxes from lysimeters located in piles have been used to approximate average annual infiltration values over several years of monitoring (Nichol et al., 2005; Andrina, 2009). Since this method averages data over several years, little to no insight is gained towards the magnitude of individual infiltration events or infiltration over a particularly dry or wet year. An alternate method described by Barbour et al. (2016), high resolution isotopic profiling was completed on drill cores to estimate rainfall and snowmelt infiltration at several waste rock piles in British Columbia. Despite the success of these studies, more long-term field investigations are required to develop new techniques to estimate recharge to waste rock piles and assess the variability across a range or climates.

In order to reliably predict solute concentrations/loadings from a waste rock pile, there must by a robust understanding of the solute transport system. Tracer testing and flushing of blasting residuals have been used to characterize transport processes such as the pore water velocity and the significance of preferential flow, as well as more complex processes including the influence of particle size distribution, variability of basal solute loadings/concentrations, and the effects of diffusive mass transfer (examples: Diodato and Parizek, 1994; Erikson et al., 1997; Nichol et al.,

2005; Blackmore et al., 2014). The breakthrough curves produced from tracer tests in waste rock generally exhibit long tailing of concentrations following the arrival of the centre of mass. The examination of late time tracer concentrations during tailing often provide valuable evidence as to the processes influencing the long-term evolution of concentrations, such as the importance of diffusion. The correct characterization of processes influencing late time concentrations is particularly important when considering the length of time required to monitor stockpiles.

1.2 The Diavik Waste Rock Project

The hydrologic, geochemical, thermal, gas transport, and microbial evolution of waste rock has been researched at the Diavik mine since 2006. Three 14 m tall experimental waste rock test piles were constructed containing a variety of instrumentation in order to characterize the behaviour of waste rock at the site. The mine is located about 300 km NE of Yellowknife NWT, Canada (Figure 1.1). The mean annual air temperature at the mine site is -9°C, mean maximum temperatures of 18°C in July and mean minimum temperatures of -31°C in January/February (Environment Canada, 2012).

At Diavik, waste rock is segregated based on Sulphur content: Type I <0.04 wt.%, Type II 0.04-0.08 wt.%, and Type III >0.08 wt.%. Type I is considered to be non-acid generating, Type II is considered to have uncertain acid generating potential, and Type III is considered to be potentially acid generating due to low neutralization potential. The test piles facility includes a Type I pile, a Type III pile, and a covered pile, as well as a series of shallow active zone lysimeters (Figure 1.2).

Figure 1.1. Location of the Diavik Diamond Mine (Neuner et al., 2013).

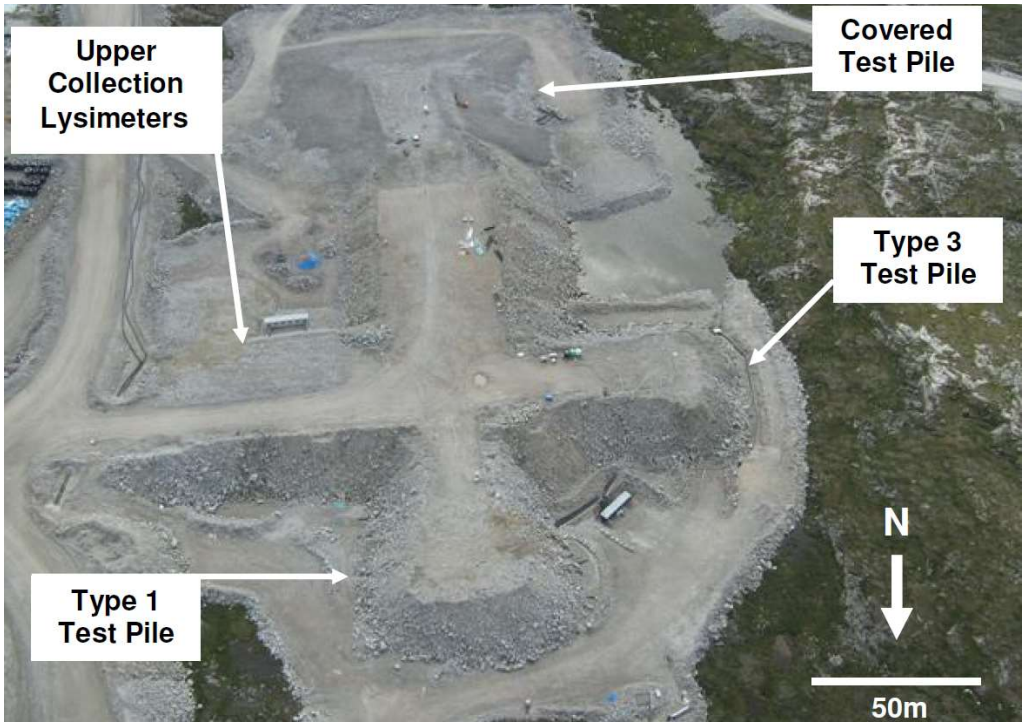

Figure 1.2. Aerial view of the Diavik test piles field site (Neuner, 2009).

1.3 Scope of work

The focus of this thesis is to improve the hydrologic characterization of waste rock in a permafrost environment influenced by regular freeze-thaw. Earlier work outlining the hydrology of the Diavik Waste Rock Project can be found in: Neuner, (2009); Neuner et al. (2013); Fretz, (2013); Momeyer, (2014); and Krentz, (2014).

The objectives of this thesis are:

1. Investigate the results from a ten-year tracer test with low recovery and long tailing of concentrations. Assess breakthrough curves to constrain estimates of the pore water velocity and describe the solute transport system, including the possible influence of

diffusive mass transfer between mobile and immobile domains, as well as influence from ice formation.

2. Evaluate the use of stable isotopes to quantify snowmelt infiltration through the batters of a test pile and determine the overall significance of batter recharge to the total basal outflow.
3. Map the distribution of ice in the deconstructed Type I test pile, provide a preliminary description of ice formation in the full scale pile, and assess the possibility of ice formation in the Type III test pile.
4. Describe the mapped moisture contents and stable isotopes in pore waters from the deconstructed Type I test pile. Compare the mapped moisture contents to moisture contents from TDR probes.

1.4 Organization of thesis

This thesis contains five chapters, three chapters have been written as standalone papers, plus introduction and conclusion chapters. Chapter 1 provides an introduction to the topics discussed in the succeeding chapters. Chapter 2 presents an eight-year dataset on the hydrology of the Type I test pile, followed by insights gained from the deconstruction of the test pile. This chapter discusses the mapped moisture contents and ice distribution in the pile and develops a conceptual model for water flow in the test pile. This chapter also presents the distribution of ice observed in the full scale pile during excavations. Chapter 3 uses deuterium and oxygen-18 isotopes to quantify snowmelt infiltration to the batters of the test pile, believed to be a significant component of the water balance. These isotopes are also used to investigate that significance of evaporation and ice formation in the test pile. Chapter 4 examines the results

from a ten-year tracer test study. This chapter considers the evolution of late time solute behaviour at low concentrations in order to investigate the processes influencing solute transport in a test pile. Chapter 5 presents the most important conclusions from this thesis and recommendations for future work

Chapter 2 Hydrologic learnings from monitoring and deconstructing a partially frozen waste rock test pile

2.1 Introduction

An understanding of the hydrologic behaviour of waste rock is key to considering when an active or decommissioned waste rock pile at a mine site may yield drainage with elevated solute concentrations. Waste rock stockpiles can be several kilometers in length and several hundred meters in height, in many cases behaving as reservoirs of potential contaminants (Nichol et al., 2005) such as blasting residuals (Bailey et al., 2013). The oxidation of minerals in waste rock can lead to reaction products including acidity and dissolved metals (Blowes et al., 2003). Infiltration through a waste rock pile serves as a method of transport for these contaminants (Smith et al., 1995), often times posing a significant environmental concern and financial liability to mining companies (Cidu, 2011; Sracek et al., 2004).

In cold climates, water flow is modified by temperature. Below 0^{o}C, freezing of water causes the immobilization of pore water and a reduction in the permeability of the porous material, altering the hydrologic behaviour of the waste rock pile and influencing the geochemical evolution of the waste rock pile (Sinclair et al., 2015). These effects have been mostly undocumented in scientific literature, corresponding to a knowledge gap in the behaviour of waste rock piles located regions of permafrost; a knowledge gap of particular importance to fill given increased mining activities at Northern latitudes.

The hydrologic (Neuner et al., 2013), thermal and (Pham et al., 2013b), geochemical evolution (Smith et al., 2013a; Bailey et al., 2013; Bailey et al., 2015) of waste rock in an area of continuous permafrost has been studied at the Diavik Diamond Mine, NWT, Canada (Figure 2.1)

since 2006 using three 14 m high experimental waste rock test piles. At Diavik, waste rock is segregated by sulphur content into three categories: Type I <0.04 wt.%, Type II 0.04-0.08 wt.%, and Type III >0.08 wt.%. Type I is considered to be non-acid generating, Type II is considered to have uncertain acid generating potential, and Type III is considered to be potentially acid generating due to low neutralization potential. The focus of this paper is on the uncovered test pile containing Type I material.

Located approximately 300 km NE of Yellowknife, NWT Canada, Diavik is in a semi-arid region. The mine is located in the 20 km^2 East Island situated on the 60 km long Lac de Gras, which discharges into the Copper Mine River. The mean annual air temperature is -9°C, mean maximum temperatures of 18°C in July and mean minimum temperatures of -31°C in January/February (Environment Canada, 2012), creating conditions conducive to permafrost formation in waste rock piles.

Figure 2.1. Location of the Diavik Diamond Mine (Neuner et al., 2013).

The active zone of the uncovered test piles reaches a maximum thickness during the late summer (Pham, 2013a). It has been demonstrated that ice accumulation within the inactive zone has an impact on drainage from the waste rock (Sinclair et al., 2015). However, assumptions regarding the presence of ice are largely speculative. Characterization of the distribution of ice in the test pile during its most thawed state has represented a significant knowledge gap in describing the hydrologic behaviour of the test piles.

The crest of the uncovered Diavik test piles accounts for 45% of the infiltration surface, the remaining area is composed of batter regions, which have slopes at the angle of repose. Work to determine batter infiltration estimates completed by Krentz (2014) demonstrated that snowmelt infiltration occurred through the batters of a test pile, but not the crest. Sublimation and wind

scouring were found to effectively remove snow from the crest, preventing snowmelt recharge from occurring through the surface (Figure 2.2). Given the proportion of the surface of the batters to the crest of the pile, and accumulation of snow, infiltration through the batters is believed to represent a significant component of the water balance, possibly having an influence the distribution of ice. The influence of high infiltration through the batters to the general hydrologic behaviour of the test pile has direct implications to the characterization of flow and solute transport in the pile.

Figure 2.2. Photo showing the distribution of snow on the Type I test pile, March 16, 2008. Snow has mostly been removed from the crest and has accumulated on the batters (West batter shown). From: Neuner, 2009.

Data obtained over eight years of continuous flow and geochemical monitoring of the Type I waste rock test pile are presented to describe the hydrologic regime. Following the monitoring period (2007-2014), the test pile was deconstructed to observe, in part the distribution of ice,

map moisture contents, and determine concentrations of blasting residuals and stable isotopes in pore waters. The objectives of this paper are: 1) characterize the formation of ice in the pile, 2) evaluate the distribution of rainwater and snowmelt in the pile, 3) provide a preliminary assessment of rainwater and snowmelt contributions to basal drainage, and 4) investigate the spatial distribution of moisture contents in the pile and make comparisons to TDR data. Through the integration of these learnings, an improved conceptual model of water flow within the waste rock pile is presented.

2.2 Methodology

2.2.1 Experimental facility

The test piles field site is shown in Figure 2.3. The construction and instrumentation of the Type I experimental test pile is described in detail by Smith et al. (2013b) and Neuner et al. (2013). The test pile was constructed and instrumented from 2004-2006 using standard mining equipment. Waste rock was end-dumped from a ramp onto the 50 x 60 m base of the test pile. The pile was 14 m high with batters on three sides at the angle of repose (38°).

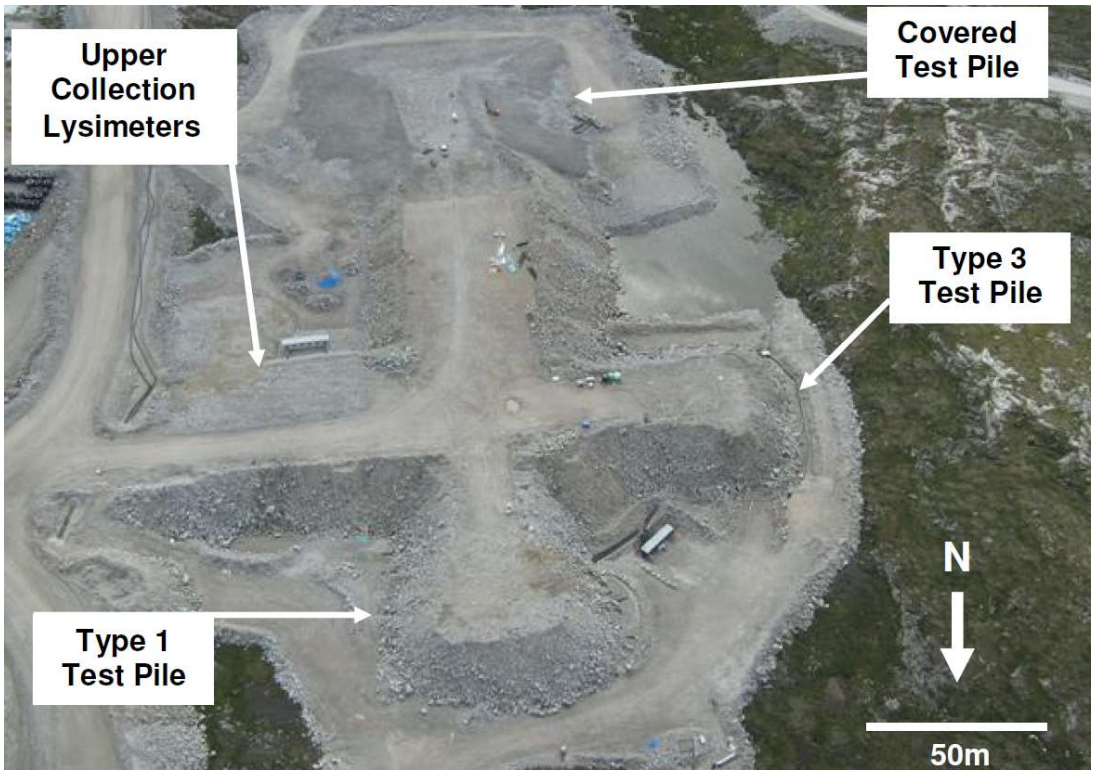

Figure 2.3. Aerial view of the Diavik test piles field site (Neuner, 2009).

A schematic of the test pile is given in Figure 2.4. The base was lined with a high density polyethylene geomembrane (HDPE) liner sloped to the SW at a 1.4% grade. A basal drain was oriented diagonally across the base of the pile. The liner and basal drain were covered with 0.3 m of <50 mm processed kimberlite crush to prevent damage during test pile construction. Drainage from the basal drain was directed into an instrumentation trailer where continuous measurements of flow were recorded using a tipping bucket. Sampling for geochemical analysis occurred at a frequency of approximately three days during periods of discharge.

Three clusters of two 2 x 2 m and two 4 x 4 m basal collection lysimeters (BCLs) were constructed on top of the crush layer, each lysimeter had 1 m high walls. Flow from the lysimeters was directed towards the instrumentation trailer for geochemical sampling and

continuous flow monitoring using tipping bucket rain gauges (Young Model 2202). Self-regulated heating cable was placed in the basal drain and lysimeter drain lines, as well as across the bottom of the lysimeters, to prevent temperatures in the drains from falling below 5°C.

Instrumentation to monitor the geochemical, hydrological, microbiological, gas transport, and thermal behaviour internal to the pile was installed, shown in Figure 2.5. TDR probes and soil water solution samplers (SWSS) were surrounded by matrix materials placed during installation. Time domain reflectometry (TDR) probes were designed following Nichol et al. (2002, 2003). The TDR probes were calibrated and then placed on waste rock tipping faces. Several probes were damaged during construction, working probes remained at 2, 3, 6, and 9 m depth (Fretz, 2013).

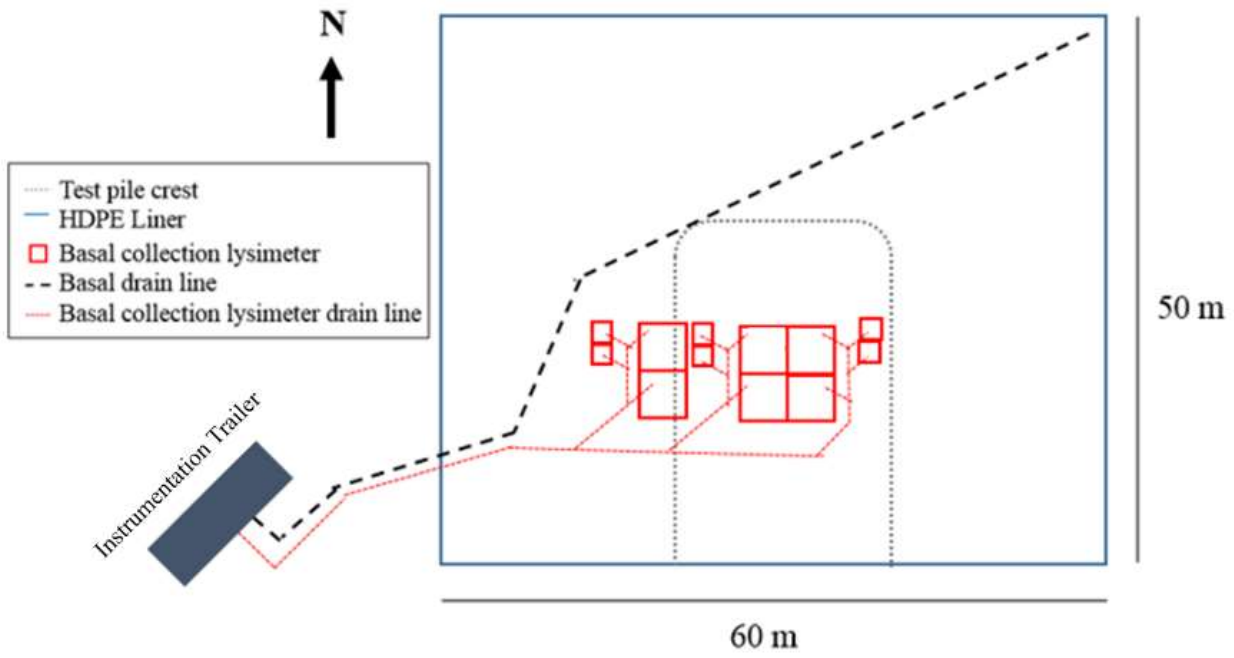

Figure 2.4. Layout of the Type I experimental test pile, modified from Smith et al. (2013b).

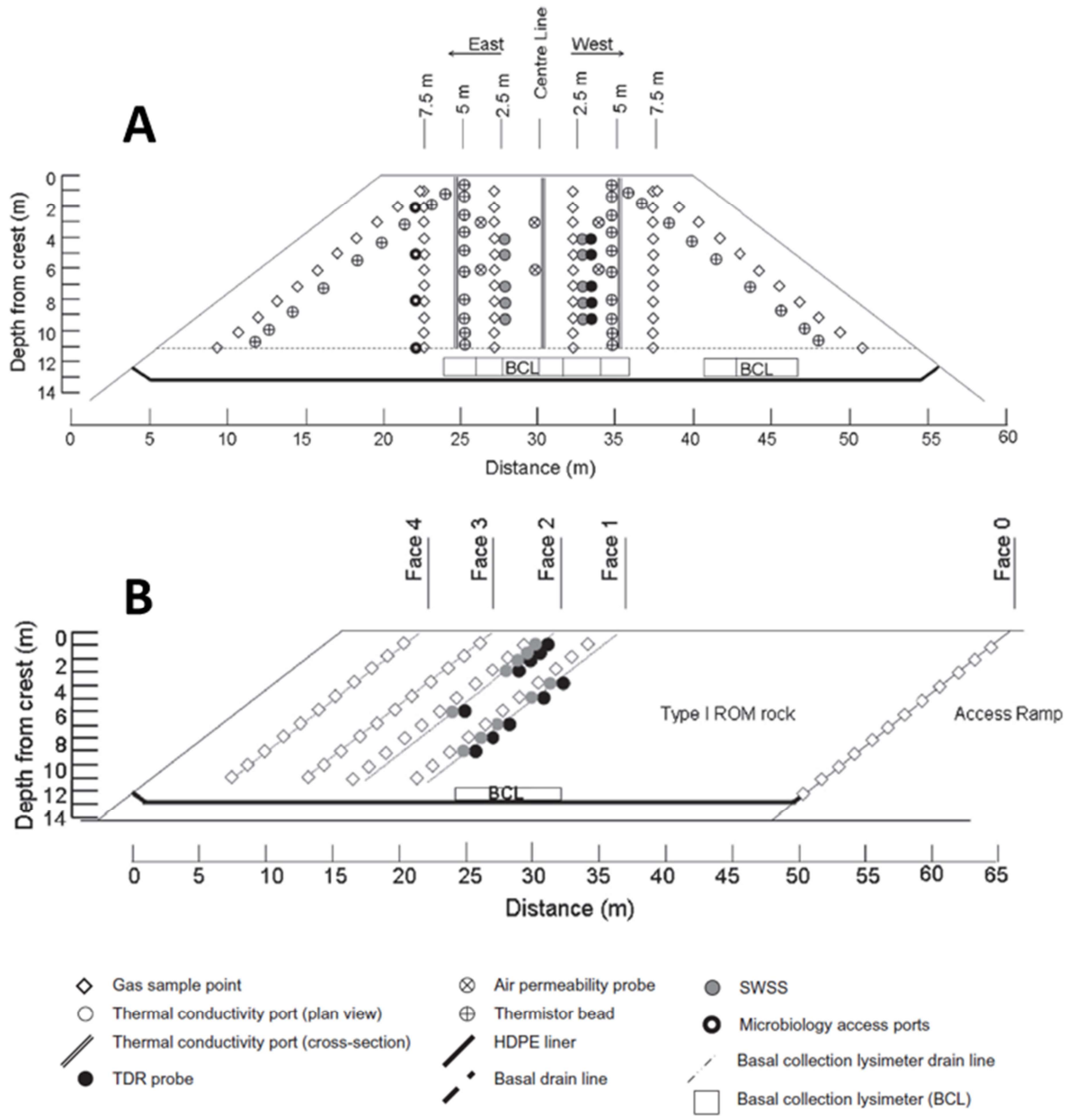

Figure 2.5. A) East-West Cross-section and B) North-South profile Type I test pile showing the locations of instrumentation (Smith et al. 2013b).

2.2.2 Test pile deconstruction

The Type I test pile was deconstructed following eight years of continuous monitoring (2007-2014). A detailed description of the deconstruction process is provided in Atherton (2017), the methods relevant to this paper are described here. The pile was excavated and sampled using six

lifts as shown in Figure 2.6. The first five lifts were completed by excavating two 1.2-3.0 m deep trenches along the length of the pile. Trenches were sloped at an angle of approximately 3:1 to comply with mine safety regulations. Sampling transects were oriented perpendicular to the trenches and samples were collected every 3 m. Transects were completed every 5 m from the southern edge of the basal liner and named accordingly– example, the transect 15 m from the southern edge is referred to as the 15 m Line, shown in Figure 2.7. The sixth lift was excavated as two 1.2 m deep trenches along the 15 and 35 m transects. The deconstruction process required approximately 11 weeks to complete, July-September 2014.

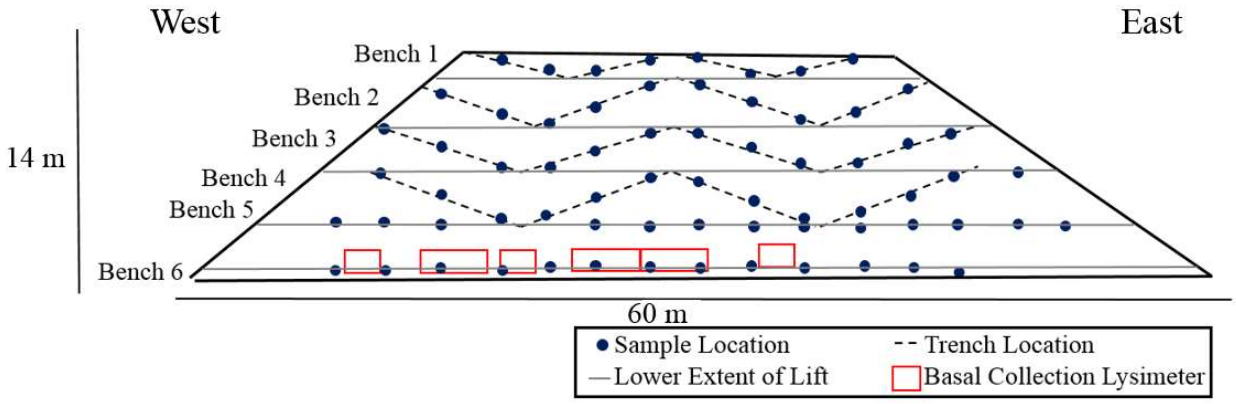

Figure 2.6. West-East cross section schematic showing the approximate locations of excavated trenches and sample locations.

Figure 2.7. Approximate positions of the 15 m and the 35 m sampling lines across the partially deconstructed Type I pile (Atherton, 2017).

2.2.2.1 Volumetric moisture content

Volumetric moisture content (VMC) was determined by the use of soil drying cans. At each sample site, the upper 15 cm of material was removed to expose fresh matrix, where moisture had not evaporated following excavation. Soil cans (4 cm long, 6.5 cm diameter) were inserted into the matrix to collect a sample. Following collection, samples were emptied from soil cans onto individual drying trays and sealed with plastic wrap to prevent evaporation. Samples were weighted, then oven dried for 24 hrs at 105ºC, and weighted again. Drying samples for longer than 24 hrs was found not to have an impact on the results obtained. No significant rainfall events occurred during the deconstruction process, therefore the observed distribution of moisture is not misrepresented by rainfall events during this time period.

2.2.2.2 Pore water collection

Pore water extraction methodology is described in detail by Atherton (2017). In brief, material was sieved to a grain size fraction <1 cm, placed in 69 oz. plastic sample bags and immediately frozen until pore water extraction could be undertaken. Extraction of pore water was completed using a centrifuge. pH, Eh, alkalinity, and concentrations of NH_3-N, H_2S, Fe^{2+}, and PO_4^{3-} were determined immediately following extraction. Analysis of other dissolved cations, anions, hydrogen and oxygen isotopes were completed at the University of Waterloo.

2.2.2.3 Ice mapping and sampling

The spatial distribution of ice was mapped with the aid of a Trimble Differential GPS linked to the Diavik GPS base station. Samples of ice lenses that were collected for geochemical analyses were brushed of loose sediment and placed in Ziploc bags. The presence of stable atmospheric conditions within the Type I pile have been documented (Amos et al., 2009), therefore, sample oxidation was not expected to occur following collection. Samples were stored at room temperature until fully melted. Water was extracted from the sample bags using syringes triple rinsed with sample water. The measurement of geochemical parameters and analysis were completed in the same manner as the above described pore water samples.

2.3 Results

This section provides an overview of results from observations and measurements. Interpretation of these results are given in the discussion section.

2.3.1 Precipitation

The record of annual rainfall at Diavik is shown in Figure 2.8A, the average annual rainfall recorded over nine years was 104 mm, with the three years prior to deconstruction being 72 mm cumulatively below the yearly average. Measurements from a snow gauge operated by the Diavik Environment Department are shown in Figure 2.8B. These data indicate an average annual snowfall of 150 mm (water equivalent) from 2007-2014; note that annual totals reflect snowfall over the winter season, approximately October-April. Approximately 60% of the total precipitation at Diavik occurred at snow during the period of measurement.

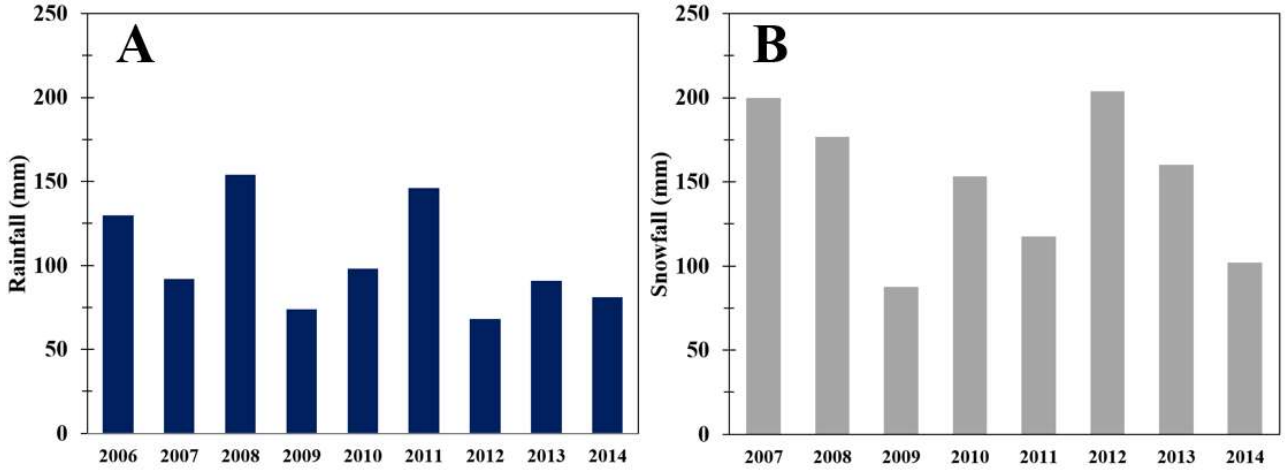

Figure 2.8. Measurements of A) rainfall and B) snowfall (water equivalent) at Diavik Diamond Mine.

2.3.2 Hydrologic summary of test pile during the monitoring period

2.3.2.1 Infiltration

Infiltration was estimated using a modified Penman Monteith method (PM) (Figure 2.9) which requires atmospheric data such as temperature, relative humidity, wind speed, and net radiation to determine potential evaporation. Fretz (2013) used this method to determine infiltration to a series of lysimeters at Diavik. It is important to recognize that the estimates apply only to rainfall infiltration through the crest of the waste rock pile, not the batters. A total of 324 mm of rainfall is estimated to have infiltrated the crest of the Type I test pile from 2007-2014. The average annual infiltration over this period was 41 mm, with the last three years being cummulatively 58 mm below the yearly average. It is anticipated that infiltration to the test pile occurred primarily through the batters due to their size (55% of the infiltration surface) and accumluation of snow.

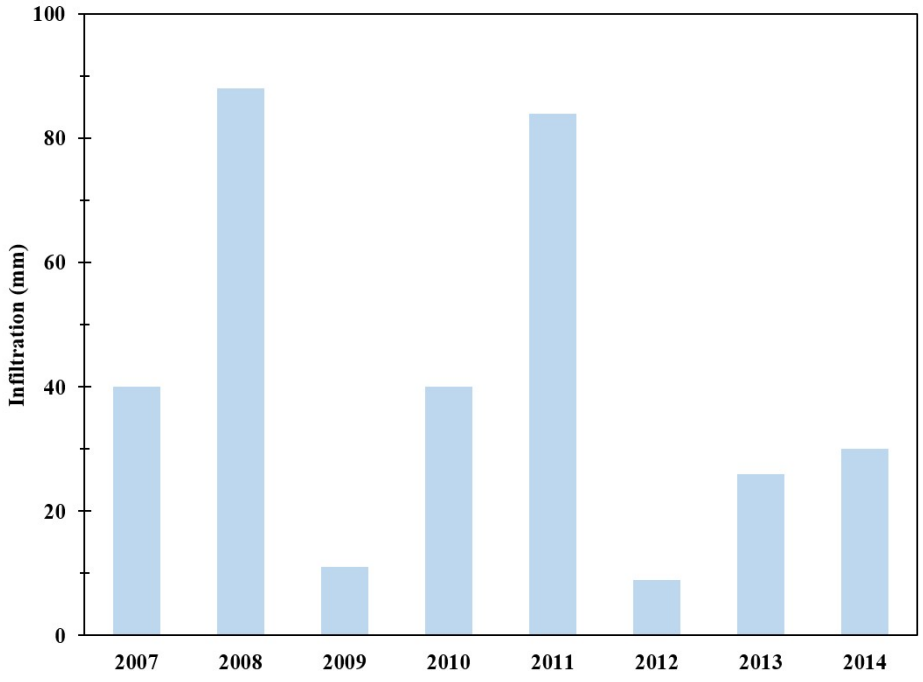

Figure 2.9. Estimation of rainfall infiltration through the crest of the test pile.

2.3.2.2 Volumetric moisture content

Volumetric moisture content of matrix material was estimated using a TDR probe at 2, 3, 6, and at 9 m below surface are presented in Table 2-1. TDR provides a valid estimation of moisture contents only when temperatures are above freezing. The measurements presented here represent annual values of stabilized moisture contents reported while the temperature was above freezing at the given depth- determined using the nearest thermistor. Moisture contents from years when TDR readings did not reach a steady state value have been omitted. The values reported in 2014 represent moisture contents measured in June, immediately prior to deconstructing the waste rock pile. For the interpretation of these data, note that Neuner et al. (2013) reported a porosity of 25% for matrix material, accounting for 7% of the bulk volume of the waste rock. VMC at 2 m show a two-year period of increasing moisture content and a three year period at 3 m, followed by a state of dynamic equilibrium (2009-2012). Moisture contents at 6 and 9 m remained low, relative to 2 and 3 m, showing no evidence of a state of equilibrium.

Moisture contents at all depths in 2014 were notably lower than those reported over 2008-2012. This trend is difficult to interpret given the loss of data in 2013 caused by flooding to the instrumentation trailer. Declining moisture contents may have been caused by lower than average infiltration in 2012-2014, as well as a combination of processes operating in earlier years such as: surface evaporation, wind driven internal evaporation, and a downward hydraulic gradient caused by drying related to basal ice formation.

Table 2-1. Average volumetric moisture contents for thawed period, measured by TDR in the Type I test pile.

Depth (m)	Volumetric Moisture Content (%)							
	2007	**2008**	**2009**	**2010**	**2011**	**2012**	**2013**	**2014**
2	6	20	14	20	17	Omitted	No data	3
3	10	13	24	22	24	21	No data	5
6	4	16	12	7	Omitted	10	No data	3
9	4	7	Omitted	Omitted	Omitted	9	No data	Omitted

2.3.2.3 Outflow

Daily flow volumes from the Type I basal drain and BCLs are shown in Figure 2.10. Years with increased discharge from the basal drain correlate with years of increased infiltration (Figure 2.9). Cumulatively, 222 m^3 of water discharged from the basal drain of the test pile, the equivalent of 74 mm of infiltration through the crest and batters; this is low when compared to infiltration estimates. Flow from the basal collection lysimeters occurred without a clear trend over time or relationship to the behaviour of the basal drain. Cumulatively, 0.74 m^3 of water discharged from eight of the 12 BCLs, corresponding to 9.2 mm across the footprint of BCLs which produced flow, approximately 3% of the estimated infiltration through the same footprint at surface.

Flooding of the instrumentation trailer in December 2012 resulted in the loss of power to Type I instrumentation, data loggers, and internal heat trace system. Power was restored in September 2013. Reduced outflow was observed from the basal drain and BCLs from 2012-2014, partially coinciding with the loss of heat tracer to the test pile. This may indicate damage to the drainage

system occurred as a result of the loss of the heat trace over winter months, possibly having an influence distribution of ice in the test pile.

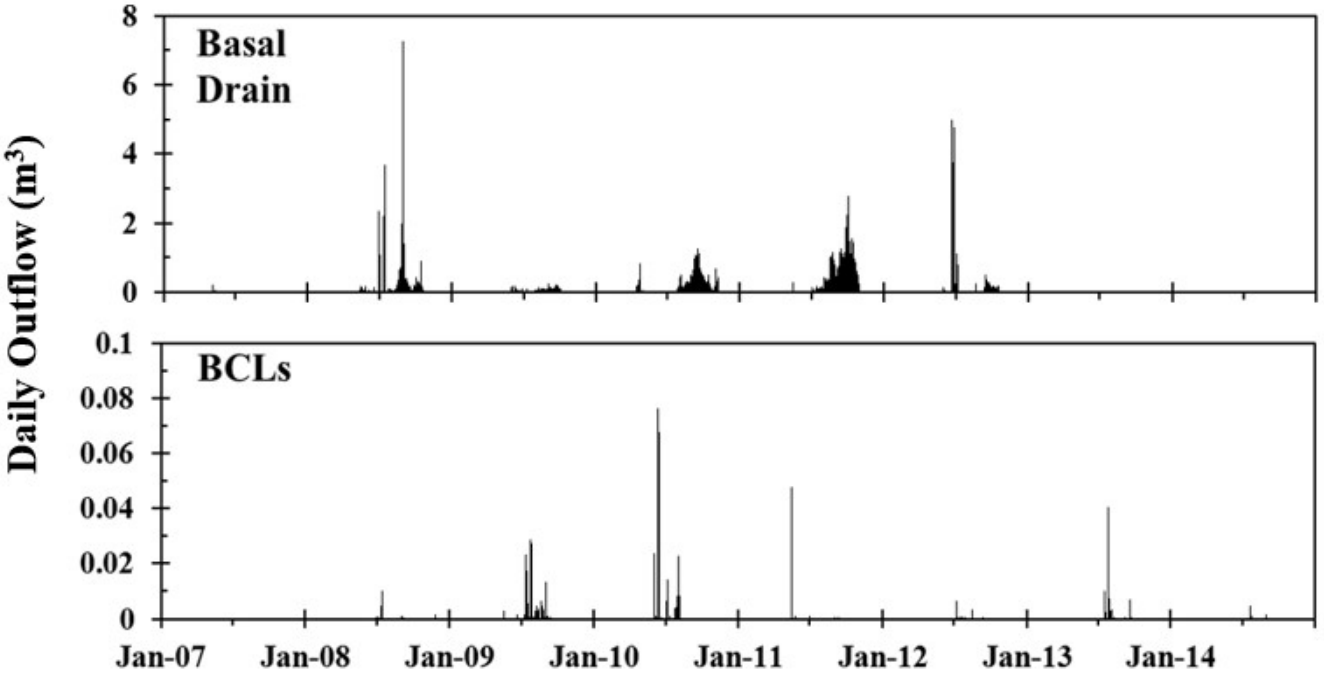

Figure 2.10. Daily outflow from the Type I basal drain and basal collection lysimeters (BCLs).

2.3.2.4 Thermal regime

Thermal monitoring has shown that the pile is frozen from December-May each year, during this time discharge did not occur. Thawing progressed through the summer from the surface toward the base (Pham, 2013b). Migration of the thaw front through the spring and early summer created the potential for the flow of water to be directed away from the frozen core and toward the batters (Sinclair et al., 2015). Figure 2.11 shows that a portion of the core of the test pile remained frozen through the year, resulting in a 12 m active zone. The BCLs, were located in a frozen area of the pile, flow from these (Figure 2.10) may have been permitted by the heat trace placed in the bottoms of the lysimeters.

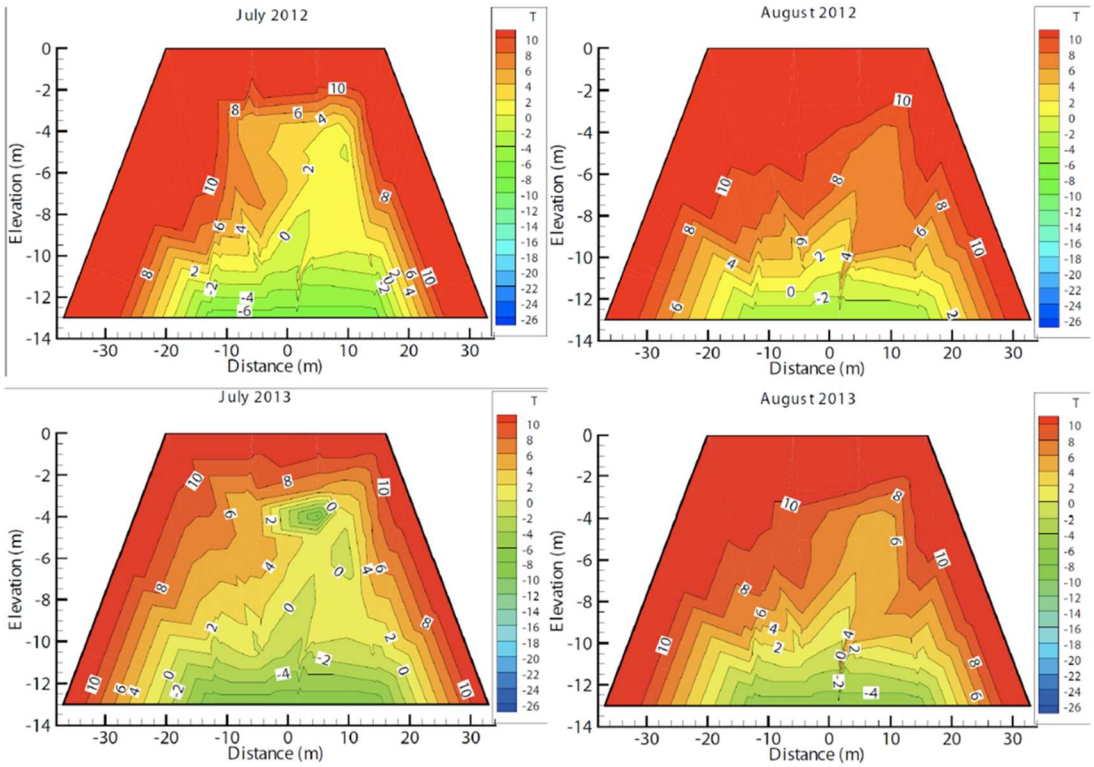

Figure 2.11. Thermal contours of the Type I test pile in the summer months (Pham, 2013a).

2.3.3 Test pile deconstruction

2.3.3.1 Volumetric moisture content

VMC measurements obtained during deconstruction reflect a snapshot within the Type I waste rock pile and do not illustrate seasonal or long-term variability. In general, moisture contents increased with depth, showing little lateral variability (Figure 2.12). Localized areas of increased moisture content (8%) existed between 4 and 7 m depth, likely a result of discrete areas of decreased grain size. Below 10 m, moisture contents were above field capacity (10-15% Neuner, 2009). An area of elevated moisture contents can be visually identified in Figure 2.13, providing an additional perspective. At 11 m depth, increased moisture contents were located in the NE

batter region, thought to be a consequence of batter infiltration draining downslope along the basal liner towards the basal drain outlet.

Table 2-2 provides a comparison of VMC measured by TDR immediately prior to deconstruction and the measurements made during deconstruction using soil cans. These measurements were found to agree with each other. This creates support for TDR readings over the monitoring phase. TDR data at 9 m was omitted due to freezing conditions at the time of measurement, however thawing had occurred at the time of excavation.

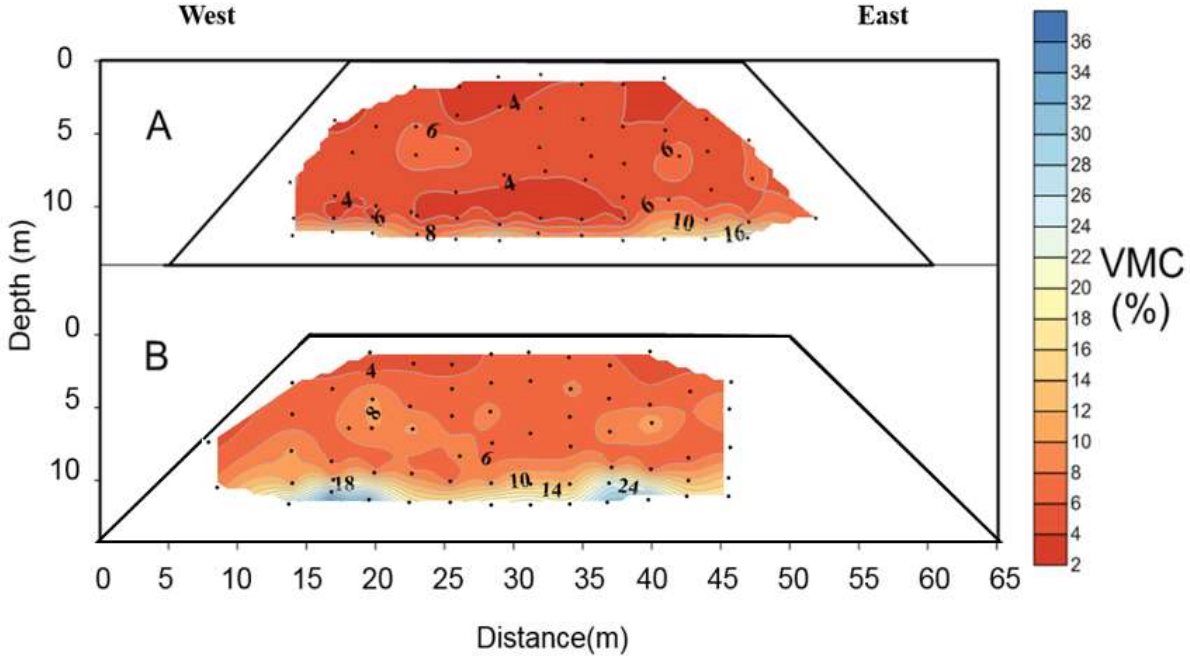

Figure 2.12. Contour plots of volumetric moisture content at the A) 15 m line, and B) 35 m line of the Type I test pile (collected July-September 2014).

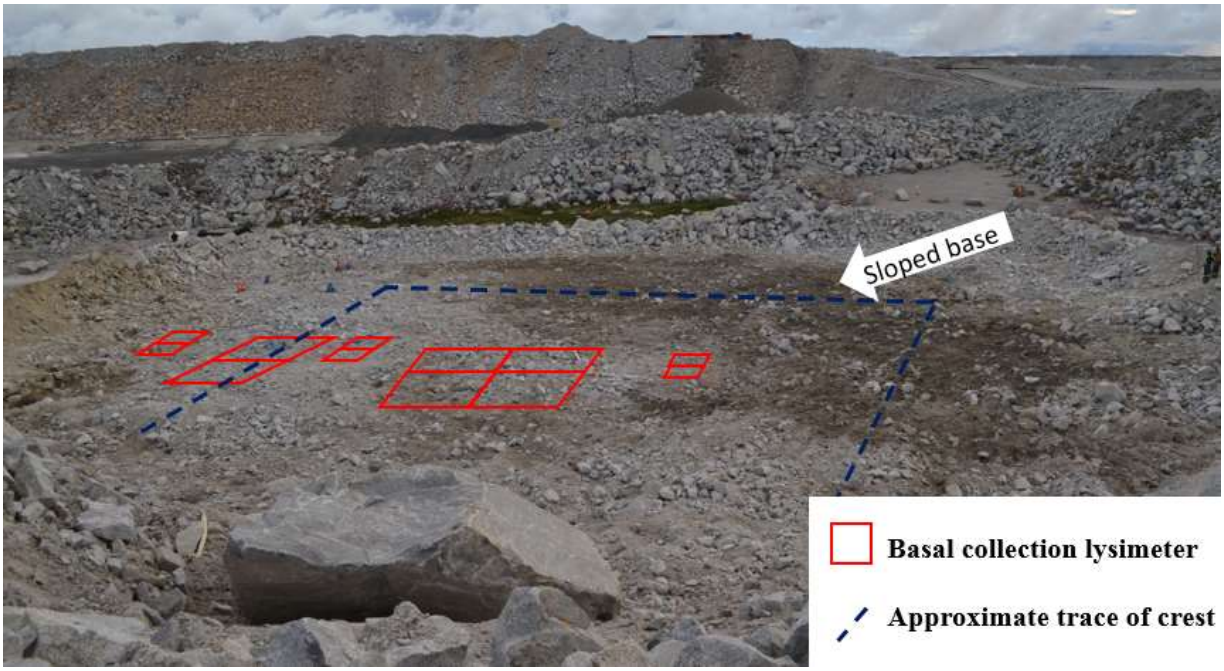

Figure 2.13. Photograph of the Bench 5 surface sampled during deconstruction. Approximately 11 m below the original ground surface (2-3 m above the base).

Table 2-2. Comparison of VMC measured by TDR and using soil cans during deconstruction.

Depth	Volumetric Moisture Content (%)	
	TDR	Soil Can
2	3	4
3	5	4
6	3	5
9	Omitted	5

2.3.3.2 Blasting residuals

Depletion of chloride concentrations from initial conditions provides evidence of the first pore water flush of the waste rock pile. Pore water extractions from the 15 and 35 m transects in general show increasing chloride concentrations downward (Figure 2.14). Concentrations in the upper 3 m range from 0.02-28 mg/L. Between 3-6 m depth the range of concentrations observed increased to 10-52 mg/L. Below 6 m depth, chloride concentrations significantly increased to

>100 mg/L, however localized areas with concentrations <10 mg/L were also observed at similar depths. Bailey et al. (2013) provides a detailed analysis of blasting residual concentrations in the test piles, reporting maximum chloride concentrartions of 2800 mg/L from the basal drain from the Type I pile. Leach testing revealed spatial variability in the initial conentrations between samples which was attributed to the proximity of the sample to a blasting hole. Isolated areas of high or low concentrations observed during deconstruction likely reflect an effect due to distance of the material from a blast hole.

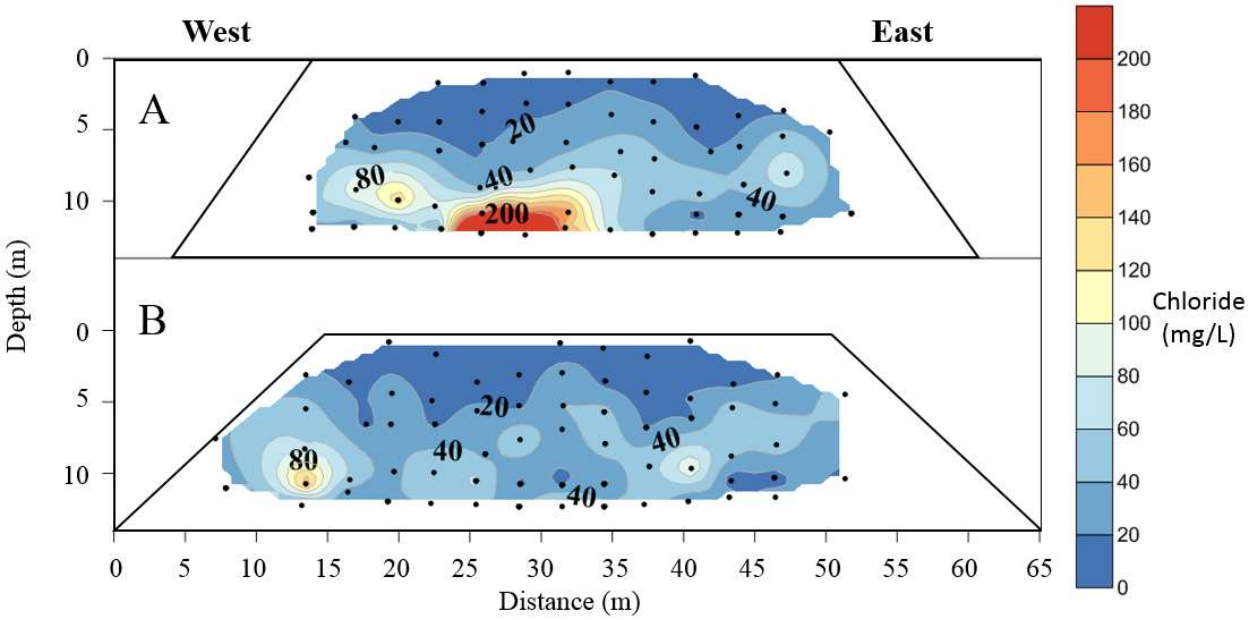

Figure 2.14. Chloride concentrations obtained from pore water extractions collected during Type I test pile deconstruction across the A) 15 and B) 35 m transect lines.

2.3.3.3 Ice distribution

Ice within the test pile can be characterized in terms of three major forms (Figure 2.15): granular ice crystals held in matrix material, discontinuous ice lenses filling large void spaces, and laterally continuous ice lenses filling large void spaces. Discrete sections of granular ice crystals located in matrix material as shown in Figure 2.15A were observed at a depth of 9 m within the batters of the pile. Small ice lenses (10-25 cm; Figure 2.15B) were often proximal to frozen matrix, typically found beneath boulder and large cobble-sized waste rock. Discrete seams were observed in some discontinuous ice lenses (Figure 2.15C) and have been interpreted as freeze-thaw seams produced by partial thawing of a lens followed by ice growth later in time. Laterally continuous ice extending to the base of the pile was encountered at a depth of approximately 12 m in the batters. Continuous ice was characterized by laterally extensive ice reaching a width of approximately 15 m, filling large void spaces between cobbles and boulders (Figure 2.15D). At this depth, trace amounts of discontinuous ice lenses and granular ice were observed within the core of the pile, shown schematically in Figure 2.16. First order calculations were completed to determine the volume of water held in storage by continuous and discontinuous ice. This assumed the continuous ice filled the available pore space where it was observed and the discontinuous ice occupied 1% of the pore space volume of the regions where it was observed. An estimated 4 m^3 of ice was present as discontinuous and an estimated 1087 m^3 as continuous-mainly in the batters. This equates to about 1000 m^3 of water assuming a density of 0.92 g/m^3 for ice.

A mass balance was completed using: PM estimates of rainfall infiltration through the crest of the test pile, recorded outflow from the drain and BCLs, and estimates of storage in the forms of ice and moisture contents mapped during deconstruction. These components of the water

balance for the test pile were used to approximate an average rate of infiltration (snowmelt and rainfall) through the batters of the pile from 2007-2014. The components of the mass balance are shown in Table 2-3. The mass balance yielded a cumulative estimate of batter recharge of about 970 m^3, corresponding to an annual infiltration rate of approximately 73 mm. This value is less than expected. Annual snowmelt infiltration through the batters of the Type III pile is estimated to be about 77 mm/yr (Chapter 3). Assuming PM estimations of rainfall infiltration to the crest of the pile provide a good indication of rainfall infiltration to the batters, cumulative batter infiltration may be about 118 mm/yr (rain and snow). Differences in the estimated batter infiltration for the two piles may be caused by: 1) Variable snow pack on the two piles due to wind redistribution, or 2) the PM calculation not being representative of rainfall infiltration to the crest of the Type I pile. Further investigation is required to determine the factors influencing infiltration to the Type I pile.

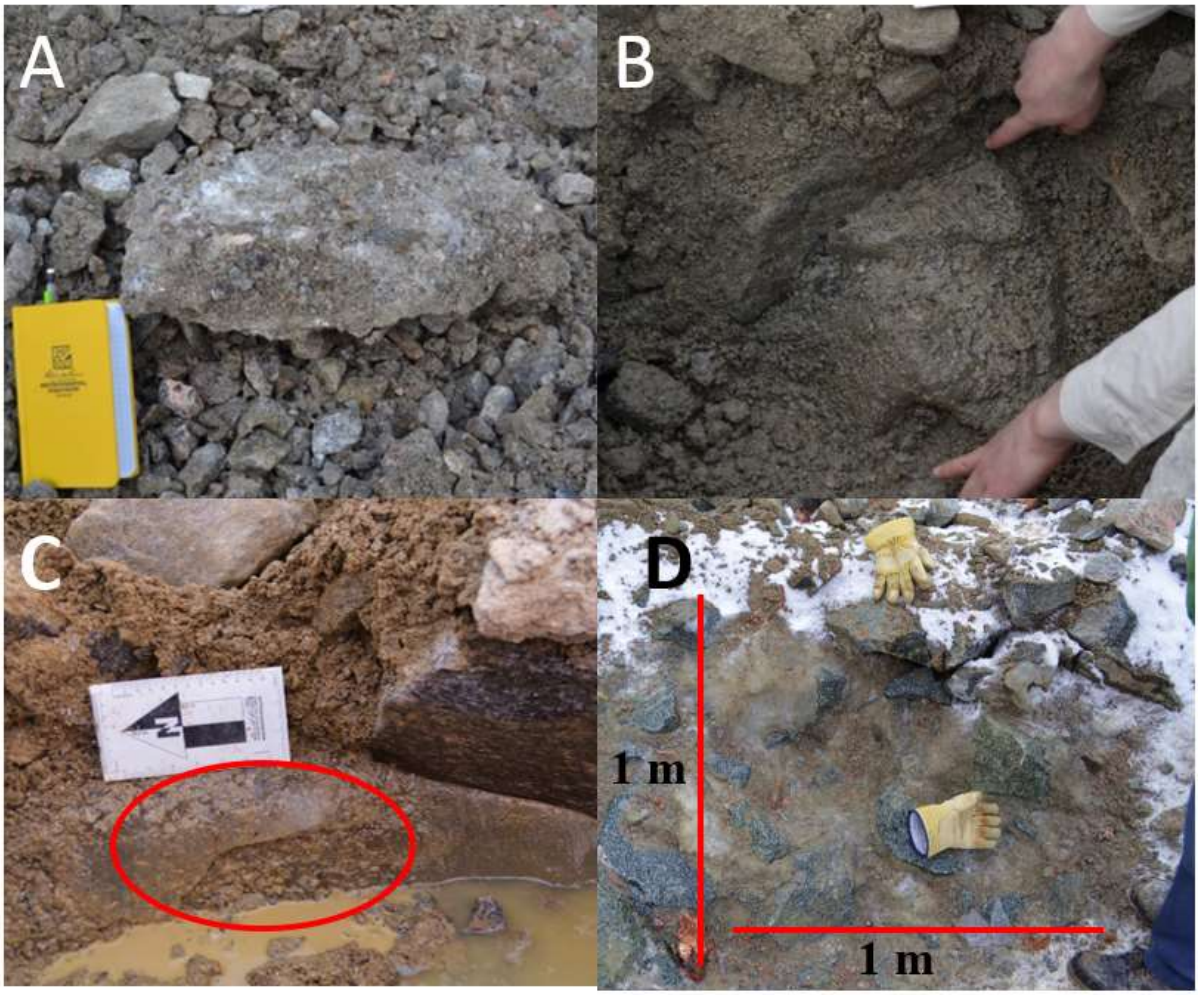

Figure 2.15. Types of ice encountered in the Type I waste rock pile: (A) centimeter scale ice crystals filling pores in matrix material, (B) discrete ice lens filling a large void space, (C) ice lens containing a freeze-thaw seam, and (D) continuous ice lens filling large void spaces.

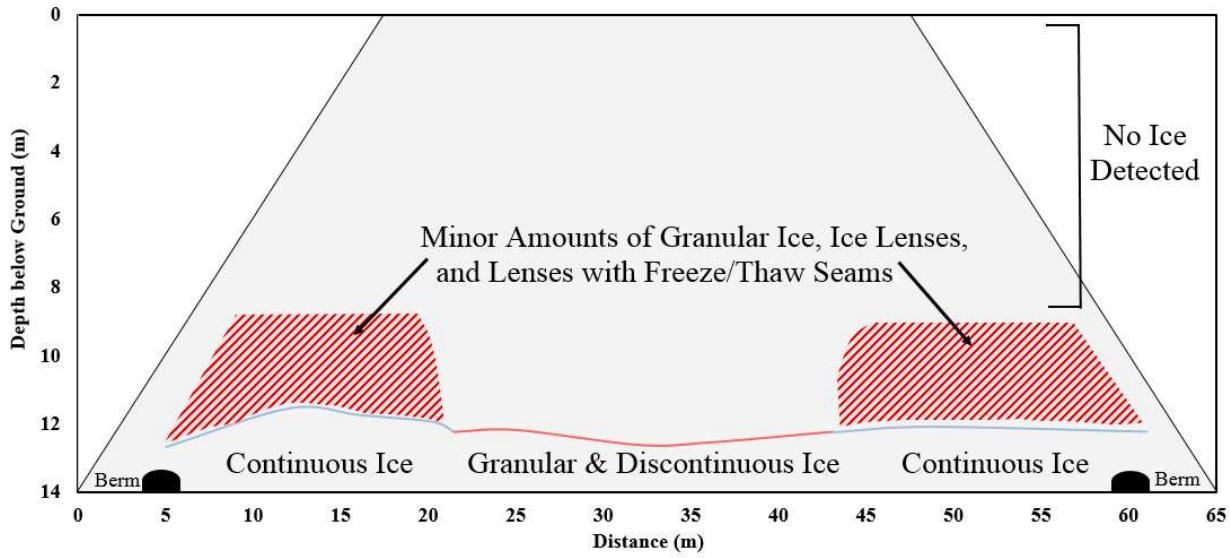

Figure 2.16. West-east schematic cross-section showing the distribution of ice in the Type I test pile.

Table 2-3. Water balance of the Type I test pile, estimating infiltration through the batters. Data from 2007-2014.

	Infiltration (m^3)	**Storage (m^3)**	**Outflow (m^3)**
Crest (rainfall)	437		
Batters (rain and snow)	966		
Ice		1000	
Moisture Content		180	
Basal Drainage			223

As shown in Figure 2.4, the alignment of the basal drain was mainly through batter areas of the pile, which contained a significant amount of ice. Ice lens formation immediately above the drain reached a minimum thickness of 0.25 m in the NE and a maximum of about 2 m in the SW area of the pile. Excavation revealed that the drain was filled with ice; it is unclear if this was a result of turning off the heat trace immediately prior to deconstruction, or related to the flooding event in 2013 (note the decrease of outflow Figure 2.10), or if it predated these events. In general, the BCLs were free of ice. However, one lysimeter which had never produced drainage

(1BWBlys2S- located in the batter), was found to be filled with water and had a thin layer of ice at the bottom. Significant damage to the lysimeters occurred during excavation, preventing testing of the drain lines.

2.3.3.4 Solute exclusion

Nitrate, sulfate, and chloride concentrations measured in extracted pore waters and ice samples are shown in Figure 2.17. All concentrations displayed were measured in samples collected below 11 m depth, mean concentrations and standard deviations were calculated from these data. In general, the mean concentrations of these anions in ice were lower by 1-2 orders of magnitude when compared to the mean values for pore waters. Mean nitrate concentrations for pore water and ice were 932 mg/L and 39 mg/L (standard deviations= 2356 mg/L and 75 mg/L), respectively. Mean sulfate concentrations for pore water and ice were 1124 mg/L and 232 mg/L (standard deviations 1151 mg/L and 274 mg/L), respectively. Mean chloride concentrations for pore water and ice were 72 mg/L and 4 mg/L (standard deviations= 151 mg/L and 4 mg/L), respectively.

The observed reduction in concentrations from pore water to ice is explained by the process of solute exclusion, whereby solutes are rejected from the crystalline structure during ice growth, resulting in the remaining fluid phase becoming concentrated with solutes as freezing proceeds. Solute exclusion has been shown to lead to enriched concentrations at depth in soils as downward freezing proceeds, leading to the flushing of effluent with increased solute concentrations the following summer (Lewkowicz and French, 1982). Conceptually, freezing of the active zone of the test pile results in temporary enrichment during the winter followed by

dilution upon thawing. Permafrost aggradation at the base of the pile results in a permanent shift in the solute distribution since the ice does not melt. A description of the behaviour of these solutes in drainage from the Type I test pile is provided in Bailey et al. (2013).

The effective distribution coefficient describes the ratio between the solute concentration in ice and the concentration in the unfrozen phase. Low distribution coefficients indicate significant solute exclusion from the frozen phase and enrichment to the unfrozen phase (Overduin, 1997). This ratio can range from 10^{-3} to about 1, being a function of: 1) freezing rate, 2) the initial concentration of the solution, 3) the solution type, 4) the temperature gradient near the phase interface in the unfrozen soil, 5) the mechanism of heat and solute transfer, and 6) the crystallographic orientation of growing ice crystals (Hallet, 1978; Overduin, 1997). The effective distribution coefficients of nitrate sulfate and chloride were found to be 0.04, 0.2, and 0.06, respectively, calculated using the observed mean concentrations. Since the aqueous concentration of these solutes at the time of ice formation is unknown, there is some uncertainty associated with the calculated distribution coefficients. The distribution coefficients observed here are expected. These values are consistent with laboratory experiments completed by Konrad and McCammon, (1990) for a cooling rate of less than 1ºC/day, which is consistent with the thermal regime of the test pile.

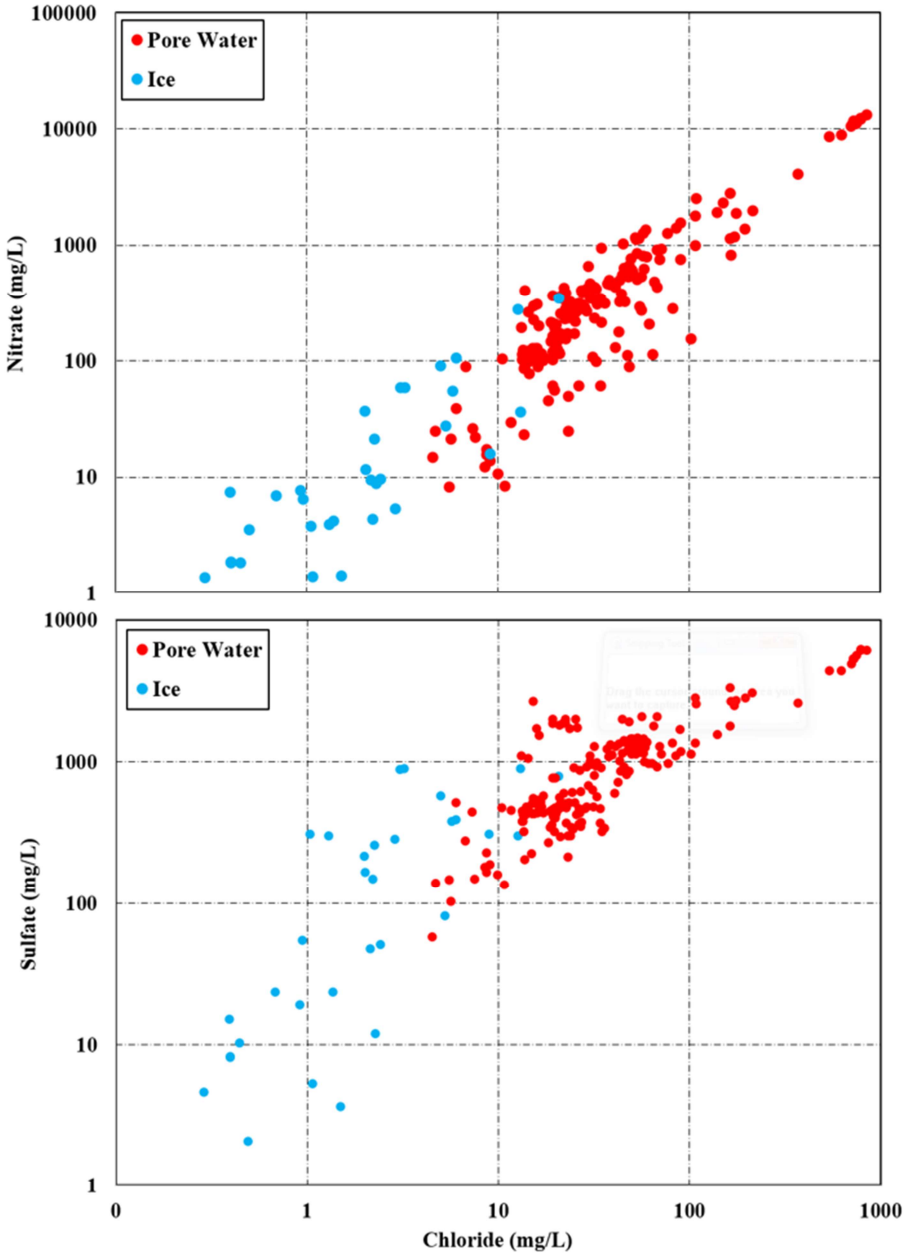

Figure 2.17. Comparison of nitrate vs. chloride and sulfate vs. chloride concentrations between ice samples and pore water samples collected during the deconstruction of the Type I test pile.

2.3.3.5 Ice and pore water isotopic analysis

δD and $\delta^{18}O$ are measured in terms of their deviation from the Vienna Standard Mean Ocean Water (VSMOW). Seasonal variation is caused by wetter vs. drier and colder vs. warmer periods (Clark and Fritz, 1997). Compared to snowfall, rain is enriched with δD and $\delta^{18}O$, this helps to describe if a water sample from the test pile originated from snowmelt, rainfall, or a mixture of the two (examples: Sracek et al., 2004; Barbour et al., 2016).

The isotopic signature of infiltrating meteoric water lies along the local meteoric water line (LMWL). The LMWL at Diavik has been established to be $\delta D = 7.5 \times \delta^{18}O - 2.4$ (Chapter 3). The LMWL and mean composition of rain and snow at Diavik are shown in Figure 2.18, error bars indicate the standard error of the mean. Also shown on the plot are ice and pore water samples from test pile deconstruction, BCL drainage samples, and SWSS collected from 2008 and 2009. Ice samples were collected from beneath the crest and batters of the pile, while pore water, BCL, and SWSS were collected solely from beneath the crest. Comparison of these data provides an understanding of the distribution of rainfall and snowmelt recharge across the crest and batters. BCL drainage from beneath the crest and ice samples collected from the batters appear to be mostly "snow like". Pore waters collected beneath the crest during deconstruction, SWSS samples collected beneath the crest, and ice samples, taken beneath the crest are dominantly "rain like". However, contributions from snowmelt are evident in some pore water and ice samples. In general, all samples did not significantly deviate from the LWML, although, the majority of samples plot slightly below, reflecting a minor influence by evaporation (Allison, 1982).

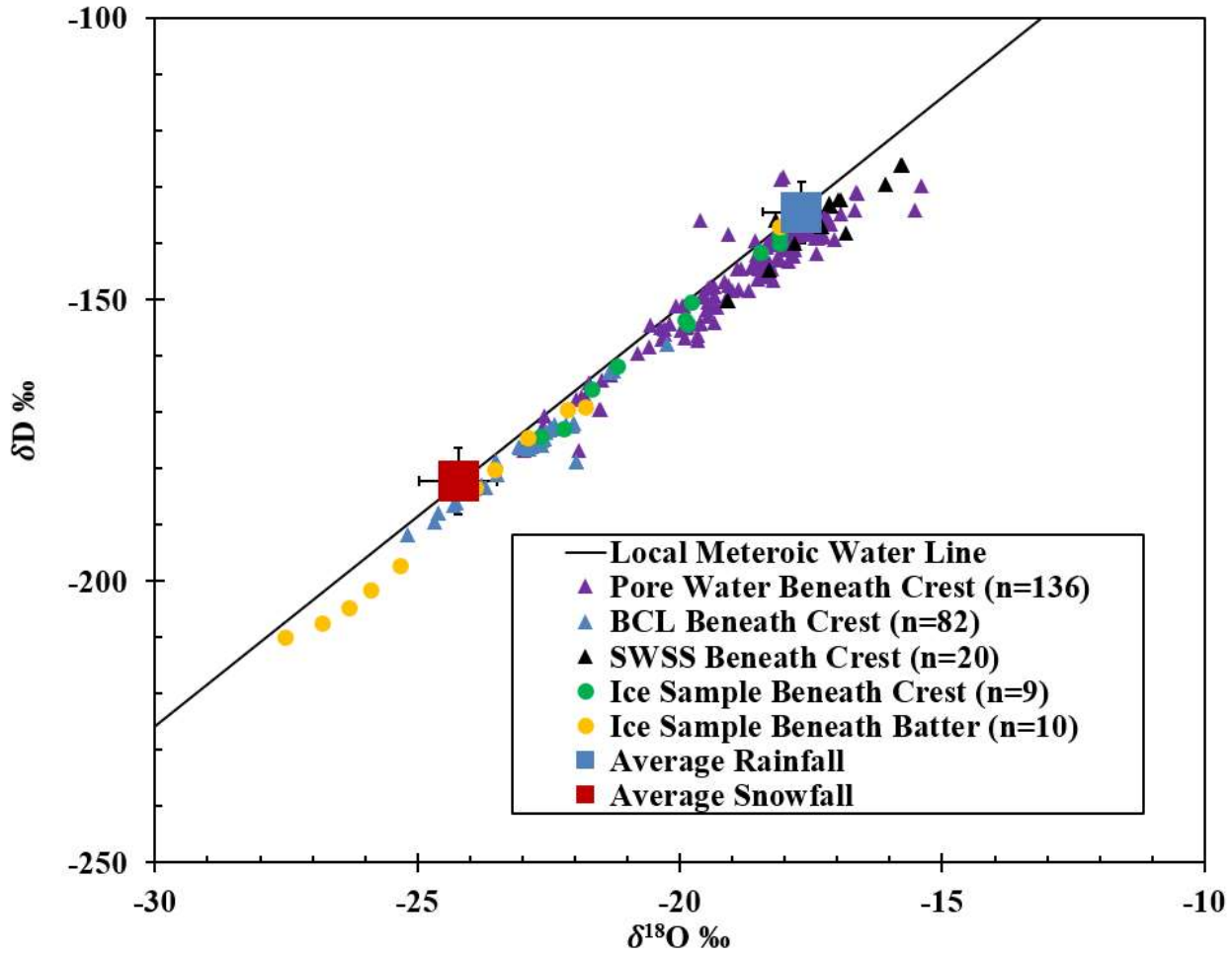

Figure 2.18. Oxygen-18 and deuterium concentrations in pore waters, BCL drainage, and ice lenses collected from the Type I test pile, plotted along with average isotopic ratios of precipitation collected from Diavik. Error bars show the standard error of the mean concentrations.

In order to understand the significance of rainfall versus snowmelt recharge to the test pile, the rainfall composition of water samples was calculated using equation 2.1– where δ_{snow} represents the respective mean of δD or δ^{18}O value for snow measured at Diavik, δ_{rain} is the mean value for rainfall measured, and δ_{sample} is the value measured in sample. Since it is possible for a sample to have δD and δ^{18}O concentrations greater than the mean rainfall or less than the mean

snowfall, rainwater compositions less than 0% and greater than 100% can be calculated, this does not invalidate the data, it is merely a reflection of the natural variability of these isotopes.

Figure 2.19 shows that pore waters sampled beneath the crest primarily originated from rainfall, snowmelt water was not detected in the upper 10 m. At depth, pore waters were composed of rainfall and snowmelt recharge. The upper 10 m of the 15 m and the 35 m lines were on average 95% and 88% rainfall. SWSS show an average rainfall composition of 103%. Below 10 m, waters were more "snow like", on average 52% rainfall for the 15 m line and 60% for the 35 m line. As shown by the inset in Figure 2.19 increased moisture contents observed at 11-14 m depth are associated with more "snow like" water, suggesting the majority of the water in the pile was derived from snowmelt.

$$Rainwater\ Composition = \frac{\left[\frac{\left(\delta D_{snow} - \delta D_{sample}\right)}{\left(\delta D_{snow} - \delta D_{rain}\right)} + \frac{\left(\delta^{18}O_{snow} - \delta^{18}O_{sample}\right)}{\left(\delta^{18}O_{snow} - \delta^{18}O_{rain}\right)}\right]}{2} * 100 \qquad (2.1)$$

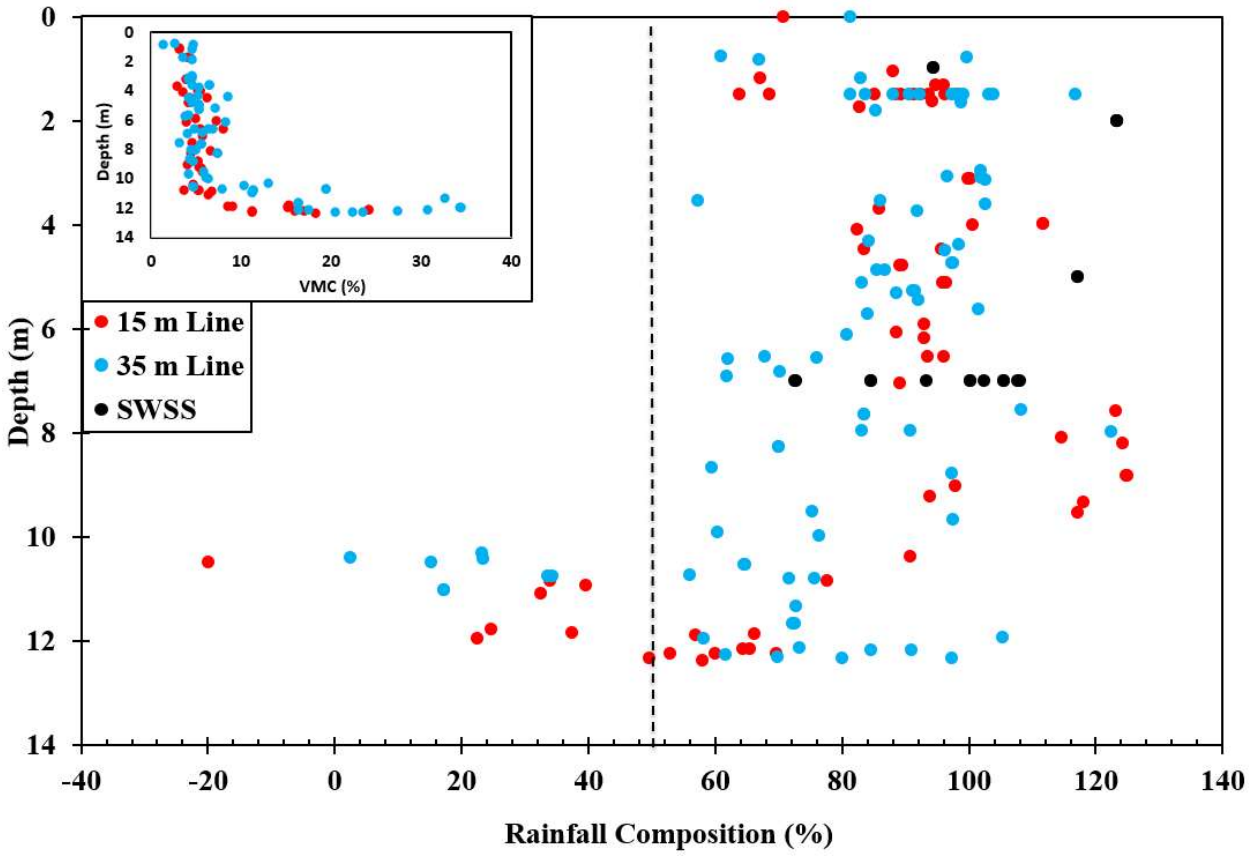

Figure 2.19. Rainfall composition determined using δD and $\delta^{18}O$ measured in SWSS samples and pore waters sampled during the deconstruction of the Type I test pile, collected from 15 m and 35m transect lines. Inset shows volumetric moisture contents (VMC) measured from the same transects.

2.3.4 Basal drain isotopic analysis

δD and $\delta^{18}O$ concentrations measured in the basal drain are shown in Figure 2.20. Similar to ice, pore water, and BCL drainage, outflow from the basal drain plotted slightly below the LMWL, along the line $\delta D = 7.5 \times \delta^{18}O - 4.1$, indicating slight influence by evaporation (Figure 2.20A). Discharge can be seen to be dominated by snowmelt (Figure 2.20B), suggesting snowmelt infiltration through the batters was the primary source of recharge to the test pile. An annual trend of drainage becoming increasingly "rain like" through the summer months is shown to

have been disrupted in 2013. This may indicate that the loss of heat trace to the pile during flooding resulted in damage to the drainage system due to freezing.

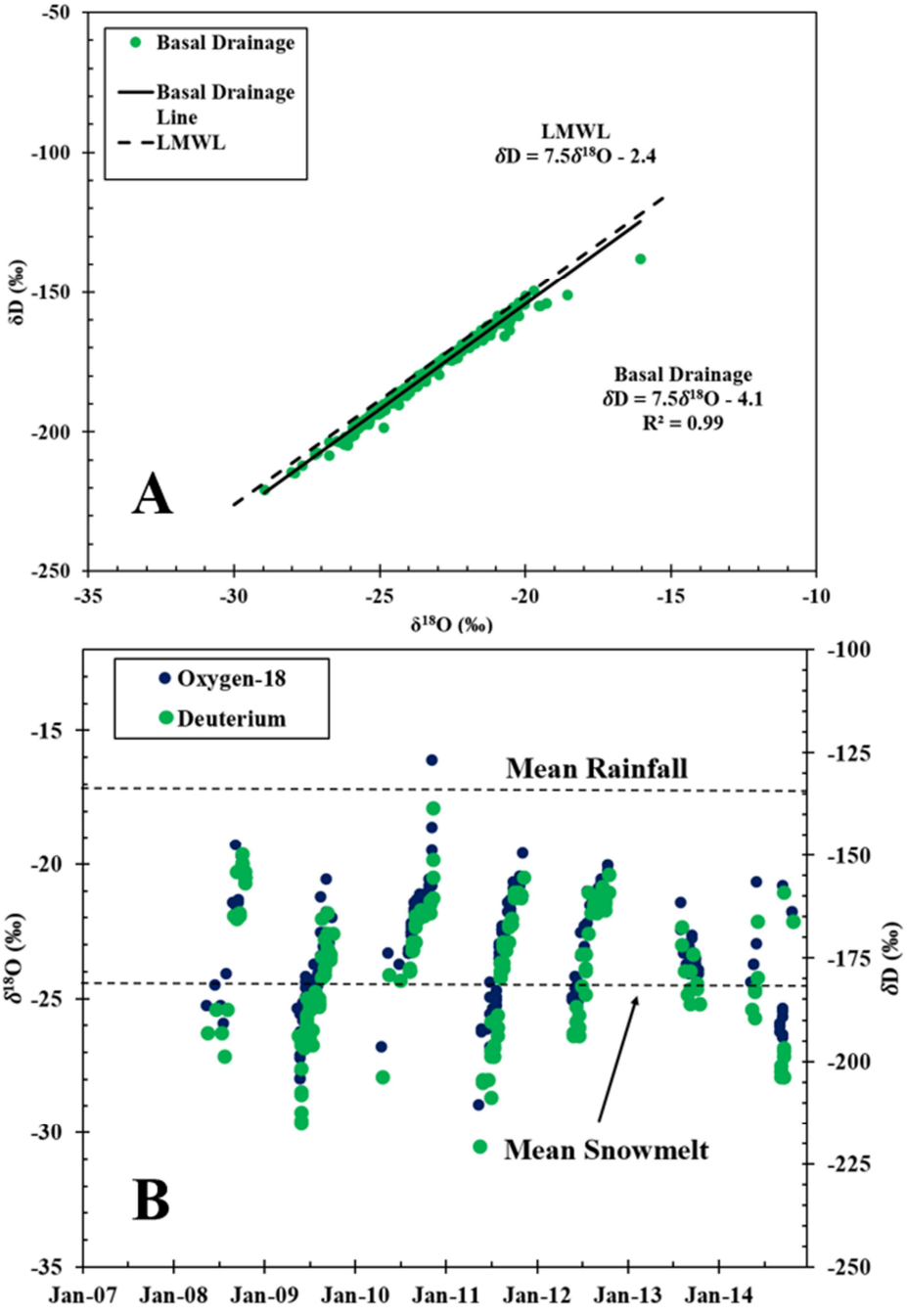

Figure 2.20. Oxygen-18 and deuterium concentrations from the Type I basal drain. A) Regression of δD and $\delta^{18}O$ and B) δD and $\delta^{18}O$ concentrations over time.

2.4 Discussion

2.4.1 Test pile scale processes

2.4.1.1 Waste rock first flush

Based on data obtained from eight years of monitoring the Type I waste rock test pile and data collected during deconstruction, the matrix material in test pile had not undergone a full pore volume flush. Concentrations of chloride in pore waters mapped during deconstruction serve as an indicator of the depth to which the matrix material was flushed by flow through the pile. Bailey et al. (2013) demonstrated that following the first pore volume flush of a series of 2 m deep lysimeters at Diavik, chloride concentrations in effluent sharply declined below approximately 20 mg/L. Concentrations measured in pore water samples above this threshold were consistently observed below a depth of approximately 6 m in the test pile (Figure 2.14), indicating the upper 6 m of matrix had been flushed while greater depths had not.

Moisture contents from TDR corroborate the interpretation of mapped concentrations of blasting residuals. Moisture contents at 2 m depth show a two year wet-up period (2007-2008) and a three year wet-up period (2007-2009) at 3 m depth; here, the term "wet-up" is used to describe moisture contents maintained above field capacity (10-15%, Neuner, 2009). During wet-up, moisture contents increased each year until field capacity had been reached. Wet-up was followed by a state of dynamic equilibrium characterized by little variation in peak amplitude on an annual basis. Once moisture contents above field capacity were established, the flushing of blasting residuals was able to occur. Moisture contents reported at 6-9 m indicate relatively dry conditions existed at these depths. Since moisture contents were generally below field capacity at these depths, the transport of blasting residuals did not occur.

2.4.1.2 Evaporation

Allison (1982) demonstrated that the δD and $\delta^{18}O$ regression line produced from water influenced by evaporation in an unsaturated porous material can have a slope as low as 2. Few studies have been completed regarding the effects of evaporation on δD and $\delta^{18}O$ in unsaturated waste rock. Sracek et al., (2004) reported a regression of $\delta D = 2.4\ \delta^{18}O - 66.0$ from a waste rock pile at Mine Doyon where internal evaporation was found to be significant. Using a modified Penman method (1948), Fretz, (2013) identified two predominant infiltration seasons at Diavik, May and September-mid October. Potential evaporation was found to be too high during June-August for infiltration to occur, unless large rainfall events (>10 mm) occurred; runoff was found to not occur. As a general statement: given the significance of evaporation to the test piles water budget, it is interesting that Figure 2.18 and Figure 2.20A suggest that evaporation had a minor influence on waters which recharged the test pile. When considering the seasonality of infiltration at Diavik, the similarity between the regressions of drainage and pore waters to the LMWL becomes apparent: When potential evaporation is high (June-August), there are very few rainfall events large enough at Diavik to result in infiltration beyond the evaporation horizon. Furthermore, when potential evaporation is low (May and September-mid October) rainfall largely infiltrate. The result of this is that water which has been significantly influenced by evaporation comprises a relatively small component of the test pile water balance.

2.4.1.3 Distribution of recharge

The consequence of wind scouring of snow off the crest of the pile and accumulation on the batters (Krentz, 2014) is reflected in δD and $\delta^{18}O$ concentrations. The majority of pore water

and SWSS samples indicated that water beneath the crest of the test pile was dominantly from rainfall recharge. Ice samples from the batters of the pile originated from primarily snowmelt. Pore waters collected from below 10 m, ice samples from beneath the crest, and BCL effluent demonstrated "snow like" components. A possible explanation of the occurrence of snowmelt water beneath the crest at the base of the pile could be caused by infiltration through the NE area of the batters, which then flowed within the lower 3-4 m of the pile towards the drain outlet and into lysimeters along the flow path. Batter-derived waters were most likely able to reach 3-4 m above the base of the pile by flowing above frozen zones (ice formations and areas below 0°C) where the hydraulic conductivity was near zero.

The batters of the test pile occupy approximately 55% of the infiltration surface. However, it is clear that the batter domain strongly controlled the hydrologic behaviour of the test pile. Combined rain and snowmelt infiltration to the batters was estimated to be about 73 mm/yr using a mass balance. Elevated VMC at the base of the pile (Figure 2.19) and discharge from the basal drain (Figure 2.20B) were found to be primarily snowmelt, indicating these waters originated as batter recharge. This highlights the requirement for reliable snowmelt infiltration estimates in future work on the covered and Type III test piles.

2.4.1.4 Ice formation

Mapping of ice in the Type I pile demonstrated that ice distribution was not well correlated with areas of the pile which remained below freezing temperatures through the summer (Figure 2.11 and Figure 2.16). The majority of the ice in the test pile was located within the batters, where thermistors reported temperatures of 0-6°C in surrounding areas during the late summer (Figure

2.11). It is conjectured that the limited timeframe of above freezing temperatures in the batters did not provide a sufficient period to allow for significant melting of continuous ice lenses to occur. It is expected that melting occurs following a stepwise process beginning with ice in small pores first followed by sequentially larger pores, due to the decreasing ratio of surface area and increasing pore volume. This means once large continuous ice lenses have formed in the waste rock, a sustained melting period will be required to fully thaw the region.

The distribution of ice was influenced by the thermal regime of the pile as well as the amount of recharge received by the crest and batters. In the batters, ice lens thickness had been limited by temperature rather than infiltration. This is supported by the occurrence of freeze-thaw seams in discontinuous ice lenses overlying continuous ice. Additionally, pore spaces in frozen batter regions appeared to be filled with ice, suggesting an adequate supply of recharge. Conversely, the amount of infiltration the core received appeared to limit the growth of ice in this region. The core of the pile remained below freezing temperatures below 12 m depth annually (Figure 2.11). Here ice was discontinuous leaving pore spaces unsaturated. Relative to the batters, the crest of the waste rock pile received lower infiltration due to a lack of snowmelt recharge.

2.4.1.5 Conceptual model

Learnings from eight years of monitoring followed by test pile deconstruction have been integrated to develop a hydrologic conceptual model for the Type I pile, shown in Figure 2.21. This conceptual model highlights: 1) Wind scouring causing removal of snow from the crest and accumulation on the batters. 2) Vertical flow in the upper region of the pile and lateral flow at depth caused by the combined influences of the sloped basal liner, ice formation in the batters,

and the 0°C isotherm in the core. Flow lines indicating a flux past the continuous ice layer and out of the pile are highly speculative. The purpose of these flow lines is to represent drainage prior to the observed decrease in outflow in 2012, the ice distribution may have been different at that point in time permitting some extent of outflow to occur. Drainage which had occurred in 2012-2014 may have resulted from melting induced by heat trace or leakage though basal ice. Infiltration during this period of low basal outflow likely led to increased ice formation.

Pham (2013b) discusses a period of gradual permafrost formation at the base of the test piles, leading to the development of the frozen core. Prior to the formation of permafrost in the test pile, flow at the base of the pile would have been in contact with the basal liner. During permafrost and ice formation at the base of the pile, the hydraulic conductivity of the waste rock decreased towards zero causing lateral flow to be initiated slightly above these regions, as shown in the conceptual model.

The model proposed here for the Type I pile differs from the conceptual model of flow in the Type III test pile presented by Sinclair et al. (2015), in part due the configuration of the basal liners. The Type III basal liner was sloped to divert flow away from the centre of the pile towards the North and South batters, water was collected by two independent toe drains located at opposing ends of the pile, creating a drainage divide through the middle. The Type I pile had a basal liner which was sloped to divert flow towards the drainage outlet at the southwest corner. Furthermore, it is proposed here that significant ice formation in the Type I pile induced lateral flow in the batters. Ice accumulation in the pile led to reduced drainage from the pile over 2012-2014 (and possibly earlier) - it is unknown if this was a result of heat trace failure. The influence of ice formation on the Type III pile hydrologic system is complex- this is discussed in Chapters 3 and 4 in this thesis. The Type III pile conceptual model assumed that the 0°C isotherm in the

summer months delineated the distribution of ice in the pile. The work presented here demonstrates that a significant amount of ice can remain in the batters through the summer, having an influence on internal flow fields. With an improved understanding of ice formation in the test piles, refinement of the Sinclair et al. (2015) conceptual diagram may be required.

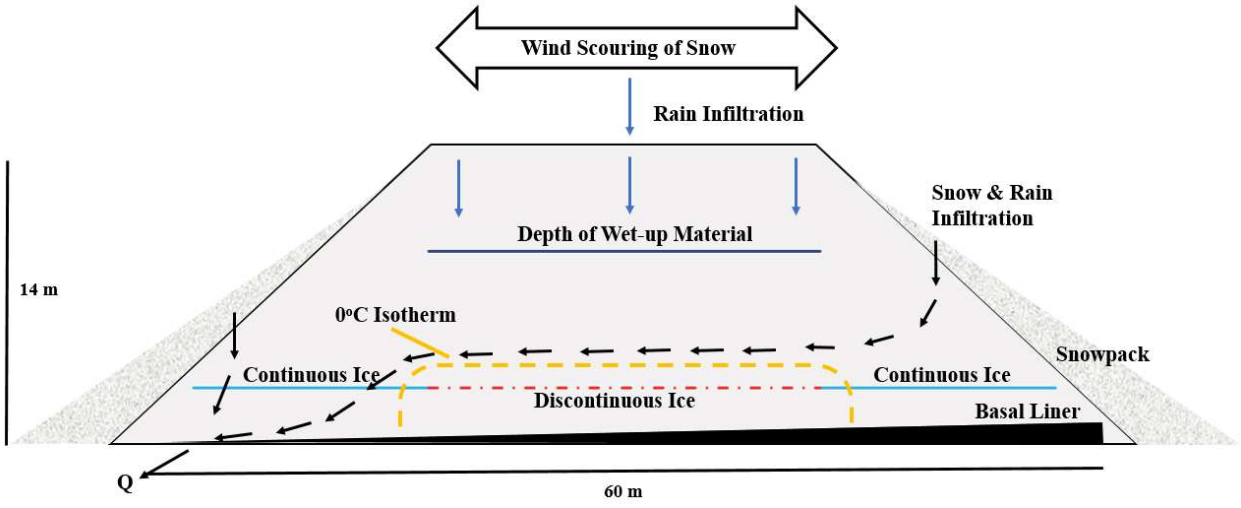

Figure 2.21. Conceptual diagram showing the distribution of infiltration across the Type I pile and the flow fields which lead to the observed ice distribution.

2.4.2 Full scale pile ice formation

Excavations of the 80 m tall full scale pile at the mine site allowed for the preliminary observations of ice formation in the full scale pile. Figure 2.22A shows a slab of frozen material held together by granular ice crystals filling voids in matrix, similar to granular ice observed in the Type I test pile. Figure 2.22B illustrates ice filling large void spaces between cobble and boulder material, similar to the continuous ice lenses observed in the Type I test pile. Figure 2.22C provides a sense of scale for the frozen material, a thin (1-2 m) sheet of continuous large void filling ice spanning the width of the excavation (>100 m). The depth of ice formation from

the original pile surface was unable to be determined from mine records, but was on the order of 5-10 m.

The formation of continuous ice in the full scale pile indicates that the low amount of recharge experienced at Diavik is sufficient to produce extensive ice formation over a period of time. The observed continuous ice lens formation may act as a barrier to flow above potentially reactive material. Isotopic analysis of ice and overlying pore waters should be completed in order to determine if snowmelt infiltration to the full scale waste rock pile is insignificant, similar to the test piles. The full scale pile features a much larger crest area relative to the batters when compared to the test piles. This will be crucial when considering if the core or batters dominate the full scale pile flow system.

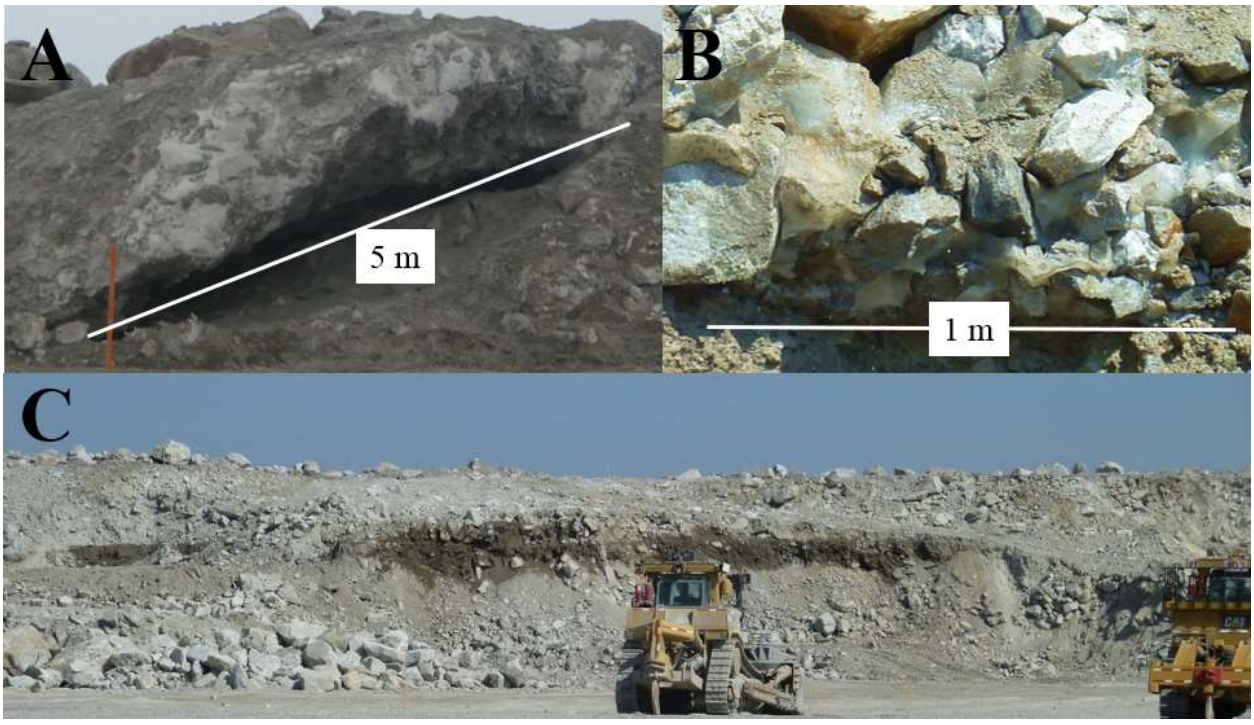

Figure 2.22. Excavations of the full scale waste rock pile at Diavik showing ice. A) A slab of material held together by ice in matrix pore spaces (taken April 2015), B) Ice filling large void spaces between clasts (taken August 2015), C) Continuous ice layer spanning across the excavation site (taken August 2015).

2.5 Conclusions

Eight years of continuous monitoring followed by test pile deconstruction provided a unique opportunity to gain an improved understanding of the hydrologic behaviour of the Type I waste rock test pile. This study yields a number of insights to the behaviour of waste rock at Diavik which may be applicable to other mine sites located in the sub-arctic:

1. Evidence indicates that the flow regime of the Type I test pile was strongly batter dominated. Basal drainage and elevated moisture contents at the base of the pile beneath the crest were found to be primarily originated from snowmelt, which is derived from the batters.

2. Zones of extensive ice formation cannot reliably be located by simply identifying areas of permafrost formation (areas below $0^{o}C$). In the Type I test pile, temperatures above $0^{o}C$ sustained in the batters through the summer months did not lead to melting of large void filling continuous ice lenses. In contrast to the batters, the core -where permanently freezing temperatures have been documented- contained little ice due to the low amount of recharge experienced through the crest.

3. Following an estimated 324 mm of rainfall infiltration through the crest, chloride concentrations originating from blasting residuals and TDR measurements suggested the upper 6 m of the pile had experienced a first flush of pore water. Below this depth, matrix material remained unflushed indicated by elevated chloride concentrations

4. In support of earlier work by Krentz (2014), isotopic analysis of pore waters indicated that wind scouring effectively removed snow from the crest of the test pile, thus preventing snowmelt recharge. This limited recharge through the crest to rainfall during

the summer months, while batters were recharged by snowmelt in the spring as well as by rainfall through the summer.

5. Solute exclusion during freezing was identified as a process influencing concentrations of nitrate, sulfate, and chloride in the test pile, this process is likely to influence concentrations of other solutes as well. Effective distribution coefficients were calculated to be 0.04, 0.2, and 0.06, respectively. Distribution coefficients in this range are consistent with the thermal regime of the pile.

6. TDR readings of VMC immediately prior to deconstructing the test pile were found to be comparable to those observed during deconstruction. This places confidence in moisture contents recorded in the Type I pile during the monitoring phase. Additionally, this suggests TDR probes can be considered to be a useful instrument to reliably measure moisture contents over multi-year projects in cold climates.

7. Deuterium and oxygen-18 isotopes were used successfully to identify rain and snow components in waters using a mass balance equation.

8. Concentrations of stable isotopes show weak alteration by evaporation. This suggests that rainfall events are either almost entirely lost to evaporation during June-August or largely infiltrate during May and September-mid October.

9. Discharge volumes from the basal drain and the BCLs were much lower than infiltration estimates. Low drainage was likely the result of significant ice formation in the test pile. A period of decreased drainage was observed from 2012-2014 (partially coinciding with the loss of heat trace to the pile), infiltration during this period likely contributed to

further ice buildup. The effects of the temporary loss of heat tracer to the Type I drainage system on the observed ice distribution and drainage from the pile remain unclear.

10. Preliminary ice characterization of the full scale pile has shown similarities to ice observed in the batters of the test pile. Further work is required to identify the significance of snowmelt recharge to the full scale pile, providing a better understanding of the amount of infiltration required for the formation of continuous ice lenses.

The work summarized here has outlined multiple learnings developed from the monitoring and deconstruction of a waste rock test pile. This research allowed for an improved hydrologic conceptual model for test pile to be produced. Future work characterizing flow and solute transport in field and full scale waste rock piles should involve accurately quantifying rainfall/snowmelt infiltration through both the crest and batters of the pile.

Chapter 3 An isotopic investigation (δD and δ^{18}O) of drainage from a waste rock test pile in a permafrost environment

3.1 Introduction

Mining activities are typically associated with stockpiling of large volumes of rock at surface during the extraction of an ore body, this is called waste rock. The oxidation of sulphide minerals contained in waste rock can cause drainage from stockpiles to contain elevated acidity and metal concentrations, this is referred to as acid rock drainage (ARD). ARD poses serious environmental and financial risks to mining companies and communities on a global scale. Hydrogeological processes have been recognized to play a significant role in determining the quality of water discharged from waste rock piles (Smith et al. 1995; Amos et al. 2014). The management of waste rock at active or legacy mine sites requires a knowledge of the relevant physical, chemical, and microbial processes taking place within a waste rock stockpile.

Characterizing infiltration is fundamental to the assessment of the hydrologic regime of a waste rock pile. Poor recharge estimates can result in misleading predictions of future solute concentrations and loadings to the environment. Several techniques used to estimate recharge to waste rock piles have been considered successful in the past: A modified Penman method (1948) was found to reliably predict infiltration to a series of 2 m deep lysimeters by Fretz (2013), and to an instrumented cover system by O'Kane et al. (1998). This method requires high resolution air temperature, relative humidity, wind speed, and net radiation data from the site in order to estimate potential evaporation. As a general statement on the method, the Penman method does not account for infiltration to the batters of stockpiles nor does it account for internal evaporation caused by air flow through the waste rock pile, which may be relevant to the water balance (Amos et al., 2009; Sracek et al., 2004). Nichol et al. (2005) and Andrina (2009)

used collection lysimeters to estimate infiltration through waste rock over the course of several years. This method required the assumption that water fluxes averaged over several years were representative of a characteristic recharge rate; providing little insight towards the effects of individual infiltrations events or recharge which occurred during particularly dry or wet years. Furthermore, in climates where snowmelt is a key component of the water balance, these methods provide little insight to quantify snowmelt infiltration. High resolution isotopic profiling of drill cores completed by Barbour et al. (2016) yielded estimates of rainfall and snowmelt recharge components to several waste rock piles at coal mines in British Columbia. Despite the success of these studies to produce reasonable infiltration estimates, additional field investigations from long-term, large-scale waste rock studies are required to develop new techniques to estimate infiltration to waste rock piles as well as assess the variability of recharge to waste rock across a range of climates.

The Diavik Waste Rock Project in Northern Canada is aimed at characterizing the geochemical (Smith et al., 2013a; Bailey et al., 2013), hydrological (Neuner et al., 2013), thermal (Pham et al., 2013), gas transport (Amos et al., 2009; Chi et al., 2013), and microbial evolution (Bailey et al., 2015) of waste rock at the Diavik Diamond Mine. Located approximately 300 km NE of Yellowknife, NT (Figure 3.1), Diavik is in a semi-arid area with continuous permafrost. The mean annual air temperature at the mine site is -9ºC, a maximum of 18ºC is reached in July and a minimum of -31ºC is reached in January/February (Environment Canada, 2012). The climate results in freeze-thaw dynamics which introduce complexity to the characterization of the waste rock behaviour.

Figure 3.1. Location of Diavik Diamond Mine, NWT, Canada.

At Diavik, waste rock is segregated by sulphur content into three categories: Type I <0.04 wt.%, Type II 0.04-0.08 wt.%, and Type III >0.08 wt.%. Type I is considered to be non-acid generating, Type II is considered to have uncertain acid generating potential, and Type III is considered to be potentially acid generating due to low neutralization potential. Three 14 m tall instrumented experimental waste rock test piles were constructed in 2004-2006 using these materials: a Type I, a Type III, and covered pile (Smith et al. 2013b). This focus of this paper is on the Type III test pile.

The crests of the uncovered Diavik test piles occupy 45% of the infiltration surface, the remaining area is composed of batter regions having slopes at the angle of repose. Wind redistribution of snow removes snow from the crest of the test piles, where it accumulates on the

batters (Krentz, 2014; Figure 3.2). During the deconstruction of the Type I test pile, it was found that snowmelt infiltration comprised a significant component of basal drainage and contributed to the formation of continuous ice lenses in batter regions (Chapter 2). These findings highlight the requirement for snowmelt infiltration estimates to better characterize the significance of snowmelt to the water budget of the waste rock pile. Quantifying batter infiltration, interpretation of solute loads released from the test piles (Sinclair et al., 2015), and assessment of possible ice formation have remained significant unknowns in the hydrologic characterization of the Diavik test piles. Recharge estimates on the batters of a northern latitude waste rock pile influenced by wind redistribution of snow have not been investigated to the present day. These estimates are required to develop a conceptual model of hydrologic and geochemical processes occurring within a waste rock pile at the field scale and possibly full scale.

Figure 3.2. Photo showing the distribution of snow on the Type I test pile, March 16, 2008. Snow has mostly been removed from the crest and has accumulated on the batters (West batter shown). From: Neuner, 2009.

Stable isotopes (δD and δ^{18}O) are an important tool to study the water cycle, providing insight to groundwater recharge, runoff, evaporation, and mixing (Clark and Fritz, 1997). The application of δD and δ^{18}O analysis to the field of waste rock hydrology has been limited (examples: Sracek et al., 2004; Barbour et al., 2016). Concentrations of these isotopes in precipitation are largely temperature dependent, resulting in distinctive signatures in rainfall and snow. In this paper, stable isotope analysis is used to estimate the proportions of snowmelt and rainwater in the drainage water from the Type III test pile using a nine-year dataset. Infiltration estimates and outflow measurements are used to evaluate water storage in the test pile, possibly indicating the formation of ice. This study provides an improved understanding of snowmelt recharge to the batters and the significance of snowmelt to the overall flow system in the waste rock pile.

3.2 Methodology

3.2.1 Experimental facility

The construction and instrumentation of the Type III experimental waste rock test pile is summarized in detail by Smith et al. (2013b) and Neuner et al. (2013). To summarize, construction and instrumentation occurred from 2004-2006 using standard mining equipment. Waste rock was end-dumped from a ramp onto the 50 x 60 m base of the test pile. The pile is 14 m tall with batters on three sides at the angle of repose (38^{o}). The base of the test pile was graded (0.5-2%) away from the centre line towards the North and South halves of the pile and lined with an impermeable HDPE geomembrane in order to direct basal flow towards the drains for collection. The basal drainage system collects water from the north half of the pile using the North drain and from the South half using the South drain. The drains direct flow into instrumentation huts where geochemical sampling occurs approximately every three days during

times of discharge and flow is continuously monitored using custom made tipping buckets. At the time of construction, the liner and basal drains were covered with 0.4 m of Type I 1.25 inch clean crush to prevent damage during test pile construction. Three clusters of two 2 x 2 m and two 4 x 4 m basal collection lysimeters (BCLs) were constructed on top of the crush layer. Flow obtained from lysimeters is directed towards the instrumentation trailer for geochemical sampling and flow monitoring using Young Model 2202 tipping buckets (rain gauges). Self-regulated heating cable was placed in the base of the BCLs as well as in the basal drain and BCL drain lines to prevent temperatures in the drains from falling below 5ºC. Instrumentation to monitor the geochemical, hydrological, microbiological, gas transport, and thermal behaviour internal to the pile were installed across four tip faces as waste rock was dumped from a ramp towards the pad of the test pile. Thermal behaviour is monitored using multiple thermistor strings, each with 12 beads. Two strings were offset 5 m from the centre of the pile, extending 12 m below surface. Additionally, strings were located along the North and South batters, beginning at 5 m from the centre of the pile, extending approximately 12 m below surface (Pham et al., 2013). The general layout of the test pile is shown in Figure 3.3 and a schematic to the BCLs is shown in Figure 3.4. The crest of the test pile occupies a surface area of approximately 1350 m^2, while the batters have an infiltration surface of approximately 1650 m^2 across a horizontal plane.

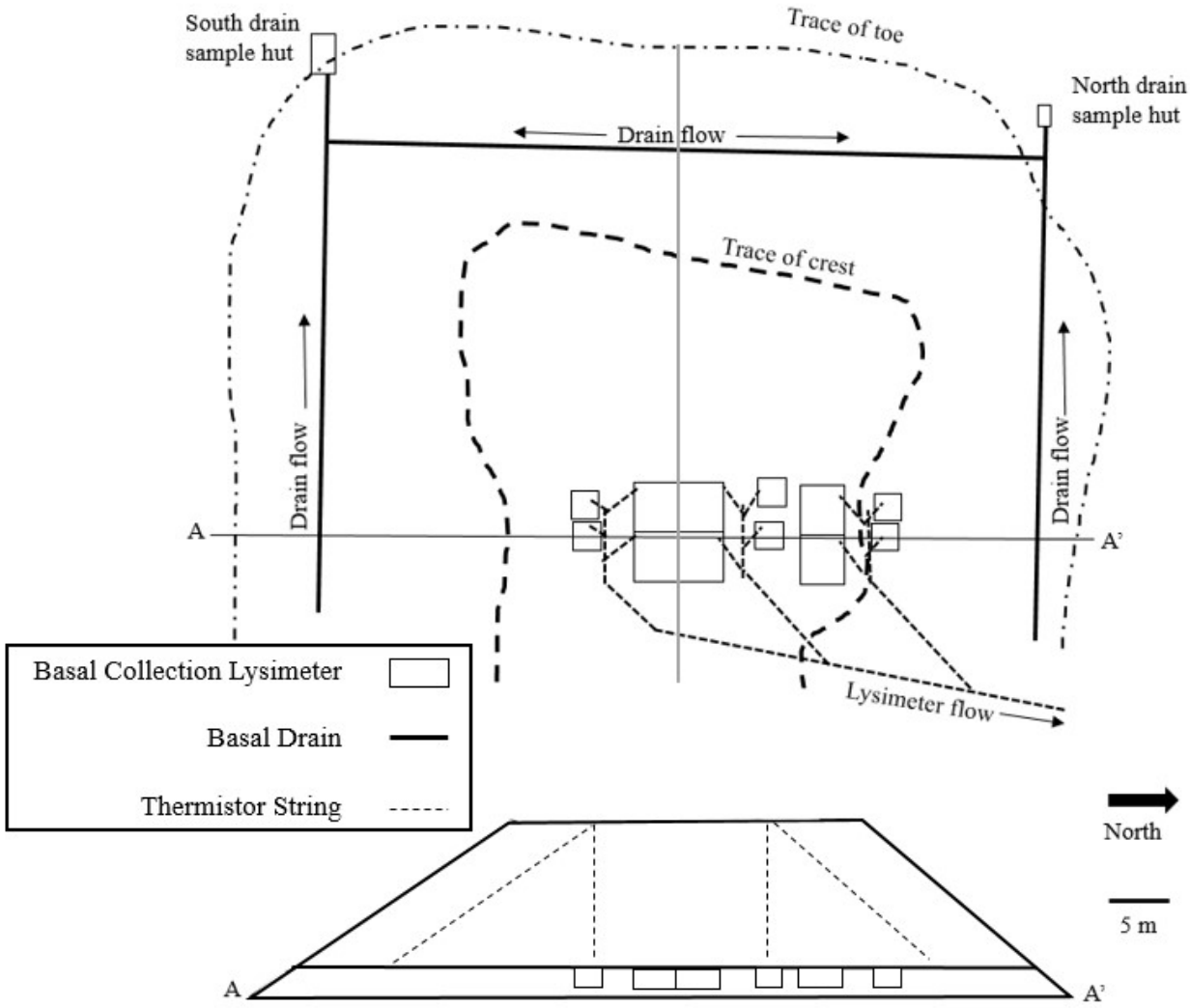

Figure 3.3. Schematic of the Type III test pile, showing basal collection lysimeters and basal drains (modified from Sinclair et al., 2015).

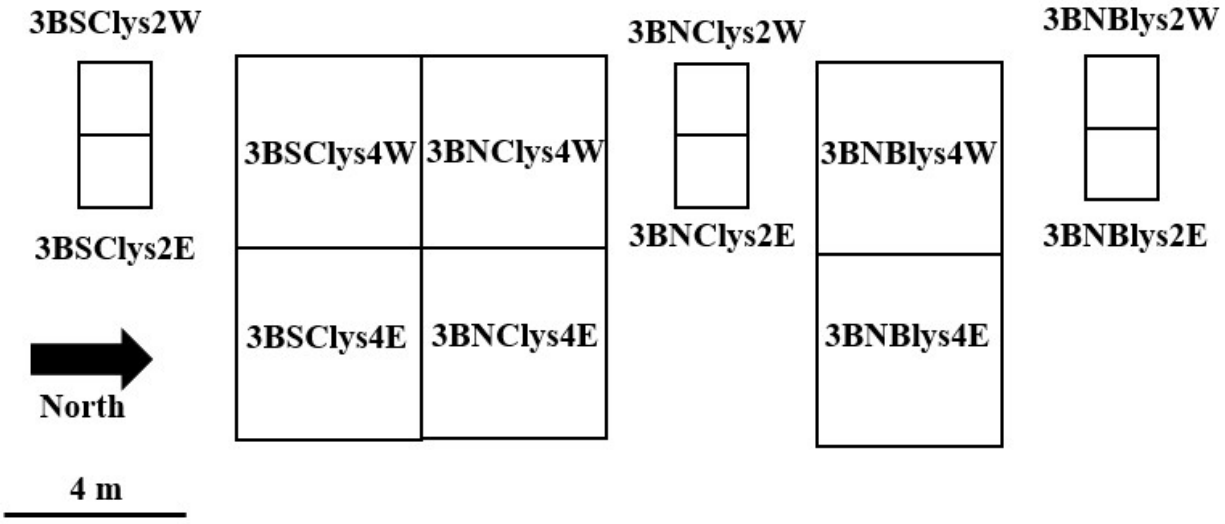

Figure 3.4. Layout and naming of BCLs in the Type III test pile.

3.2.2 Precipitation sampling

Precipitation samples were collected from 19 L plastic buckets that were cleaned using deionized water before a forecasted precipitation event. Water samples were collected from the buckets the day after select rain and snowfall events using a syringe, then distributed into collection bottles. Samples were stored in HDPE bottles without headspace and kept refrigerated until analysis was completed. Following collection, precipitation samples were analyzed for pH, Eh and EC on site. δD and δ^{18}O measurements were completed at the University of Waterloo using a PICARRO L2130-i analyzer.

3.2.3 Background for stable isotope analysis

δD and δ^{18}O concentrations are given in terms of their deviation from the Vienna Standard Mean Ocean Water (VSMOW). Seasonal variation of isotopic concentrations results largely from periods of wetter vs. drier and colder vs. warmer weather (Clark and Fritz, 1997; Barbour et al.,

2016). Compared to snowfall, rain is enriched with δD and $\delta^{18}O$, this helps to describe if a water sample originated from snowmelt, rainfall, or a mixture of the two.

The formation of a regression line from δD and $\delta^{18}O$ concentrations serves as a tool to broadly describe processes that may occur in the hydrologic system of interest such as evaporation, condensation, and mixing. When this regression is created using isotopes obtained from precipitation, it is referred to as the Local Meteoric Water Line (LMWL). At the global scale, precipitation data forms a regression with a slope of 8 and is known as the Global Meteoric Water Line (GMWL; Craig, 1961). Arid regions such a Diavik typically have a LMWL with a slope of less than 8 due to evaporation occurring as the rain falls through a dry air column, this is referred to as the amount effect (Friedman et al., 1962). Allison (1982) described the influence of evaporation on δD and $\delta^{18}O$ concentrations of waters in a porous material, finding the regressions to have a slopes near 2.4-4.7. The regression formed by waters affected by evaporation is known as the Local Evaporation Line (LEL).

Deuterium excess (d-excess) provides a measure of the relative proportions of δD and $\delta^{18}O$ (equation 3.1). Using *Figure 3.5*, d-excess can be visualized as an index of deviation from the GMWL (GMWL d-excess= 10‰). D-excess values are the reflection of the physical conditions of the oceanic source area of an air mass (humidity, air temperature, and sea surface temperature) rather than δD and $\delta^{18}O$ concentrations which are largely correlated with the conditions of the site where precipitation occurs. This means that once an air mass has formed, d-excess becomes essentially a fixed value (Harvey, 2001).

$$Deuterium\ excess = \delta D - 8.0\ x\ \delta^{18}O \qquad (3.1)$$

Alteration of d-excess may result from partial evaporation of rain falling through a dry air column or evaporation occurring while in a rain gauge prior to collection resulting in low or negative d-excess in precipitation. An increase of d-excess in water may result from the addition of moisture during the transport of the air mass (Harvey, 2001; Froehlich et al., 2002). Evaporation or addition of moisture in a meteoric water sample is not desired since it alters the concentrations of δD and $\delta^{18}O$; with context to this paper, skewed δD and $\delta^{18}O$ concentrations may lead to a poorly constructed LMWL and the misrepresent the proportions of rainwater and snowmelt in drainage. Various investigations have found it useful verify the quality of δD and $\delta^{18}O$ concentrations measured in meteoric waters by calculating d-excess and eliminating low quality samples (Gammons et al., 2006; Welker, 2000; Harvey 2001, 2005; Harvey and Welker 2000). This paper adopts the acceptable d-excess limits of 3-15‰ for the construction of the LMWL, derived from the moisture exchange model presented in Merlivat and Jouzel (1979).

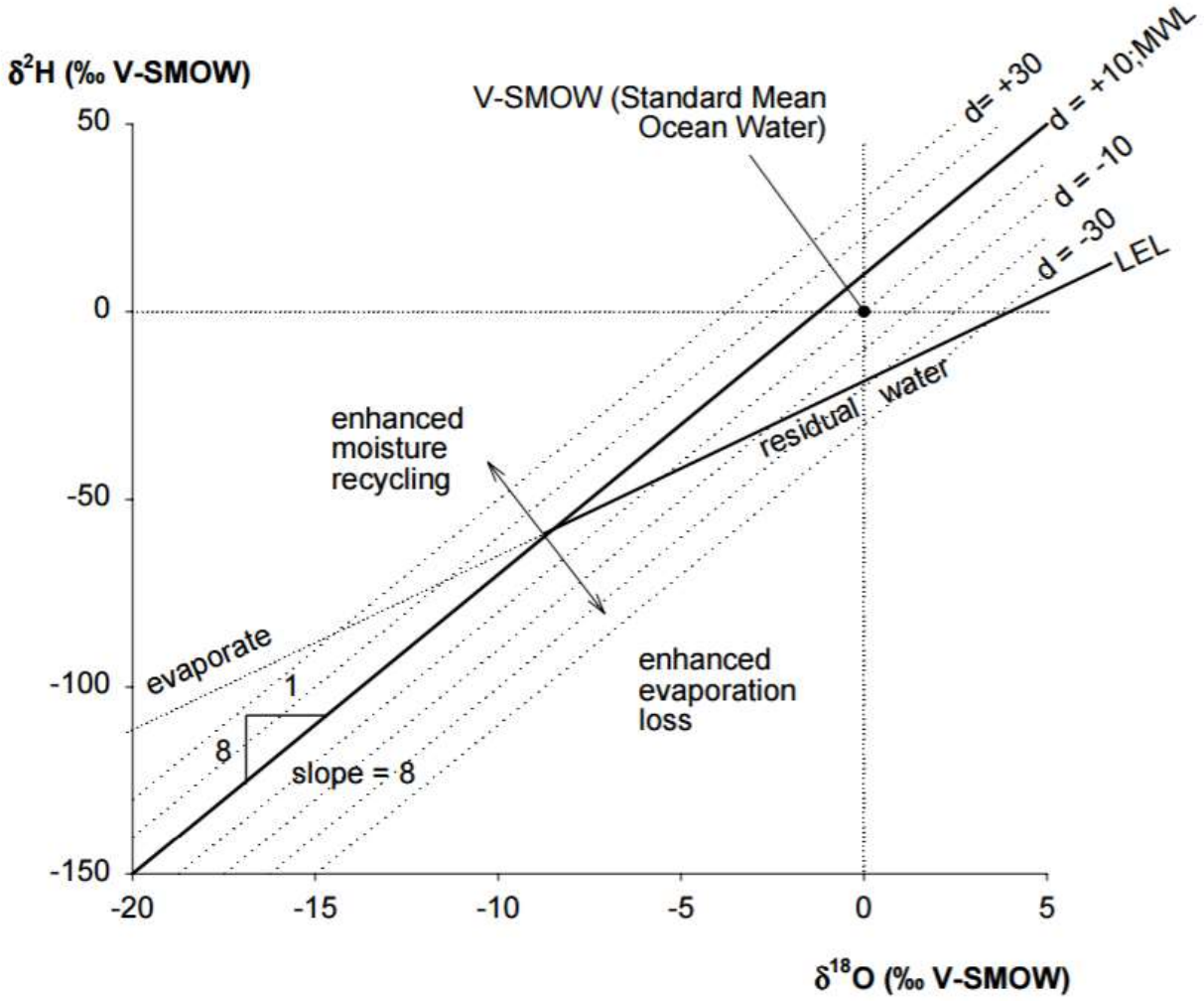

Figure 3.5. Diagram showing the global meteoric water line (MWL slope= 8, d-excess= 10‰), local evaporation line (LEL slope<8), ocean water (SMOW), and relative changes of d-excess (d). Obtained from Froehlich et al. (2002).

3.3 Results

3.3.1 Precipitation

Figure 3.6A shows the record of annual rainfall at Diavik over the duration of the test piles study, the average being 103 mm, with the last four years being approximately 78 mm cumulatively below average. Measurements from a snow gauge located approximately 500 m from the test piles site operated by the Diavik Environment Department are shown in Figure

3.6B. These data indicate an average annual snowfall of 158 mm water equivalent from 2007-2015; note that annual totals reflect snowfall over the winter season, approximately October-April. Approximately 60% of the total precipitation at Diavik occurred as snow during the period of measurement.

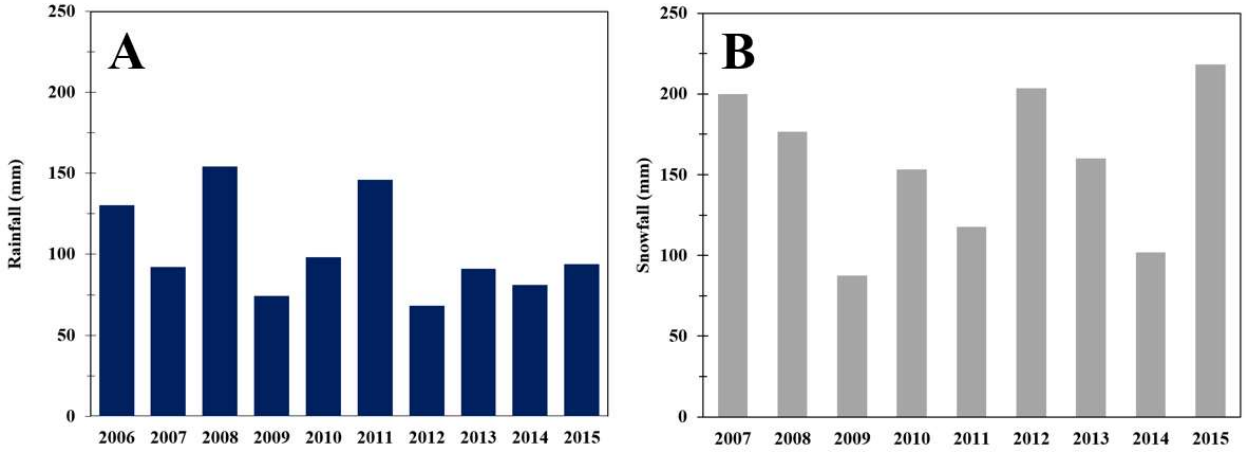

Figure 3.6. Measurements of A) annual rainfall and B) snowfall at Diavik Diamond Mine.

3.3.1.1 Isotopic characterization of precipitation

δD and δ^{18}O were measured in 34 samples of precipitation, mostly collected over 2014-2015. Mean summer and winter temperatures at Diavik range over approximately 49°C, this large difference in temperature causes the observed range of δD to be large, about 132.0‰ (-92.3‰ to -224.3‰) as shown in Figure 3.7A. The distribution of d-excess in precipitation at Diavik is shown in Figure 3.7B. It can be seen that snow typically has a larger d-excess than rain. Chauvenet's Criterion (Taylor, 1997) was used to identify outlier δD and δ^{18}O concentrations within the rain and snowfall precipitation datasets as well as d-excess, however, none were identified.

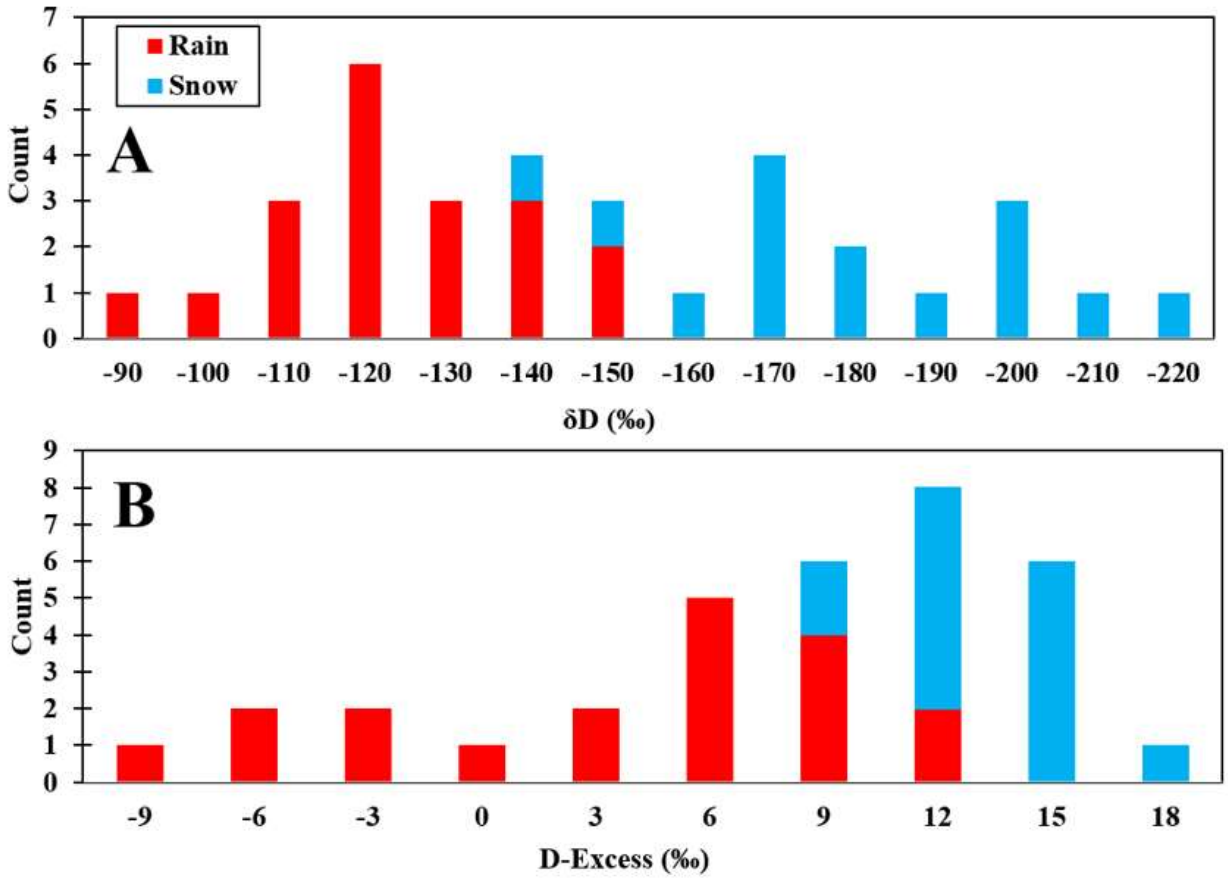

Figure 3.7. Distribution of A) δD measured in rain and snow samples and B) deuterium excess calculated from precipitation samples collected from Diavik.

For the development of the LMWL, the dataset was limited to samples where d-excess was 3‰ to 15‰ in order to maintain integrity of the analysis. This removed nine samples which had potentially been exposed to evaporation during the rainfall event, partially evaporated while in the collection bucket, or had a secondary input of water. The LMWL was found to be $\delta D = 7.5 \times \delta^{18}O - 2.4‰$, shown in Figure 3.8, reference lines indicating d-excess values of 3‰ and 15‰ are shown (slope= 8). Mean δD and $\delta^{18}O$ for rain were found to be -134.6‰ and -17.7‰ for rain, and -183.8‰ and -24.4‰ for snow, respectively, the standard error of the means are indicated by error bars on the figure.

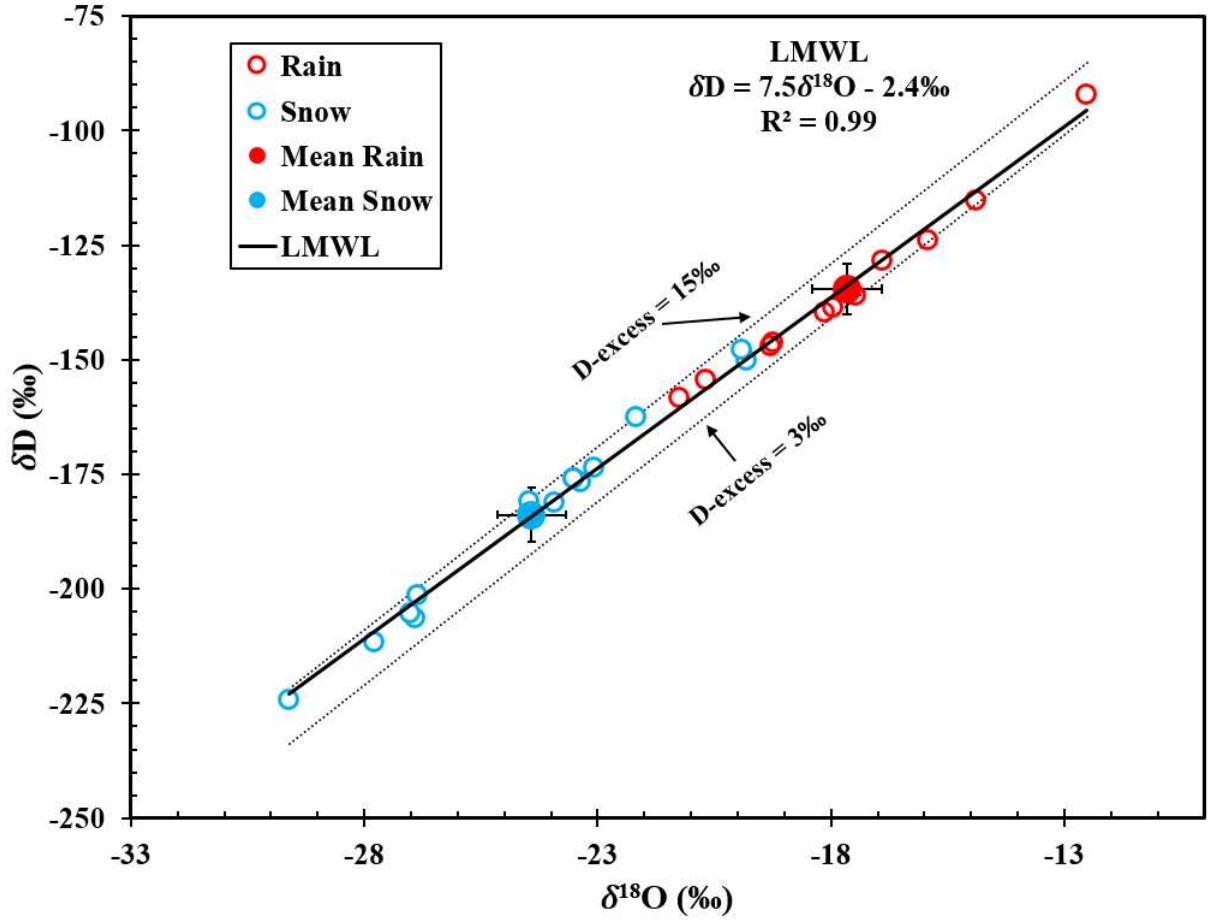

Figure 3.8 . δD and δ^{18}O of rain and snow at Diavik Diamond Mine, NWT, Canada. Error bars reflect the standard error of the mean. Reference lines indicating d-excess= 3‰ and 15‰ (slope= 8) are shown.

3.3.2 Waste rock drainage

3.3.2.1 δD and δ^{18}O concentrations

Concentrations of δD and δ^{18}O measured in the North and South outflows of the Type III waste rock test pile are shown below in Figure 3.9. Regressions for the outflow from the North and South drains yielded δD= 7.5 x δ^{18}O – 3.3‰ and δD= 7.2 x δ^{18}O – 10.3‰, respectively; recall the LMWL, δD= 7.5 x δ^{18}O – 2.4‰. It can be seen that δD and δ^{18}O concentrations from the North drain plot near the LMWL, while samples from the South drain are slightly below.

Statistical regression analysis determined that the slopes and intercepts of the following comparisons were significantly different: South Drain vs. LMWL and the North Drain vs. South Drain. In the case of North drain vs. LMWL, slopes and intercepts were statistically similar to each other. This suggests a slight influence of evaporation on the South side of the pile which does not affect the North side. Despite the statistical dissimilarity of the South drain to the LMWL and North drain, this deviation should be interpreted as relatively minor. As previously mentioned, the influence of evaporation on a δD and δ^{18}O regression generally results in a slope near 2.4-4.7 (Allison, 1982), while these data resulted in a slope of 7.2.

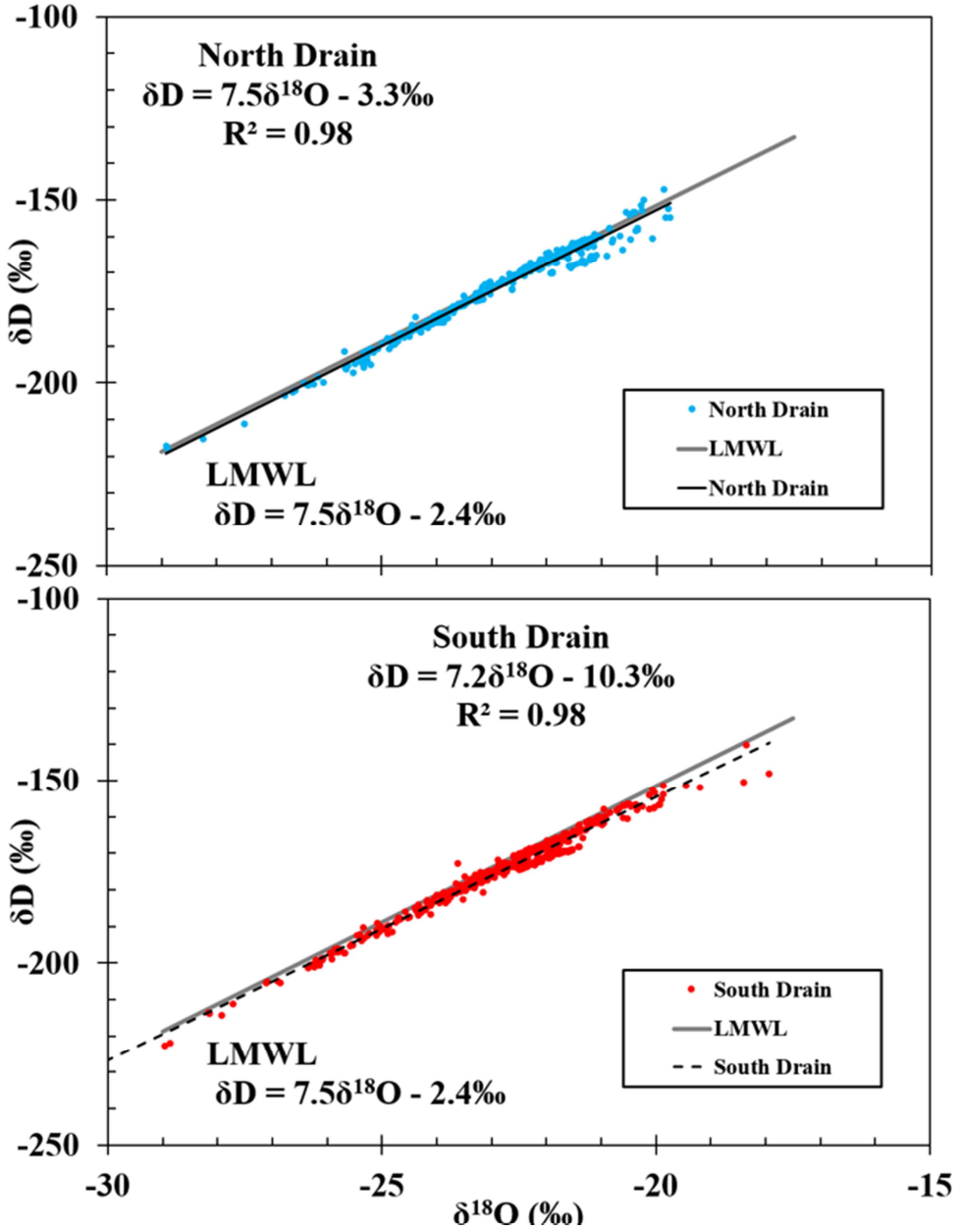

Figure 3.9. Concentrations of δD and $\delta^{18}O$ measured from the North and South Drains of the Type III waste rock test pile compared to the LMWL at Diavik Diamond Mine.

The seasonality of δD and $\delta^{18}O$ in the North and South drains is shown in Figure 3.10. In general, discharge began each season as primarily snowmelt, contributions to drainage from water with a rain source increased as the pile thawed. In the fall, freeze-up occurs from the

batters and base inwards and discharge from the drains to ceases once frozen (Pham, 2013a). As a general statement, it is interesting that δD and δ^{18}O concentrations at the time of freeze-up are dissimilar to those during the commencement of flow the following year. Freezing results in the immobilization of a water located in matrix material (matrix flow is considered dominant, Fretz, 2013), preserving the isotopic signature of the pore water at the time of freezing, shown here to contain rain and snowmelt components in the late fall. Once discharge commences in the early summer, drainage does not contain a significant rainwater component, but rather is dominantly snowmelt. This suggests that initial fluid flow in response to snowmelt through the batters does not occur through as matrix (capillary) flow at this time, but rather as noncapillary flow around matrix material. The high amount of recharge through the batters caused by snowmelt is able to migrate through larger pore spaces, effectively bypassing resident pore waters held in matrix material. Sinclair et al. (2015) outlined these effects on the geochemical evolution of the outflow. The initial flush driven by snowmelt is characterized by circumneutral pH and low solute concentrations as a result of decreased fluid residence time and limited contact with reactive matrix (Wagner et al., 2006). Following the annual flush of snowmelt, solute concentrations increased slightly while flow decreased, this was interpreted at the transition from noncapillary to matrix flow within the test pile batter.

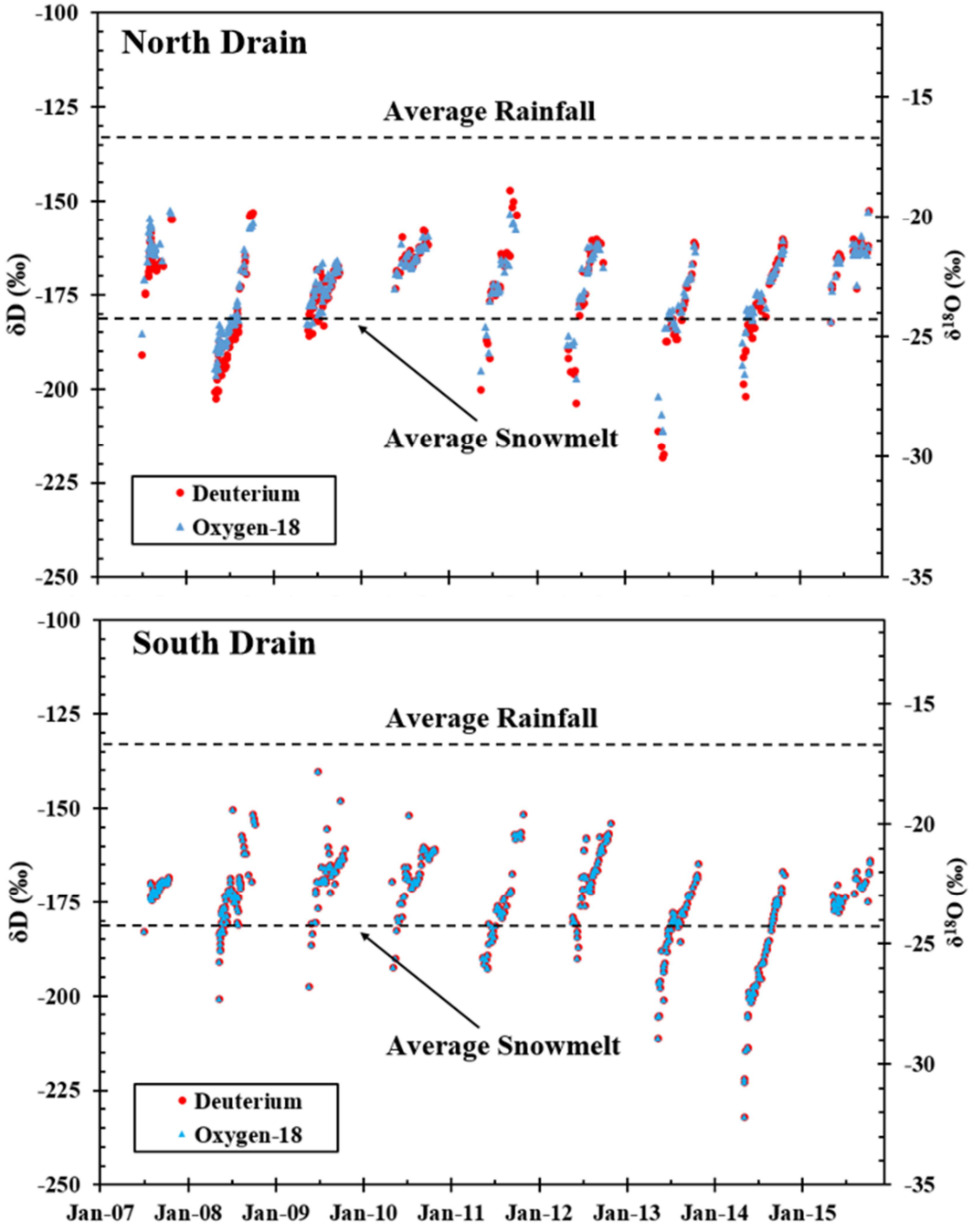

Figure 3.10. δD and $\delta^{18}O$ concentrations from the North and South drains of the Type III test pile.

3.3.2.2 Deuterium excess

D-excess in drainage from the North and South drains is shown in Figure 3.11. Compared the analysis of δD and δ^{18}O regressions, d-excess provides a better sense of the influence of processes such as evaporation and freeze-thaw on drainage. In general, d-excess values ranged from about 7‰ to 11‰, similar to measurements in precipitation. The South drain generally exhibited lower d-excess than the North drain, implying outflow from the South drain experiences a greater amount of evaporation than outflow from the North drain. This observation is consistent with the analysis of the North and South drainage regressions (Figure 3.9). Most years, the drains exhibited an annual pattern of declining d-excess over time, reflecting the shift from snowmelt dominated discharge towards an increasing rain composition over time (recall d-excess values for rain and snow shown in Figure 3.7B). The North drain in 2014 and the South drain in 2015 displayed increasing d-excess over the flow season, an interpretation of this trend is provided in the discussion section. Low d-excess was observed from both drains in 2007, implying a dominant rainwater component in the outflow, contradictory to Figure 3.10, however, this is believed to be the result of lake water used for the application of tracer tests (Neuner, 2009).

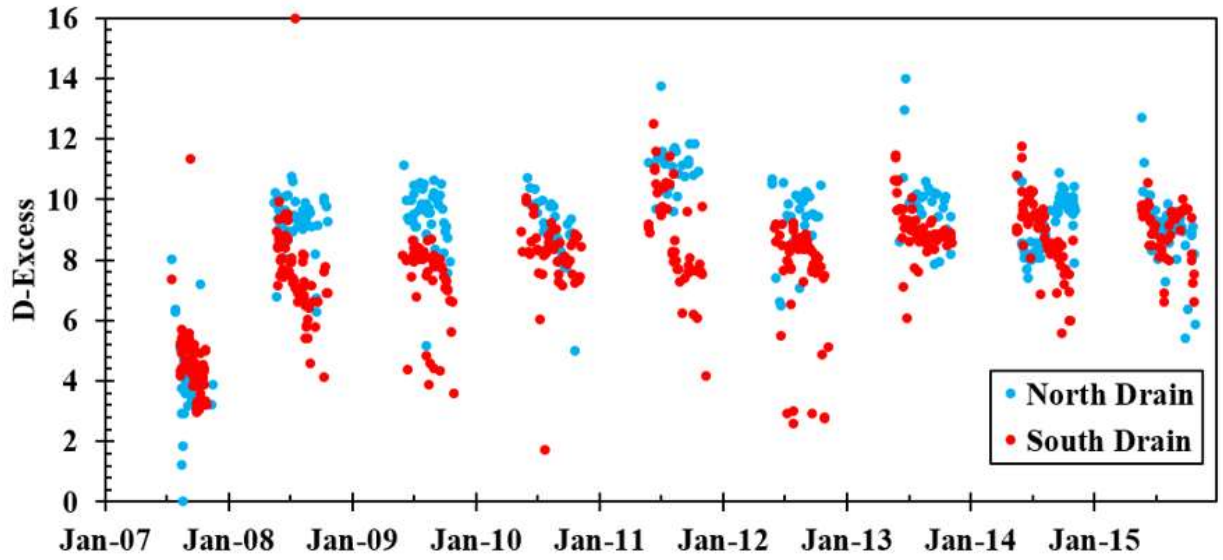

Figure 3.11. D-excess calculated from drainage from the North and South drains of the Type III test pile.

3.3.2.3 Rain and snowmelt outflow

3.3.2.3.1 North and South drains

Daily outflow volumes from the North and South drains are shown in Figure 3.12 and Figure 3.13. In general, greater volumes were observed from the South than the North, on average, 75% of annual outflow was from the South. However, years 2014-2015 show an increase in flow occurring from the North. Given the drains were designed collect water from proportionally equal areas, this disparity in flow volumes is of interest.

δD and δ^{18}O data presented in Figure 3.10 were used to estimate the proportions of snowmelt and rainwater in drainage from the test pile for each sample. These proportions were linearly interpolated between sampling events then used to determine the respective volumes of rainwater and snowmelt in drainage using the recorded volumetric discharge. This was completed using an

isotopic mass balance shown in equation 3.2– where δsnow represents the respective mean of δD or δ^{18}O value for snow measured at Diavik, δrain is the mean value for rainfall measured, δsample is the value measured in drainage, and Q is the volumetric discharge from the drain on the day of sample collection. These calculations assume evaporation and freeze-thaw have had a negligible influence on the concentrations of δD and δ^{18}O in drainage. These assumptions are justifiable given the North and South drainage regressions only deviate marginally from the LMWL (Figure 3.9).

$$Volume\ Rainwater = \frac{\left[\frac{\left(\delta \mathrm{D}_{\mathrm{snow}} - \delta \mathrm{D}_{\mathrm{sample}}\right)}{\left(\delta \mathrm{D}_{\mathrm{snow}} - \delta \mathrm{D}_{\mathrm{rain}}\right)} + \frac{\left(\delta^{18}\mathrm{O}_{\mathrm{snow}} - \delta^{18}\mathrm{O}_{\mathrm{sample}}\right)}{\left(\delta^{18}\mathrm{O}_{\mathrm{snow}} - \delta^{18}\mathrm{O}_{\mathrm{rain}}\right)}\right]}{2} * \ Q \qquad (3.2)$$

As expected from δD and δ^{18}O concentrations, outflow from the North and South drains was dominated by water originating as snowmelt, shown in Figure 3.12 and Figure 3.13, cumulative rainfall and snowmelt outflow volumes are indicated in text on the figures. Over the nine years of measurement, the mean annual rainwater outflow from the North and South drains was 14 m^3 and 34 m^3, respectively, mean snowmelt outflow was 29 m^3 and 98 m^3, respectively. Snowmelt discharge was approximately 71% of the total discharge from the North drain and approximately 77% from the South drain. These measurements indicate the total proportion of snowmelt outflow relative to the total outflow from the two drains was approximately equal.

In general, outflow from the test pile can be characterized by a brief pulse of snowmelt drainage in May followed by a period of decreased discharge. As the thawing front migrates further into the pile, larger sections are able to contribute to outflow resulting in increased volumetric discharge which becomes more rainfall like over time. Peak outflow is typically observed in September-October when the active zone of the test pile reaches its maximum, during which, contributions of rainwater to drainage were found to be the greatest, however, outflow is still

dominated by snowmelt. Peak outflow was followed by decreasing volumetric discharge as freeze-up proceeded.

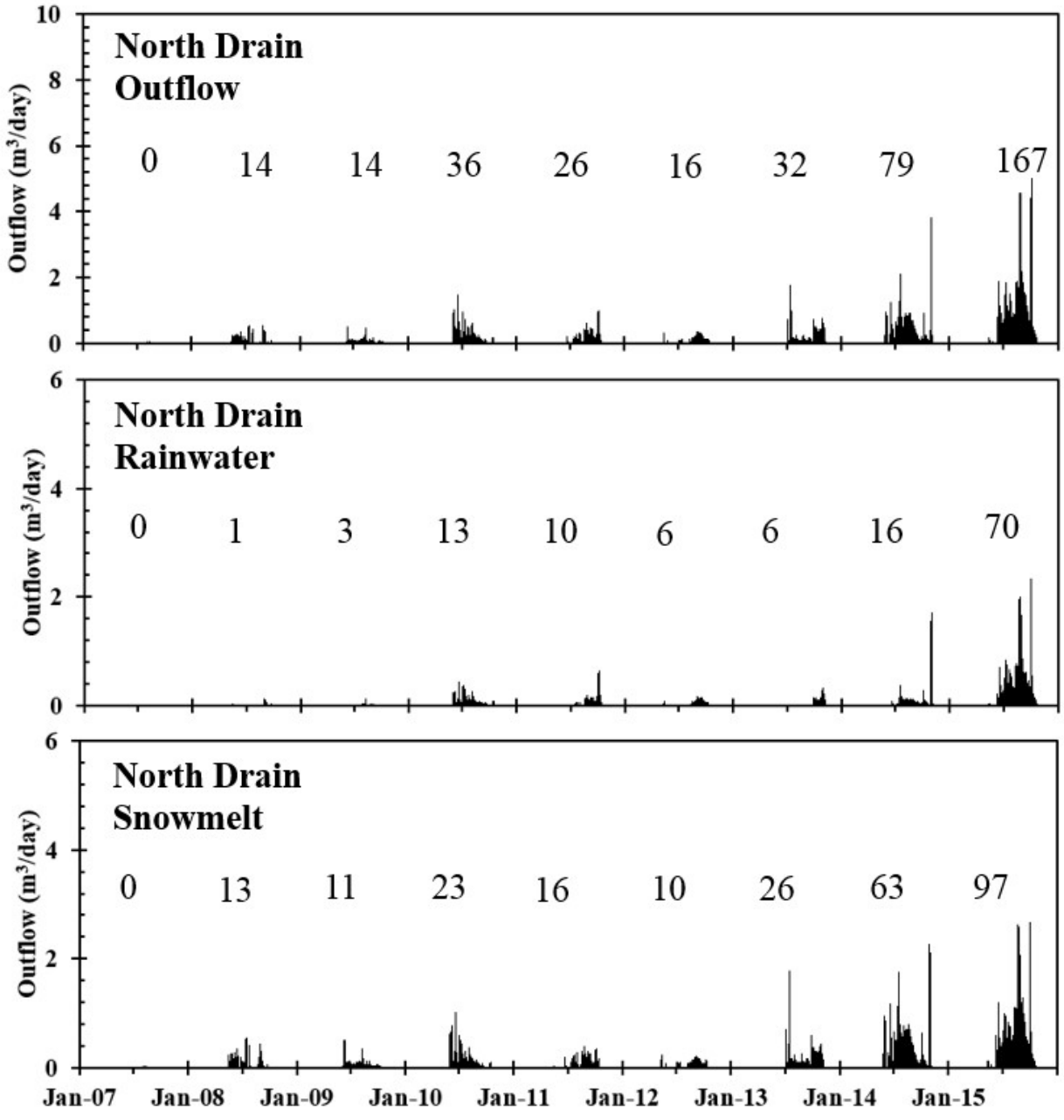

Figure 3.12. Daily outflow volumes measured from the North drain of the Type III test pile and calculated volumes of rainwater and snowmelt in drainage. Cumulative rainwater/snowmelt drainage volumes (m^3) are indicated by text.

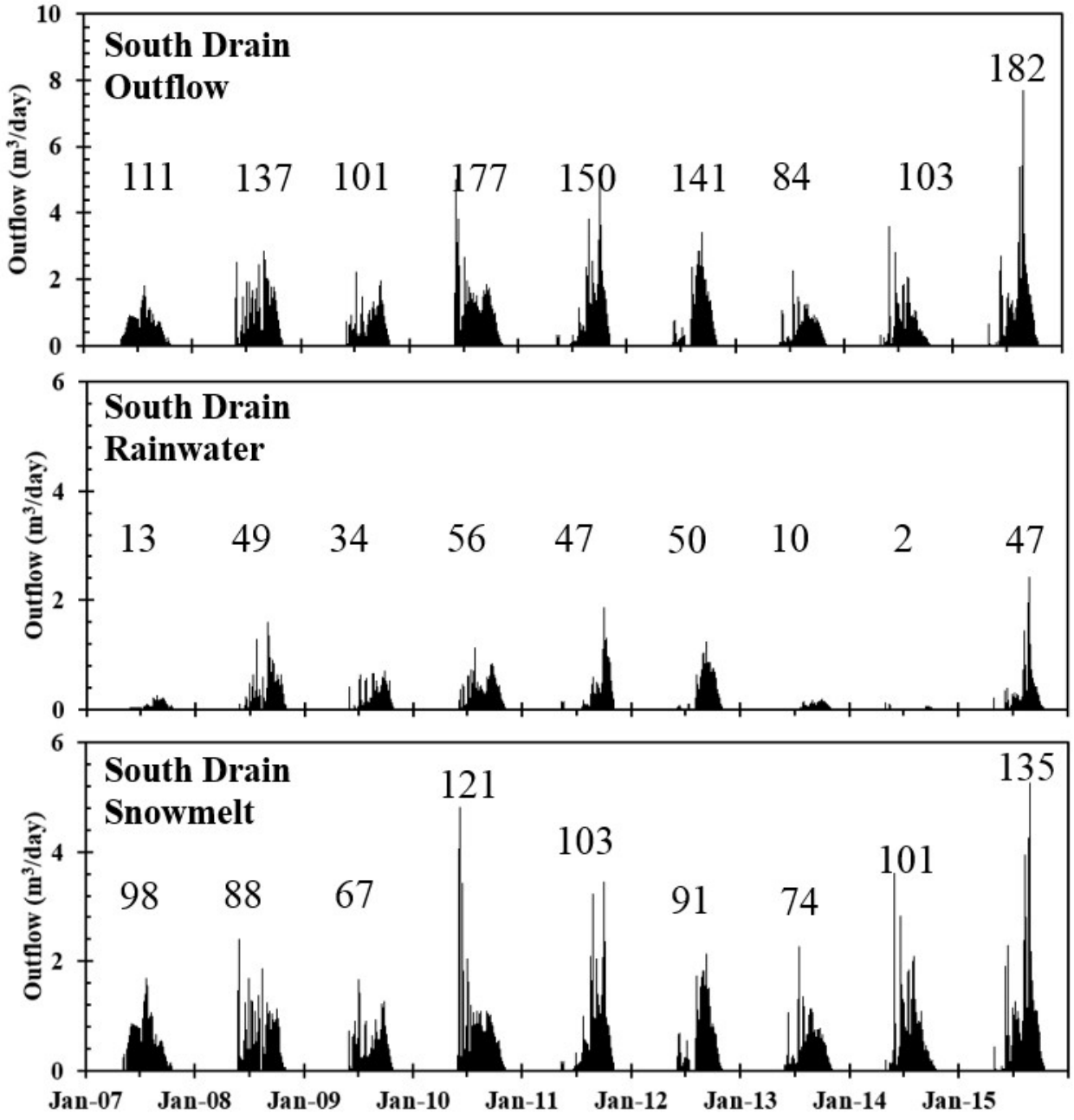

Figure 3.13. Daily outflow volumes measured from the South drain of the Type III test pile and calculated volumes of rainwater and snowmelt in drainage. Cumulative rainwater/snowmelt drainage volumes (m^3) are indicated by text.

Figure 3.14 compares total annual outflow of rainwater and snowmelt from the North drain normalized to the annual outflow of rainwater and snowmelt from the South drain. It can be seen the volumetric discharge of neither rainwater nor snowmelt from the test pile have been proportional between the two drains. Most years, the North drain contributed less rainwater to total outflow (indicated by values < 1), however in 2014 approximately 7.5 times more rainwater was discharged from the North than the South followed by near-equal volumes in 2015. Proportions of snowmelt discharge from the two drains show similar behaviour as rainwater outflow, however slightly less pronounced. The South drain contributed the majority of the snowmelt to total outflow. In recent years, the proportions approached near-equal amounts. The observed recent transition in rainwater/snowmelt discharge proportions may indicate a change in the overall hydrologic behaviour of the test pile resulting in increased flow to the North drain.

Direct measurements of snowpack on the batters of the test pile were unable to be completed due to mine safety regulations; however, Figure 3.15 provides a sense of the snow distribution between the North and South batters in the Spring, prior to snowmelt. It can been seen that the South batter accumulates more snow than the North, a consequence of wind redistribution. Therefore, dissimilar volumes of snowmelt outflow from the North and South drains are expected to some extent. The large difference in rainwater outflow from the drains is difficult to reconcile, interpretations of this are given in the discussion section.

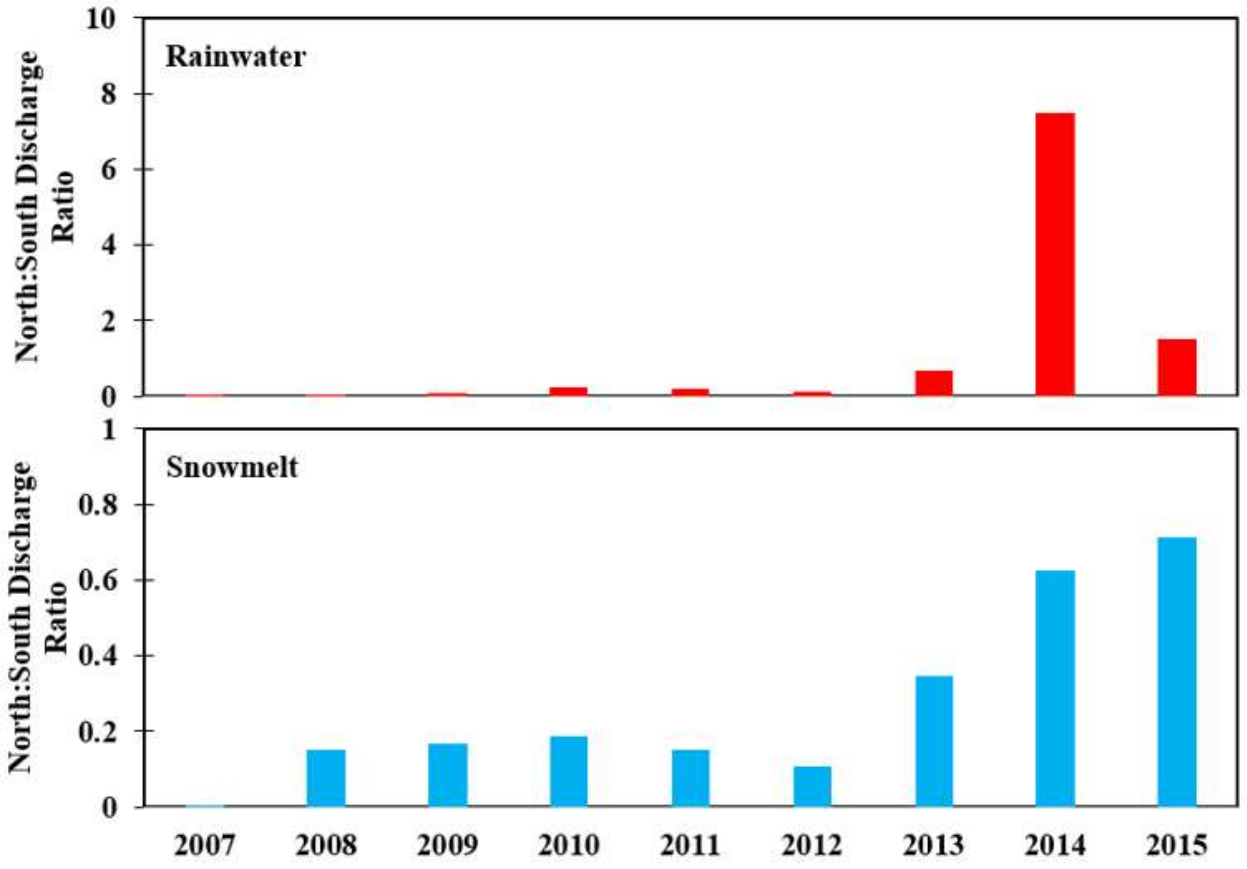

Figure 3.14. Annual ratios of rainwater and snowmelt outflow from the North-South drains.

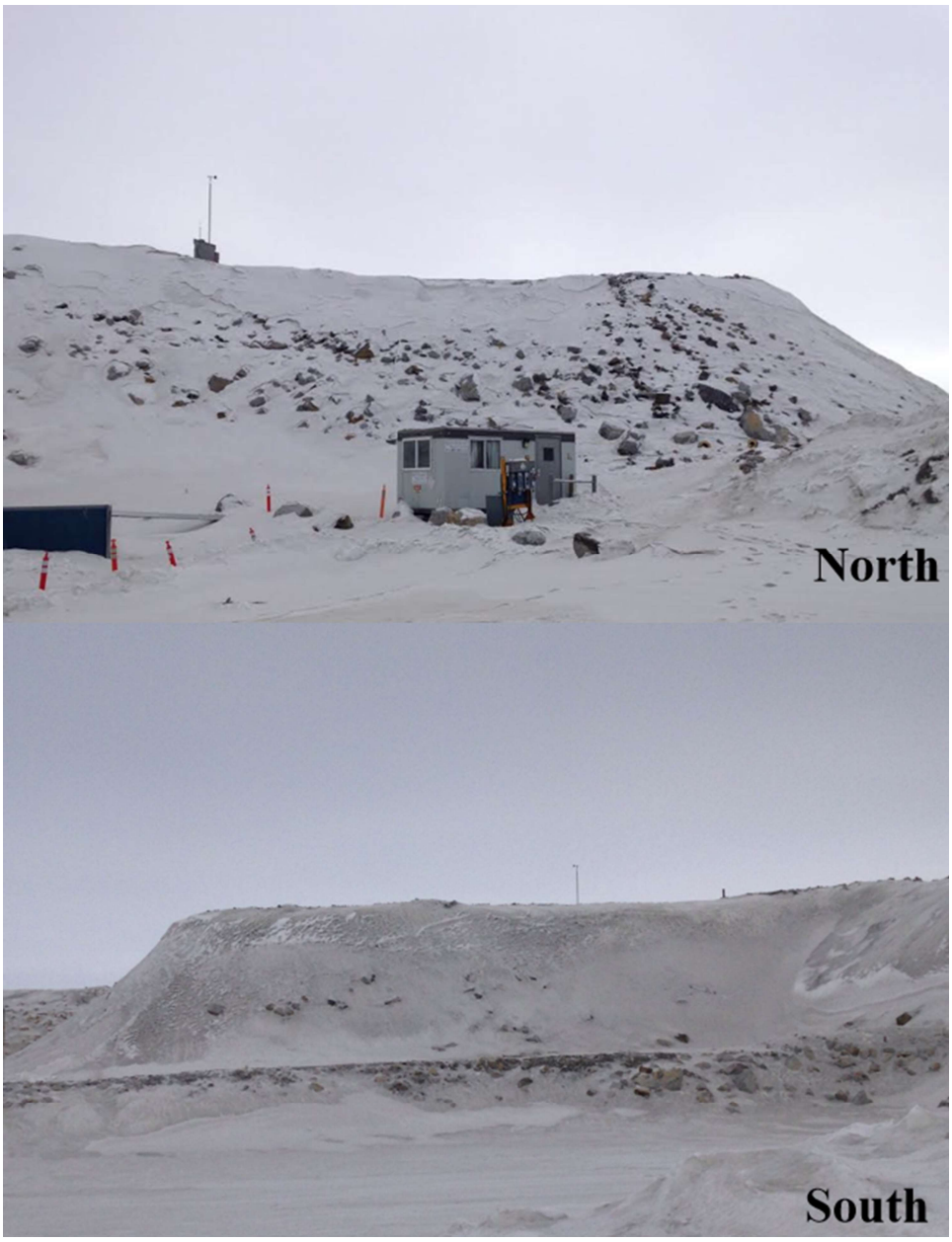

Figure 3.15. Snow distribution on the North and South Batters of the Type III test pile- photos were taken April, 2016.

3.3.2.3.2 Whole pile

Cumulative annual discharge of rainwater and snowmelt from the test pile are shown in Figure 3.16 (North and South drain combined). It is clear that snowmelt dominates outflow from the

test pile. Over nine years of monitoring, approximately 74% of the annual discharge from the test pile was snowmelt, the standard deviation of this measurement is 10%, suggesting moderate variability from year to year. Since snowmelt only infiltrates through the batters of the test pile and not the core, isotopic characterization of the outflow indicates that the flow regime of the test pile is strongly dominated by flow through the batters. This is important when considering the relative importance of the core and batters to solute concentrations and loading from the test pile. Increased flow through the batters dilutes to mass loading from the base of the pile.

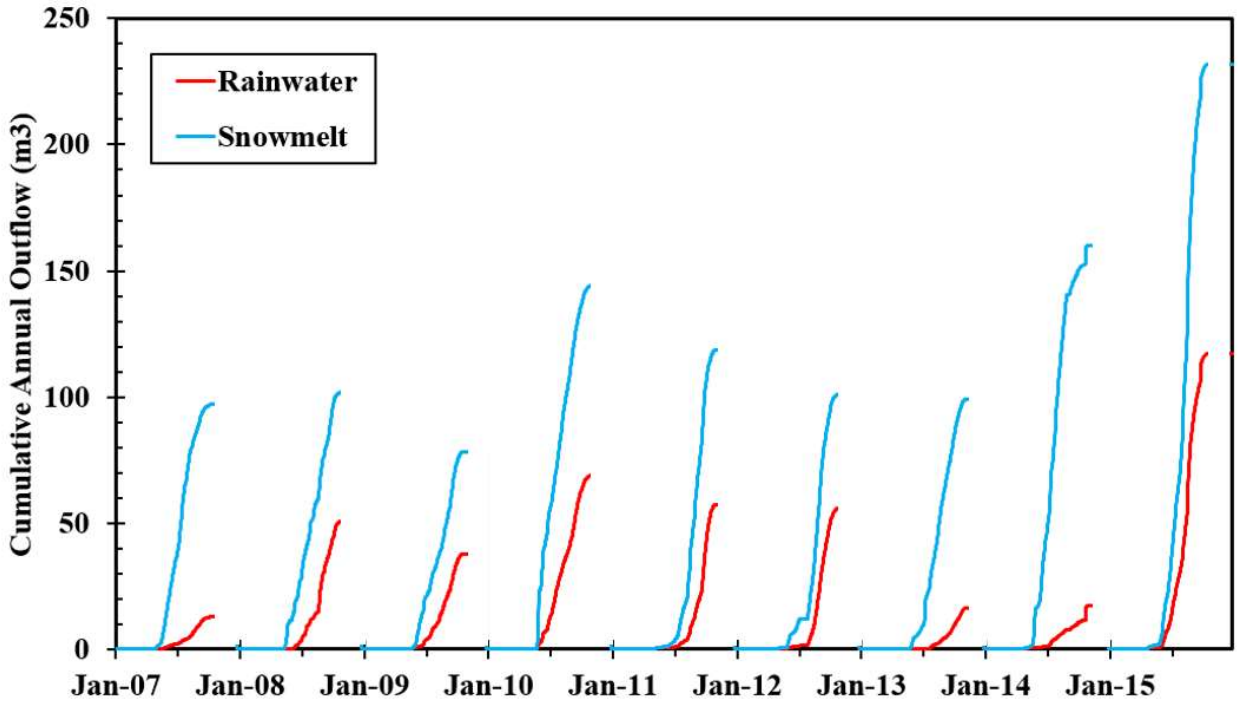

Figure 3.16. Cumulative annual rainwater and snowmelt discharge from the Type III test pile.

3.3.3 Infiltration estimation

3.3.3.1 Snowmelt

The isotopic characterization of outflow from the waste rock pile indicates that the flow system of the test pile was dominated by batter infiltration, specifically by snowmelt. This places importance on quantifying snowmelt infiltration to gain an improved understanding of the water budget for the test pile. To obtain a first order understanding of snowmelt recharge through the test pile batters, it has been assumed that snowmelt recharge occurred only through the batters (Figure 3.2; Krentz, 2014; Chapter 2) and is equal to snowmelt discharge.

Annual volumes of snowmelt discharge from the North and South drains were used to calculate snowmelt recharge to the batters of the test pile which occupy a combined surface area of 1650 m^2. Snowmelt recharge through the North and South drains was estimated to be 35 mm and 118 mm (std. deviations= 36 mm and 24 mm, showing the annual variability), respectively. When considering cumulative snowmelt drainage across the entire footprint of the test pile batters, snowmelt infiltration was found to be 77 mm (std. deviation= 27 mm), approximately 50% of the annual average snowfall.

3.3.3.2 Rainfall

Unlike snowmelt, rainwater outflow from the basal drains contains contributions from the core and batters, making it difficult to determine infiltration specific to the crest or batters. Figure 3.17 shows the combined daily outflow from the BCLs. Annual outflow volumes from individual lysimeters are shown in the units of mm to represent rainfall infiltration rates to the crest of the test pile. Infiltration estimates from lysimeters are summarized in Table 3-1, the dimensions of the lysimeters 2 x 2 m and 4 x 4 m are indicated in the lysimeter naming scheme.

Lysimeters which did not flow or produced less than 50 L in a given year have not been displayed. Note that several outlier values have been excluded from the mean calculations, as indicated in the table. Infiltration estimates from the BCLs have been compared to those determined from a modified Penman Monteith method (PM), which was used by Fretz (2013) to calculate infiltration through a set of 2 m deep lysimeters at Diavik.

Fluxes from lysimeters displayed significant variability relative to one another, ranging up to 1-2 orders of magnitude in a given year in some cases; this observation is consistent with Nichol et al. (2005). This behaviour indicates heterogeneity influencing pore water movement at a scale of greater than 4 m, such as possible boulders or ice formation. Lysimeters 3BNClys2W/2E displayed interesting behaviour; drainage was not observed from these locations over four consecutive years, followed by four consecutive years where excessive drainage was observed, ranging from 166% to 11033% of the FAO-PM estimate for the given year. The majority of BCL outflow occurred from these 2 x 2 m lysimeters, rather than the larger 4 x 4 m lysimeters. Further illustrating the variability, years of increased infiltration did not result in increased fluxes from the basal lysimeters. The cause of these complexities are not fully understood, however it may be a result of material heterogeneity or storage due to matrix wet-up or ice formation.

In general, infiltration estimates derived from individual lysimeters provide a poor representation of infiltration. However, when considering cumulative annual outflow from the all BCLs and discounting outlier lysimeters 3BNClys2W/2E, the result is comparable to those obtained from PM. Cumulative annual outflow from the BCLs ranged from 34% to 204% of the PM estimated infiltration value. Over the period of measurement, these data yield a mean rainfall infiltration of 33 mm to the crest, compared to 46 mm estimated by PM. However, given the transient nature of flow from the BCLs and small sample size, it is difficult to assess with certainty the similarity

between BCL outflow and infiltration estimations; therefore PM calculations are favoured for estimating rainfall infiltration though the crest of the test pile.

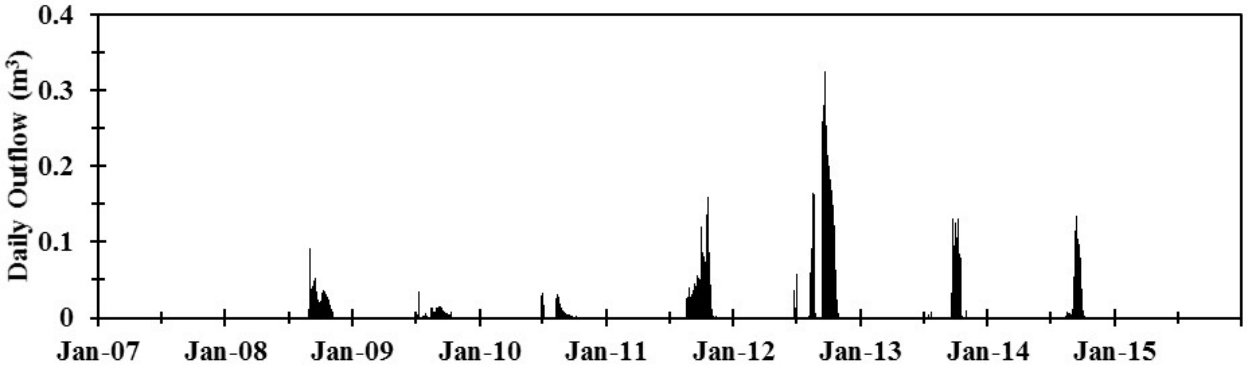

Figure 3.17. Combined daily outflow from BCLs.

Table 3-1. Infiltration estimations per unit surface area calculated using outflow volumes from BCLs. Lysimeters which flowed less than 50 L are indicated by a dash symbol (-). Outlier data has been underlined and discounted from the mean calculations.

Lysimeter	Infiltration Estimation (mm)								
	2007	**2008**	**2009**	**2010**	**2011**	**2012**	**2013**	**2014**	**2015**
3BNBlys4W			19	31	60	21	5	10	
3BNBlys4E							11		
3BNClys2W/2E					138	993	198	248	
3BNClys4W		39	-						
3BNClys4E		76	14	-	101	29	14		
3BSClys4W									
3BSClys4E		12	-		27	7	9		
3BSClys2W/2E								-	
Mean		42	17	31	63	57	10	10	
PM	92	85	10	43	83	9	26	30	38

3.3.3.3 Sensitivity analysis

The sensitivity of the isotopically determined rain and snowmelt volumetric discharge calculations to the mean δD and δ^{18}O values of snow and rain used in the calculations was investigated. This was completed by increasing and decreasing the mean isotopic concentrations by half a standard deviation (approximately 6-7% of the mean concentrations), this represents a significant variation of the mean rain and snow values. The concentrations used in the sensitivity analysis are shown in Table 3-2. Results from the sensitivity analysis are displayed in Figure

3.18, results are presented in mm to better describe sensitivity of infiltration estimates. In general, the results are sensitive to the adjustment of the mean rain and snow isotopic compositions. Following the alteration of the rain concentrations, infiltration estimates varied as high as 23% and 8% from the base case rain and snow infiltration values respectively. Sensitivity was similar when the rain and snow compositions were altered in opposing directions, as high as 39% for rain and 14% for snow infiltration. Sensitivity increased when just the snow composition was altered, differences for rain and snow in these cases were as high as 51% and 21%, respectively. Similar sensitivity was observed for trials when both rain and snow were either increased or decreased, differences as high as 75% and 28%, respectively.

To summarize: variation of the mean isotopic concentrations used in equation 3.2 by about 6% yielded rain infiltration up to 75% deviation from the base case and snowmelt infiltration results up to 28% deviation from the base case. Therefore the partitioning of rain and snow components in outflow is sensitive to the estimated mean concentrations.

Table 3-2. Parameters used for the sensitivity analysis of rainfall and snowmelt infiltration.

Condition	**Rain**		**Snow**	
	δD (‰)	**δ^{18}O (‰)**	**δD (‰)**	**δ^{18}O (‰)**
Mean values	-134.6	-17.7	-183.8	-24.4
Increase 0.5 std dev.	-125.5	-16.4	-172.8	-23.0
Decrease 0.5 std dev.	-143.6	-18.9	-194.9	-25.8

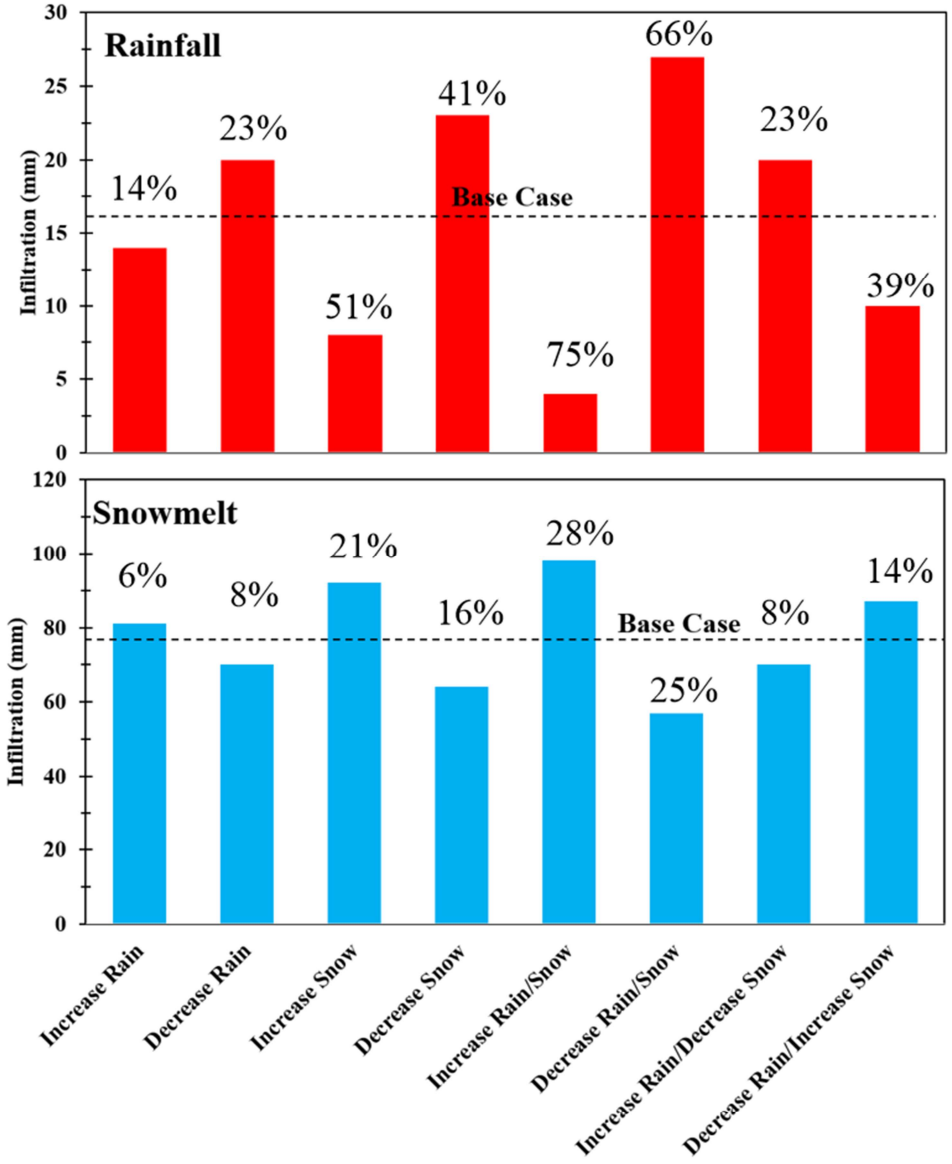

Figure 3.18. Sensitivity analysis of the mean δD and $\delta^{18}O$ concentrations to the mean annual estimate of rainfall and snowmelt infiltration calculations to the whole pile. Percent difference of each scenario from the base case are indicated by above bars.

3.4 Discussion

3.4.1 Evaporation

The effects of evaporation on δD and $\delta^{18}O$ decrease the slope of the regression line (Allison, 1982). Few studies involving these effects have been completed for waste rock hydrology.

Sracek et al. (2004) found a regression of δD= 2.4 x δ^{18}O – 66.0 caused by internal evaporation in a full scale waste rock pile at Mine Doyon. Drainage from the North and South drains plots near the LMWL, slopes of 7.5 and 7.2, suggesting evaporation at the surface of the pile or related to internal air flow (Chi et al., 2013) are not significant processes in the waste rock pile. This is interesting given that Diavik is located in a semi-arid environment, where solar radiation is thought to have a significant influence on the hydrologic behaviour of the test piles (Fretz, 2013). An explanation of these results is given by considering that rainfall events occurring during times of higher potential evaporation (June-August) are largely evaporated and therefore not available for infiltration, while rainfall events occurring during periods of lower potential evaporation (May and September-October) largely infiltrate the test pile. This concept implies that evaporation is important, however its influence is not expressed isotopically in the drainage due to the seasonal recharge profile.

Drainage from the South drain was determined to be statistically different from the LMWL and the North drain effluent, while the North drain was statistically similar to the LMWL. This suggests a minor evaporative influence on the South half of the pile which does not impact the North. Analysis of air flow through the pile (Pham, 2013a) does not show differences between the North and South sides of the pile; therefore, it is not anticipated that convective air flow would preferentially cause internal evaporation from one side of the pile and not the other. Similar to the South drain, analysis of δD and δ^{18}O in pore waters and basal drainage from the deconstructed Type I pile plotted below the LMWL (Chapter 2). The observation of these effects in this adjacent test pile suggest reduced exposure to solar radiation, which is unique to the North batter, has resulted in diminished evaporation from this region. These effects are also observable in d-excess reported from the drain (Figure 3.11). D-excess from the South drain is

consistently lower than the North drain, a consequence of evaporation. Differential evaporation between the North and South sides of the pile likely has a minimal direct effect on the hydrology, however, identification of this phenomena may provide insight to the thermal behaviour of the pile, discussed later.

3.4.2 Ice formation

Figure 3.19 shows a comparison of rainfall infiltration estimates determined using the PM method and rainwater outflow from the basal drains, both methods assume equal infiltration across the crest and batters. Calculations from 2007 have been discounted since the PM estimate includes applied rainfall events to the crest of the test pile, inaccurately representing infiltration across the footprint (crest and batters). Infiltration estimates determined from PM are generally greater those yielded from the basal drains. Cumulative rainfall infiltration estimates from the North and South Drains were 83 mm and 197 mm, respectively, highlighting the aforementioned disparity in outflow from the two basal drains. PM yielded a cumulative infiltration estimate of 326 mm over this time period, much greater than the estimates determined from outflow data. A comparison of the PM estimates to those from the basal drains indicates a significant storage component to the water balance of the test pile. This can be interpreted to represent basal ice formation. The disparity of outflow from the North and South drains suggests there is increased ice formation in the North side of the pile, unlike the symmetrical distribution of ice observed in the Type I pile (Chapter 2).

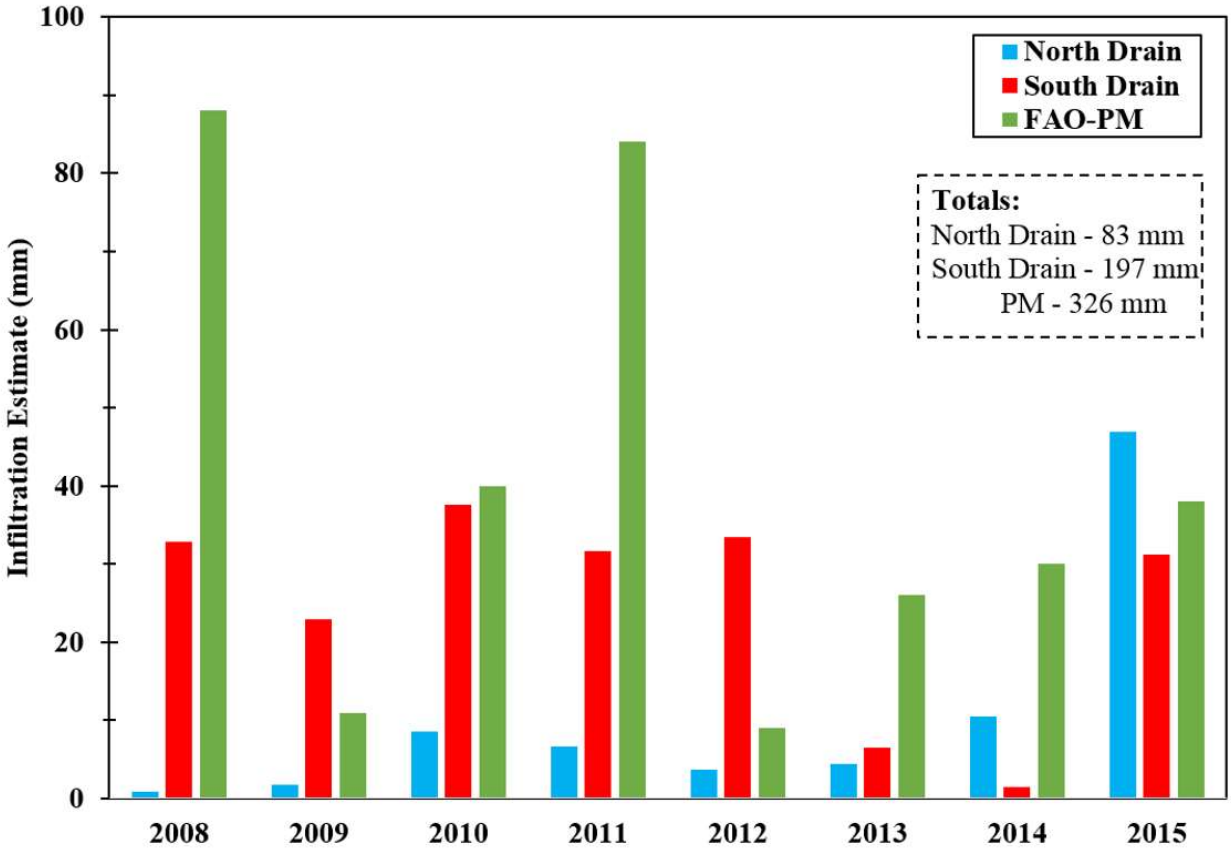

Figure 3.19. Rainfall infiltrations estimations to the Type III test pile produced by the modified PM method and rainwater discharge from the North and South basal drains.

Further evidence of ice accumulation in the test pile is shown by the evolution of d-excess from the North and South drains. Figure 3.11 reflects the transition from snowmelt dominated discharge (high d-excess) to effluent with increasing rainwater contributions (lower d-excess), occurring most years. In 2014, the drains show opposing behaviour, the South drain shows a clear trend of declining d-excess (as anticipated) while d-excess from the North drain increases; increasing d-excess was also observed in the South drain in 2015. δD and δ^{18}O in Figure 3.10 show no clear deviation from the seasonal transition of snowmelt to rainwater discharge during these instances. This progression of d-excess may reflect the discharge of water which had previously undergone multiple freeze-thaw cycles. Repeated freeze-thaw has been shown to

increase d-excess of glacial ice (Steig et al., 1998). During periods of thawing, fractionation between infiltrating water and ice results in the removal of lighter isotopes from the ice resulting in enrichment of the heavier isotopes over time. Eventually when this ice melts, the effluent will be enriched (Williams et al., 2006). Increased snowmelt outflow was observed during the flow seasons associated with melting events, suggesting the melt water had originated from ice accumulation in the batters (Figure 3.12 and Figure 3.13).

As previously stated, disproportionate outflow of water from the basal drains may result from increased ice formation in the North side relative to the South side of the test pile. It remains challenging to justify why, two possible explanations are presented:

Thermal data indicates the North side of the pile is generally colder than other regions (Figure 3.20A). Ground freezing and thawing indices from 2012 presented Sinclair et al. (2015) are interpreted here with insight gained from isotopic analysis. These indices are given in units of degree (^{o}C)-days, describing the intensity of temperature variations. A detailed explanation of these measurements can be found in Orlando and Andersland (1994). Briefly, these indices are determined using plots of degree-days over time, minimums generally occur in the Spring and maximums occur in the Fall. The ground freezing index (GFI) is the difference between the maximum and the succeeding minimum point, the Fall and the following Spring. The ground thawing index (GTI) is the difference between the minimum and the succeeding maximum, the Spring and the following Fall. GFI shown in Figure 3.20B indicates that the North side of the test pile experiences more intense cooling effects than the South. The cause of this has remained uninvestigated, the interpretation here is that this is a consequence of reduced exposure to solar radiation on the North side of the test pile through the Fall and Winter months. This concept is corroborated by the isotopic similarity of outflow from the North drain to the LWML (Figure

3.9) and the observation of consistently higher d-excess from the North Drain than the South Drain (Figure 3.11). Thawing of the test pile occurs in a more symmetrical manner than freezing (Figure 3.20C), this is understood to be a result of a more even distribution of solar radiation during the late Spring/Summer. Although the aspect of the sun is dependent on the time of day, Figure 3.21 provides a sense of the general distribution of sunlight/solar radiation the test pile receives during the late summer. As the total hours of daylight decrease, as does sunlight exposure to North facing aspects. It is proposed here that the cooler temperatures in the North side of the test pile may be conducive to increased formation of ice.

An alternative explanation to the inferred asymmetrical ice distribution is provided by examining the role of heat trace in the basal drainage system. As discussed in Chapter 2, a flooding event in the Type I/Type III instrumentation trailer resulted in the loss of power to the BCL and basal drain heat trace December 2012. The influence of this event on the distribution of ice on the pile is not understood. Upon the rewiring of the heat trace system in September 2013, greater outflow volumes were observed from the North side of the pile. This could be interpreted to indicate that the heat trace in the North basal drain had not been functional up to this point, allowing for ice formation in the drainage system. Without the measurement of temperatures inside the basal drains, this explanation is difficult to prove or disprove. Temperatures recorded in the batters of the test pile at 7, 9, and 11 m depth are shown in Figure 3.22 (note that data from December 2012-September 2013 was interpolated by Pham, (2013)). Annual minimum and maximum temperatures at the various depths are relatively consistent before and after the rewiring of the heat trace, indicating there was not an obvious change to the thermal regime in these regions. Furthermore, temperature measurements shown in appendices suggest the heat trace in the base of several of the BCLs may not fully functional, indicated by below freezing

temperatures. However, BCLs which experienced freezing temperatures showed no correlation with BCLs which did not produce flow (Table 3-1). This might indicate that the heat trace system had a negligible impact on the flow regime.

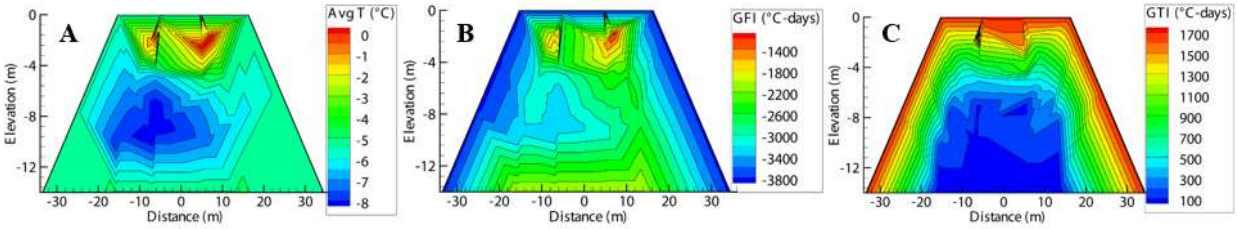

Figure 3.20. Thermal data from 2012 showing: A) average annual temperature, B) ground freezing index, and C) ground thawing index (Sinclair et al. 2015).

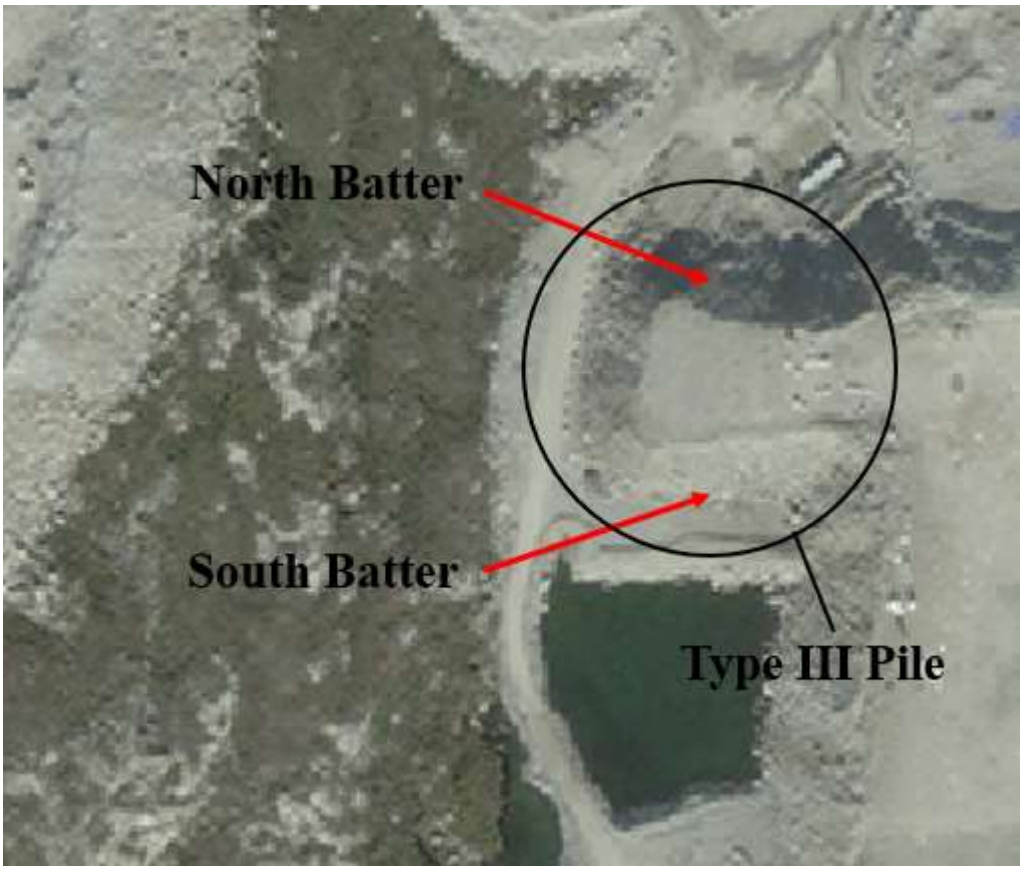

Figure 3.21. Satellite photo showing the distribution of shade on the Type III test pile, taken approximately August, 2014.

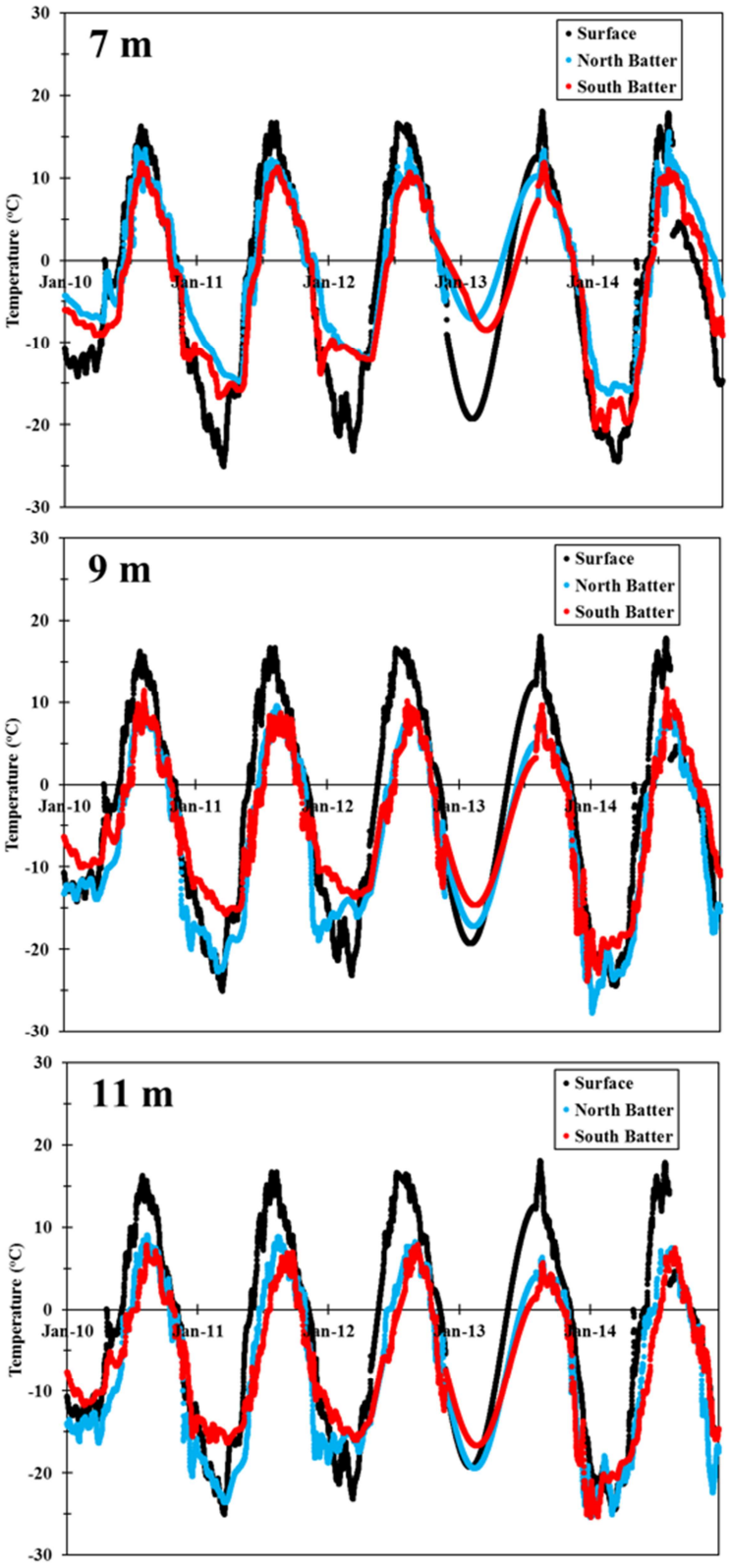

Figure 3.22. Temperatures measured at various depths (7, 9, 11 m) and near the surface (0.1 m) of the Type III test pile.

3.4.3 Batter hydrology

Snowmelt accounted for approximately 74% of the total annual discharge from the base of the test pile, making it clear that snowmelt is an important component of the pile water budget. Since snowmelt only infiltrates through the batters of the test pile, it can be concluded that greater than 74% of the total outflow observed from the test pile is derived from batter recharge. A lower limit of snowmelt recharge was estimated to be 77 mm over the batters, an average from nine years of data. However, wind driven redistribution of snow is known to affect the snowpack on North and South sides of the pile differently, infiltration estimates for the North and South batters were determined to be 35 mm and 118 mm, respectively.

3.5 Conclusions

The work here highlights the value of stable isotopes in the characterizing fluid flow processes in waste rock piles constructed in cold climates. The key findings of the research are outlined below:

1. This study demonstrates that δD and δ^{18}O can effectively be used to estimate infiltration to waste rock piles. Investigations involving the use of these isotopes in the characterization of waste rock piles have been limited in the past. The framework of this investigation can be adopted/modified to improve conceptual models, complete water balances, and investigate hydrologic processes (evaporation, condensation, freeze-thaw, etc.) occurring waste rock piles globally.

2. The annual progression of δD and δ^{18}O concentrations measured in drainage from the North and South drains displayed similar behaviour relative to one another as well as

from year to year (Figure 3.10). Outflow begins in the early summer as snowmelt, as the pile thaws and larger portions of the pile contribute to drainage resulting in increased volumetric discharge, which contains a larger component of rainwater. Peak outflow occurs in September-October and typically remains dominated by snowmelt. Outflow rapidly decreases as freezing progresses through the Fall months.

3. A comparison of annual rainwater infiltration estimates through the crest of the test pile to rainwater outflow from the basal drains indicates an increase in the storage of water (Figure 3.19). This has been interpreted as an indication of the formation of basal ice, more so in the North half of the pile. D-excess in drainage indicate the outflow of water which had experienced multiple freeze-thaw cycles, further supporting the formation of ice in the test pile (Figure 3.11).

4. Annual snowmelt recharge the through the batters of the test pile was determined to be 77 mm, without knowledge of the role of snowmelt in ice formation, this measurement should be interpreted as a lower limit. Roughly 74 % of the outflow from the pile was snowmelt, averaged over nine years of monitoring. This indicates that outflow from of the waste rock pile was strongly dominated by the batters.

5. Water fluxes from BCLs were highly variable over space and time, ranging 1-2 orders of magnitude. These local fluxes poorly represent infiltration estimates determined by PM calculations. Furthermore, years of increased infiltration did not result in increased fluxes from the BCLs. This demonstrates the heterogeneous nature of fluid flow in the waste rock pile.

6. In general, δD and δ^{18}O concentrations in drainage from the basal drains plotted near the LMWL (Figure 3.9). The lack of a significant evaporative influence observable on δD and δ^{18}O concentrations was surprising given the amount of solar radiation experienced at Diavik during the summer months. This is interpreted to be a consequence of rainfall events during times of higher potential evaporation (June-August) being largely evaporated and not available for infiltration. Rainfall events occurring during times of lower potential evaporation (May and September-October) largely infiltrate the test pile. This seasonal recharge profile prevents the influence of evaporation from being detected isotopically in drainage.

7. The cause of the interpreted increased ice formation in the North side of the test pile could not be reconciled. Two possibilities have been proposed: The first being, shading of the North batter reduces warming caused by solar radiation. This maintains a colder temperatures in the North batter region (Figure 3.20), which are more conducive to the formation of basal ice. The second possibility, heat trace in the North basal drain was improperly installed, allowing for the formation of ice in the drain. Upon rewiring the heat trace, greater outflow was observed from the North.

In addition to the estimation of snowmelt infiltration to the batters test pile, this study has led to key inferences regarding some of the processes governing flow such as evaporation, ice formation and melting of frozen zones within the test pile which are otherwise difficult to characterize. These insights are fundamental in the assessment of the hydrologic and geochemical behaviour of waste rock piles at Diavik.

Chapter 4 Assessment of a ten-year tracer test experiment from a waste rock test pile in a permafrost environment

4.1 Introduction

Waste rock piles located at mine sites are composed of large unsaturated zones with complex hydrologic behaviour. The highly heterogeneous nature of waste rock piles has been documented in numerous studies, however the effects of heterogeneity on the hydrologic behaviour and consequent release of contaminants is not well understood (Nichol et al., 2005; Fala et al., 2005; Erikson et al., 1997; Amos et al., 2014). Waste rock piles often contain a tremendous volume of material, some on the order of 500 million m^3 (McCarter, 1990). Weathering of sulphide minerals in the unsaturated zone allows for the release of dissolved reaction products such as acidity, metals, and high TDS in pore waters. The transport of pore waters and solutes to the surrounding environment is governed by internal hydrologic processes. Uncertainty in the hydrologic characterization of a waste rock pile can be problematic when making predictions of solute behaviour. Therefore, investigating the processes controlling solute transport in waste rock piles is a requirement for making meaningful predictions of the geochemical evolution of an abandoned mine, during mine closure, and also during operations (Smith et al., 1995).

In terms of knowledge of the behaviour of waste rock, the Diavik Diamond Mine is a well investigated site, hosting one of the longest duration waste rock research programs of its kind. Since 2007, the Diavik Waste Rock Project has provided a comprehensive dataset characterizing the geochemical evolution (Smith et al., 2013a; Bailey et al., 2013), hydrologic processes (Neuner et al., 2013), thermal evolution (Pham et al., 2013), gas transport (Amos et al., 2009),

and microbiology (Bailey et al., 2015) relevant to waste rock at the mine site. Located approximately 300 km NE of Yellowknife, NWT, Canada (Figure 4.1), the mine is located in a region of continuous permafrost, introducing complexity to the characterization of the behaviour of the waste rock.

Figure 4.1. Location of the Diavik Diamond Mine, NWT, Canada.

Tracer testing and flushing of conservative resident blasting residuals has been used to examine solute transport processes in numerous waste rock piles. Diodato and Parizek (1994) monitored tracer concentrations in waste rock from a coal strip mine in Pennsylvania using suction lysimeters. Tailing of the breakthrough curve (BTC) was observed and attributed to the retention

of solute in fine grained portions of the matrix during dry periods, followed by increased rates of transport after rainfall events when moisture contents were higher.

A tracer test at the Cluff Lake experimental waste rock pile in Saskatchewan, Canada was conducted by Nichol et al. (2005). This work demonstrated that the unsaturated flow system in the pile could be characterized by Richards equation in one dimension (Richards, 1931). Concentrations of tracer measured in drainage from a series of 2 x 2 m basal collection lysimeters displayed long tailing. Mass recovery from lysimeters was highly variable, ranging from 11% to 117% of the respective mass applied at surface, with an average of 34% after approximately three years. This experiment was significant in revealing a heterogeneous three domain solute transport system involving matrix flow and two types of preferential flow pathways, macropore and noncapillary.

Tracer tests completed at two field scale test piles at Antamina, Peru both exhibited long tails as described in Blackmore et al. 2014 and Blackmore (2015). The tracer tests resulted in 67% and 72% mass recovery in the first two years. Transport of the tracer was determined to be influenced by a dual porosity system where solute diffused into and out of an immobile domain according to a single mass transfer coefficient estimated by numerical modeling. A comparison of the BTCs produced by an applied bromide tracer and the flushing of internal chloride, found that chloride had a longer residence time in the advective domain and a larger mass transfer coefficient. This was determined to be a consequence of the tracers occupying different domains of flow. Bromide tracer entered the pile through the preferential flow domain during application, later partitioning into the matrix and immobile domains. Whereas, the initial transport of chloride transport was largely associated with the matrix domain, with little influence by preferential flow.

Each of the tracer test studies described here (Diodato and Parizek, 1994; Nichol et al., 2005; Blackmore et al., 2014) indicated BTCs characterized by long tails, revealing the significance of transport affected by low mobility or immobile domains; creating significant support that solute transport through waste rock should not be evaluated using a single porosity, but rather a dual porosity system influenced by advection and diffusive transfer. The conventional dual porosity model adopts a single rate to describe transfer mass transfer between the advective and diffusive domains. Similar to the dual porosity model, the multirate mass transfer model involves an advective (mobile) domain and a diffusive (immobile) domain, and diffusive solute transfer between the domains. Distinctively, the multirate model describes transfer between the domains according to a range of rate coefficients (Haggerty and Gorelick, 1995, 1998), as opposed to the single rate described by dual porosity models. Multirate mass transfer behaviour results from heterogeneity at the pore scale (such as: size/geometry of grains and pores, tortuosity, dead end pores, and interactions with pore walls), causing variability in the diffusive properties of the media. The existence of multiple rate coefficients implies that solute transfer between the mobile and immobile domains occurs over multiple timescales in the media. The potential for the influence of multirate mass transfer on solute transport is illustrated by numerous investigations modelling laboratory scale experiments (Connoughton et al., 1993; Haggerty and Gorelick, 1995, 1998; Lorden et al., 1998; Stager and Perram, 1999). Haggerty et al. (2004) compiled estimates of single rate mass transfer coefficients from 316 solute transport experiments, finding a strong correlation between the effective mass transfer time and the experimental duration- the longer the experiment, the smaller the characteristic mass transfer rate. This observation is explained by the presence of multiple rates of mass transfer; the slower the mass transfer rate, the longer amount of time required for its effect to become observable.

Despite evidence indicating that multirate mass transfer is a widely applicable model to solute transport, few field scale experiments have investigated have been completed (Haggerty et al., 2000, 2001; Ma et al., 2010).

If solute transport through a waste rock pile is significantly influenced by diffusion into immobile zones, predictions of drainage monitoring times completed using a conventional dual porosity model may be under predicted compared to estimates determined from a multirate model. Given the importance of reliable predictions of late time solute concentrations from waste rock piles, the ability for the multirate mass transfer model to describe late time solute concentrations should be investigated.

This paper builds on a preliminary investigation of tracer recovery from the Type III test pile completed by Krentz (2014). That work showed that 38% of the applied tracer mass had been recovered after seven years and mass loading from the two primary basal drainage systems was disproportionate relative to one another, demonstrating a complex transport system. Hypotheses developed in that paper attributed low tracer recovery to a combination of low velocity flow paths and ice formation. However, the effects of ice formation on the results of the tracer test versus the influence of low mobility or low velocity zones were not reconciled individually since the distribution of ice in the test pile was not fully understood and not enough time had passed to adequately characterize tailing behaviour. Chapter 2 provides a characterization of ice observed during the deconstruction of the Type I test pile, these learnings were applied in the investigation of oxygen and deuterium isotopes in basal drainage of the Type III pile (Chapter 3), supporting that ice formation had occurred in the pile, preferentially in the North side. The work presented here includes an additional three years of tracer monitoring than presented in Krentz (2014), with the objectives of improving the characterization of BTC tailing and accounting for the

unrecovered tracer mass with respect to the potential influences of multirate mass transfer and ice formation. The interpretations of the tracer test are supported by investigating the flushing of blasting residuals from the test pile.

4.2 Methods

4.2.1 Experimental facility

Construction of the test piles facility is discussed in detail by Smith et al. (2013b) and Neuner et al. (2013). The construction and instrumentation of the Type III pile occurred from 2004-2006. Waste rock was end dumped from a ramp to the 50 x 60 m base of the pile (Figure 4.3). The pile is 14 m high with batters on three sides at the angle of repose (38°). The base of the pile was graded (0.5-2%) away from the centre line towards the North and South halves of the pile and lined with an impermeable HDPE geomembrane. This configuration was designed to direct flow towards the North and South basal drains for collection, each drain collecting water from the respective half of the pile. The drains directed water into instrumentation huts where geochemical sampling occurred approximately every three days during times of discharge, flow was continuously monitored using custom made tipping buckets. Approximately 0.4 m of 1.25 inch Type I crush was placed at the base of the pile to prevent damage to the drainage system from occurring during pile construction. Three clusters of 2 x 2 m and two 4 x 4 m basal collection lysimeters (BCLs) were built on top of the crush layer (naming of the BCLs is shown in Figure 4.2). Flow collected from the BCLs was directed towards the instrumentation trailer for geochemical sampling and flow monitoring using tipping buckets. Self-regulated heat trace was placed in the basal drain and lysimeters drain lines to sustain temperatures above 5°C.

Various instrumentation (TDR, thermistors, gas sampling tubing, thermal conductivity ports) to monitor the geochemical, hydrological, microbiological, gas transport, and thermal behaviour internal to the pile were installed on four tip faces as waste rock was dumped from a ramp towards the pad of the test pile. Soil water solution samplers (SWSS) were installed along tip faces, offset approximately 2 m North and South of the centre line of the pile ranging from 2-9 m depth to obtain in-situ pore water for chemical analysis. The number of SWSS at a given depth which were actively sampled are shown in

Table 4-1. The general layout of the test pile is shown in Figure 4.3 with the locations of lysimeters and SWSS.

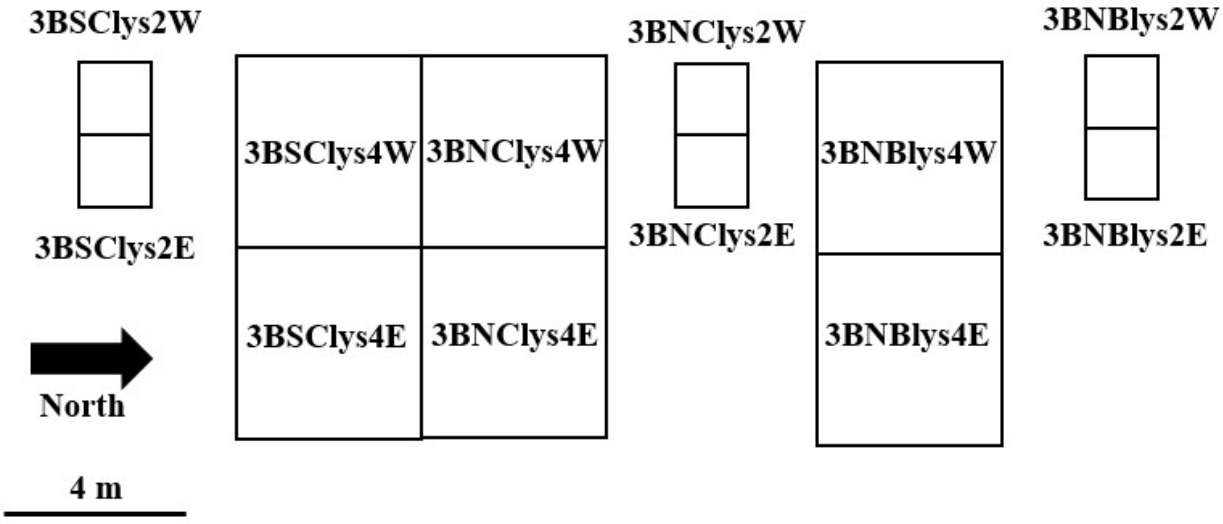

Figure 4.2. Layout and naming of BCLs in the Type III test pile.

Table 4-1. Number of sampled SWSS locations at a given depth in the Type III test pile.

Depth (m)	Number of Sample Locations
2	1
3	3
5	2
7	7
9	6

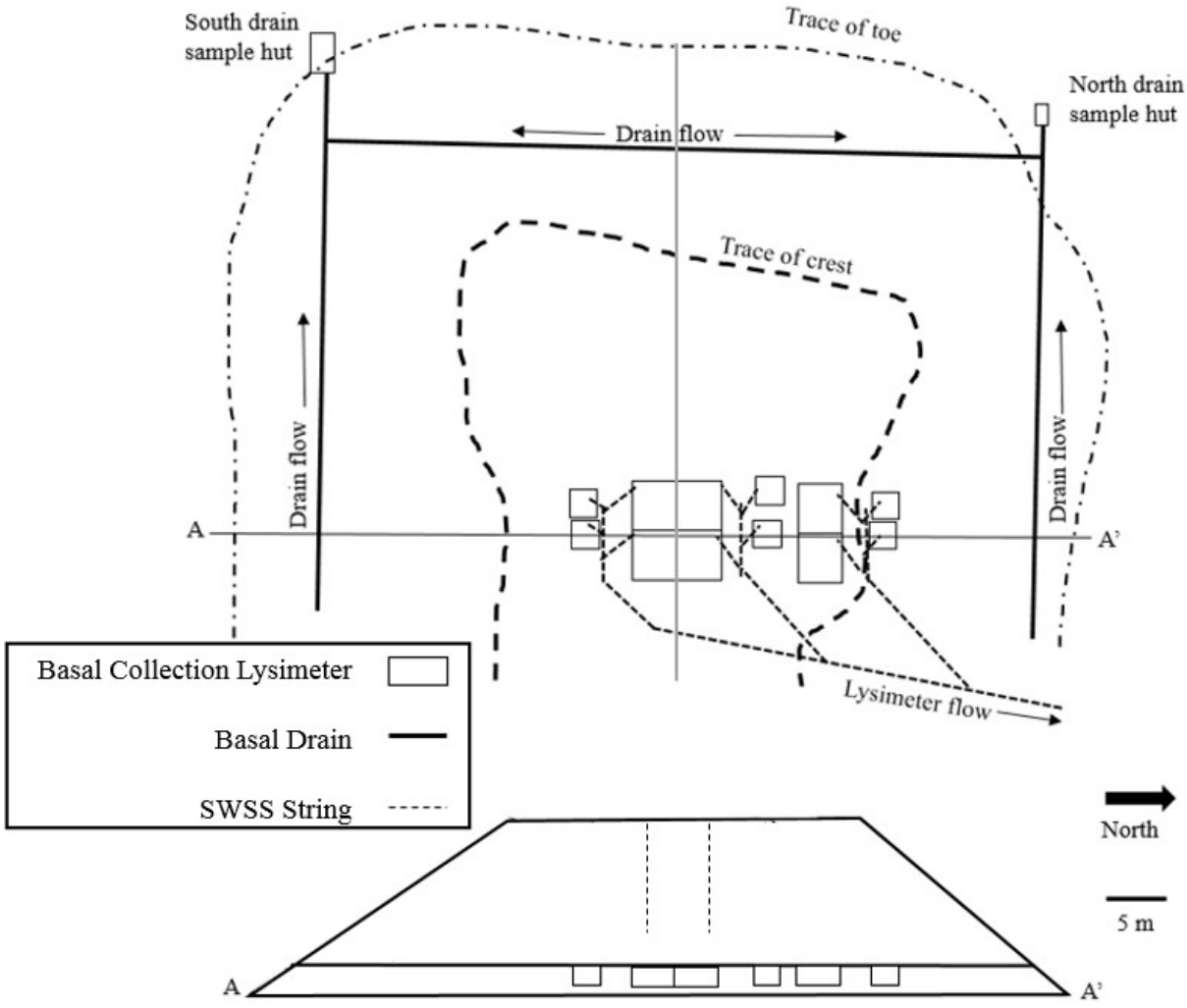

Figure 4.3. General schematic of the Type III test pile, showing locations of relevant instrumentation (Sinclair et al., 2015).

4.2.2 Application of Tracer

Following the construction of the Type III pile, a series of artificial rainfall events were applied in August/September 2006 to reproduce an average year of precipitation and initiate wet-up of the test pile, rather than wait for this to occur by natural events. The following year, several rainfall events labelled with tracers were applied to the partially wet-up test pile. The magnitude

and recurrence intervals were based on Golder Associates (2008) data. High rates (8-10 mm/hr) were intended to activate preferential flow paths in the near surface region of the pile by creating surface ponding. The magnitude and intensity of the applied events are given in Table 4-2. Rainfall events were applied across a 20 x 30 m area shown in Figure 4.4. Deuterium was used to spike a 16 mm event, the concentrations of deuterium and oxygen-18 in the event were 546.3‰ and -17.9‰. Lithium bromide and sodium chloride were added to the final applied rainfall event which was 30 mm, concentrations of bromide and chloride were 2576 mg/L and 2171 mg/L. These solutes were selected as tracers since they are known to behave conservatively and are therefore transported at a rate equal to the pore water velocity. The total applied masses of bromide and chloride were 45 kg and 38 kg respectively.

Table 4-2. Record of applied rainfall events to the Type III test pile (Fretz, 2013).

Date	Rainfall Magnitude (mm)	Rainfall Intensity (mm/hr)	Tracer
Sept 20, 2006	24	10	-
Sept 24, 2006	19	10	-
Sept 26, 2006	15	10	-
Summer 2007	Approximately 92 mm of natural precipitation occurred		
Aug 17, 2007	16	8	Deuterium
Sept 4, 2007	15	9	-
Sept 13, 2007	29	8	Cl and Br

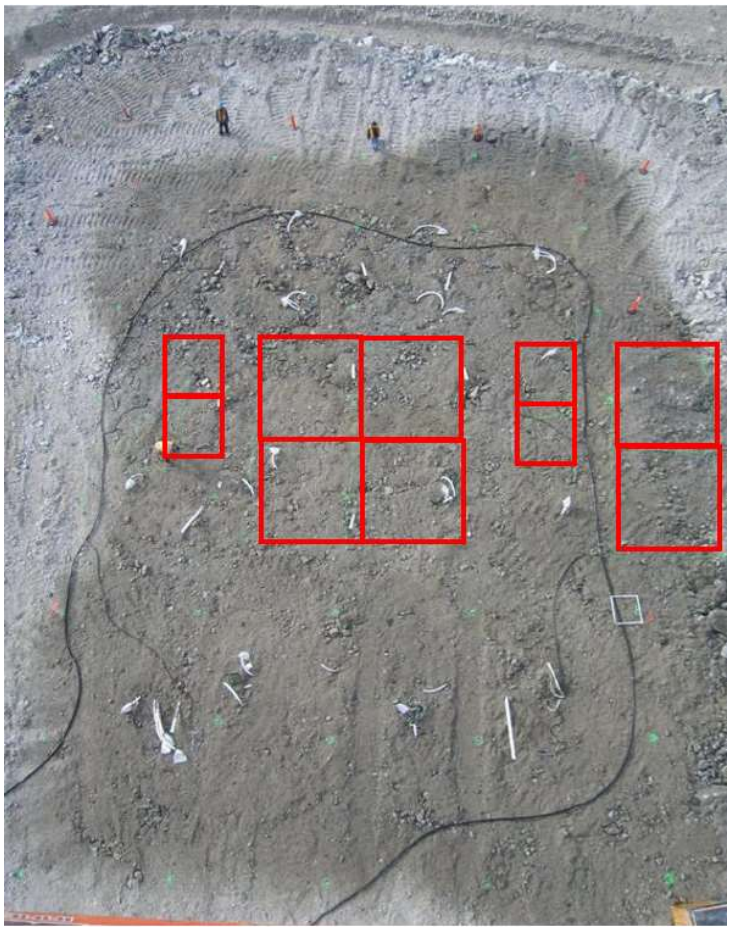

Figure 4.4. Aerial photograph taken approximately 30 m above the crest of the pile, showing the 20 x 30 m area of tracer application (Neuner, 2009). Locations of BCLs shown in red.

4.3 Results

This section presents data obtained during this investigation. Interpretations of the data are provided in the discussion section.

4.3.1 Precipitation

The record of annual rainfall at the site is shown in Figure 4.5A, the average being 102 mm, with the last five years being approximately 84 mm cumulatively below average. Measurements from a snow gauge operated by the Diavik Environment Department are shown in Figure 4.5B. These data indicate an average annual snowfall of 157 mm water equivalent from 2007-2016; note that annual totals reflect snowfall over the winter season, approximately October-April. Approximately 60% of the total precipitation at Diavik occurred as snow during the period of measurement.

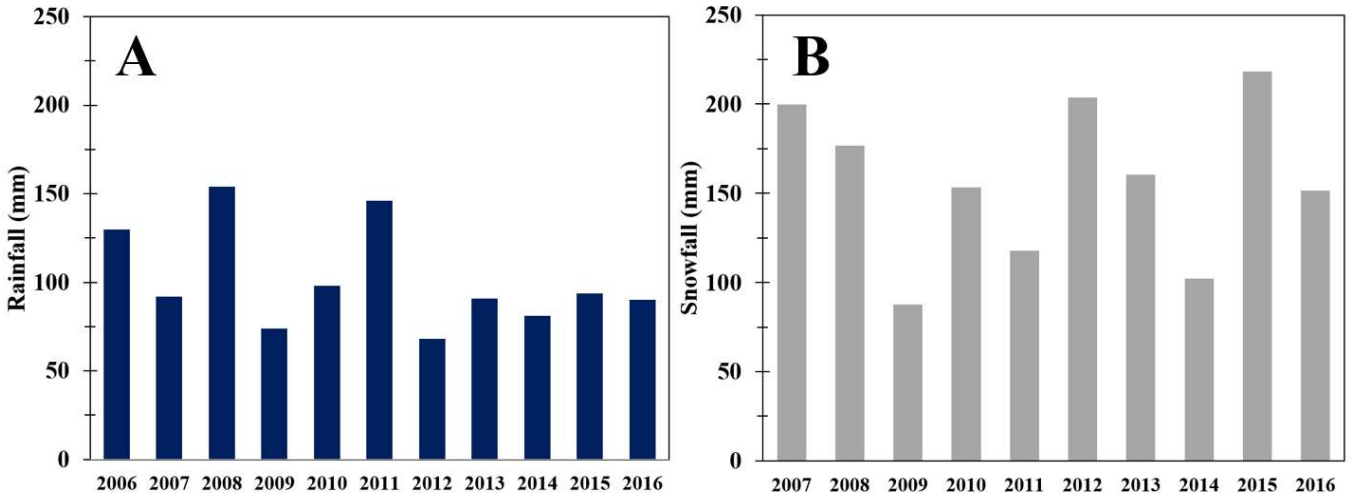

Figure 4.5. Annual totals of A) rainfall and B) snowfall at Diavik Diamond Mine.

4.3.2 Summary of thermal and hydrologic regimes

4.3.2.1 Thermal regime

Freeze-thaw cycling is known to have a dominant influence on the geochemical and hydrologic regimes of the Type III test pile (Neuner et al., 2013; Sinclair et al., 2015; Chapter 2; Chapter 3). Figure 4.6 outlines the thermal progression of a freeze-thaw cycle (Pham et al., 2013; Sinclair et al., 2015). The pile is completely frozen December-May (Figure 4.6A), during this time, discharge from the pile does not occur. A thawing front migrates inwards from the batters, thawed subsections of the batters are able to contribute drainage from the toes of the pile (May-August; Figure 4.6B). The core of the pile experiences thawing and the active zone reaches a maximum depth of about 12 m, basal drainage at this time is a combination of contributions from the batters and the core (August-October; Figure 4.6C). The depth of the active zone determined from temperature measurements in two boreholes drilled in 2013 along the centre line of the test pile is similar to the depth reported by Sinclair et al. (2015) and Pham et al. (2013); data shown in appendices. As the air temperature decreases, a freezing front migrates inward from the batters as well as from the base of the pile from the underlying frozen bedrock, discharge at this time is minimal (October; Figure 4.6D). The effects of inward cooling briefly result in the formation of a thermally isolated active zone in the centre of the pile, discharge from the base of the pile at this time has ceased (November-early December; Figure 4.6E).

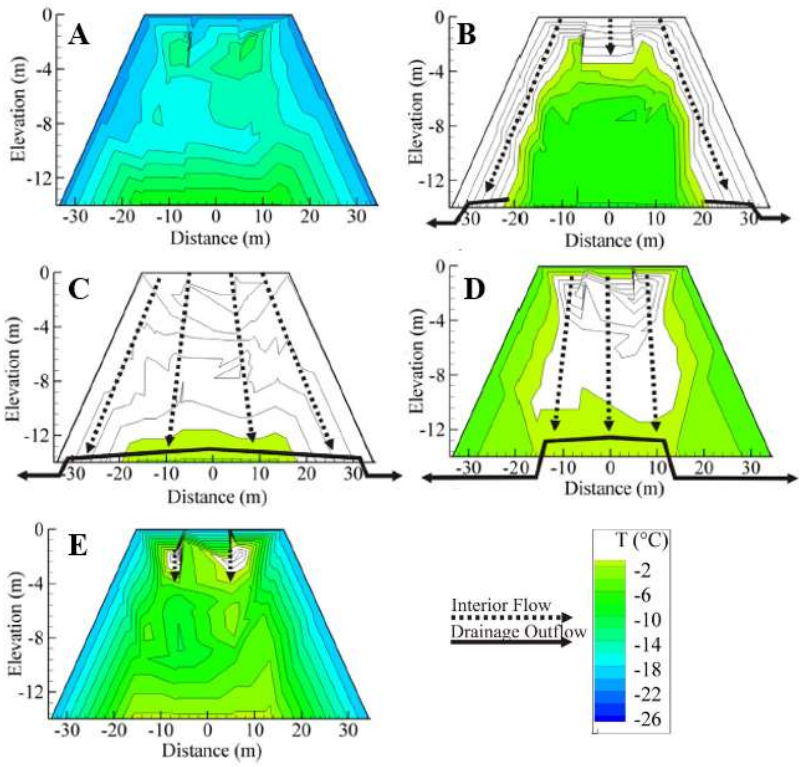

Figure 4.6. Annual progression of internal temperatures in 2012, white areas indicate temperatures greater than 0°C. Proposed flow paths to the basal drains in: A) winter, B) spring, C) summer, D) early fall, E) late fall (modified from Sinclair et al., 2015).

4.3.2.2 Infiltration

Infiltration was estimated using a modified Penman Monteith method (PM) (Penman, 1948), as described by Fretz (2013). It is important to recognize that PM estimates only apply for rainfall infiltration through the crest of the waste rock pile, not the batters. Fretz demonstrated that rainfall events occurring June-August, largely do not infiltrate waste rock at Diavik due to high potential evaporation. Potential evaporation is much lower during May and Septmember-October. Rainfall events occuring during periods of low potetnial evaporation largely infiltrate the waste rock, with little being lost to evaporation. The timing of individual rainfall events explains the different patterns observed between the records of annual rainfall and estimated

infiltration; years of high rainfall don't necesaarily correspond to years of high infiltration (Figure 4.5A and Figure 4.7).

Estimates from the period of study are shown in Figure 4.7, infiltration values for 2006 and 2007 include natural and applied rainfall events. The mean annual infiltration from rain was estimated to be 38 mm during this study (excluding applied rainfall events). Years 2012-2016 represent a five year period of below average annual infiltration, cumulatively 67 mm below. Over the 11 year study period, 487 mm of rainfall is estimated to have infiltrated through the crest of the test pile- including applied rainfall events in 2006 and 2007.

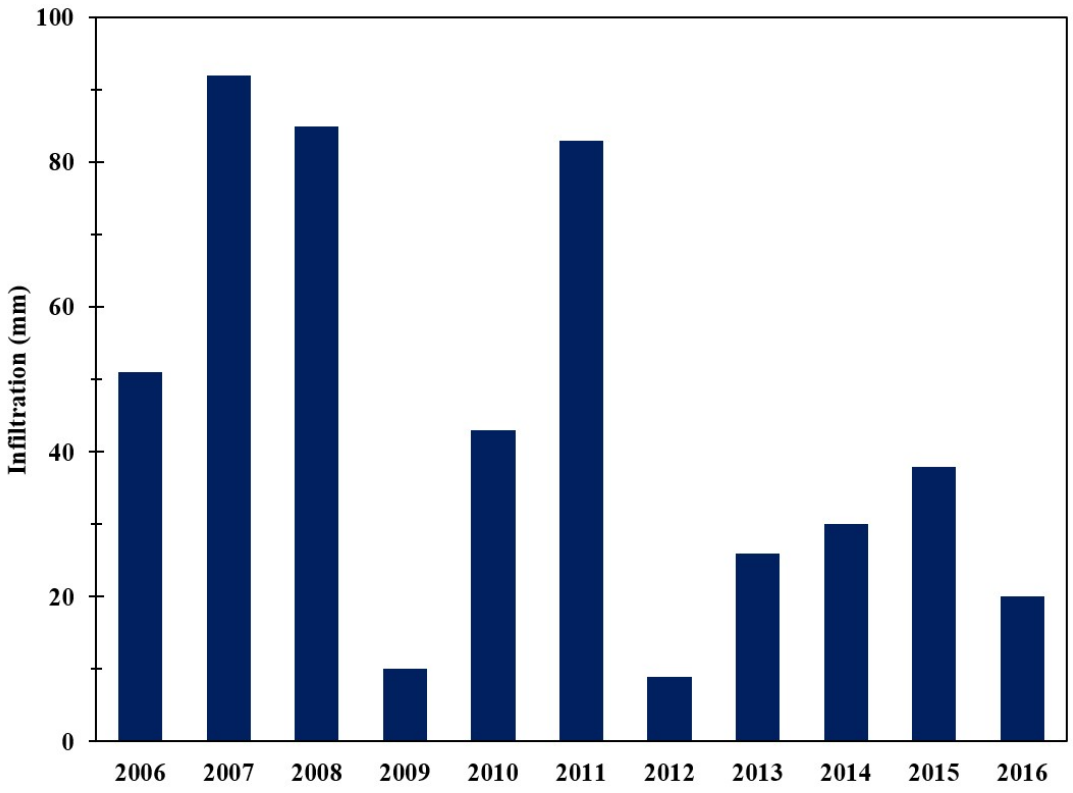

Figure 4.7. Rainfall infiltration estimates through the crest of the test pile. Estimates in 2006 and 2007 include infiltration from natural and applied rainfall events.

4.3.2.3 Moisture contents

Moisture contents measured in the Type III pile at 3, 7, and 9 m depth are shown in Figure 4.8 (data from other depths is shown in appendices). At a given depth, data from multiple laterally-offset probes are shown. For this paper, it is relevant that TDR provides valid moisture contents only when exposed to temperatures above freezing. When exposed to freezing conditions, TDR report VMC generally less than 5%, these effects are clearly shown the datasets, highlighted by sharp decreases during the onset of freezing, and sharp increases once thawed. The TDR is emplaced in matrix material, therefore the moisture contents reported here are the volumetric moisture contents of the matrix, which has a porosity of about 25% (Neuner et al., 2013; Fretz, 2013).

Fretz (2013) provided a description of the timing of wet-up within the Type III pile, to summarize: TDR probes detected a defined wetting-up trend at each depth. Following construction, moisture contents increased sequentially from the top downwards. In general, moisture contents increased each year until the matrix had reached field capacity, about 10-15% (approximately 40-60% saturation), indicating wet-up conditions had been achieved (Neuner, 2009). Following wet-up, a state of dynamic equilibrium was maintained, this was characterized by little annual fluctuation in VMC. During this period, moisture contents of matrix in the pile ranged from approximately 15-25% (60-100% saturation). The wetting front generated by the natural and applied rainfall events which occurred over 2006 and 2007 reached 7 m depth by late 2007. Wet-up was detected at 9 m during 2008. The absence of TDR sensors below 9 m introduces uncertainty in the characterization of moisture contents and wetting-up processes in the 9-14 m depth range. However, outflow from a subset of the BCLs in 2008 has been assumed to indicate the wet-up of the full thickness of the pile.

From these data, it can be seen that wetting fronts detected by multiple laterally-offset arrays located at the same depth were concurrent. This demonstrates the general uniformity of flow across the pile, despite the heterogeneous nature of the material. Wetting front velocities were 0.2-0.4 m/day in response to common rainfall events, velocities increased up to 5 m/day following greater intensity events (Neuner et al., 2013; Fretz, 2013).

The effects of the timing of infiltration events are observable in TDR. Generally once thawed, TDR indicate a seasonal high in moisture contents. As potential evaporation increases due to incoming solar radiation, little water infiltrates the surface. Moisture contents begin to decline indicating drainage. As solar radiation decreases around September, potential evaporation declines and rainfall events largely infiltrate the test pile, resulting in a sharp increase of moisture contents. However, years where there is little rainfall after September result in the continued decline of moisture until freeze-up occurs (examples: 2009, 2010, 2012, 2013, 2014).

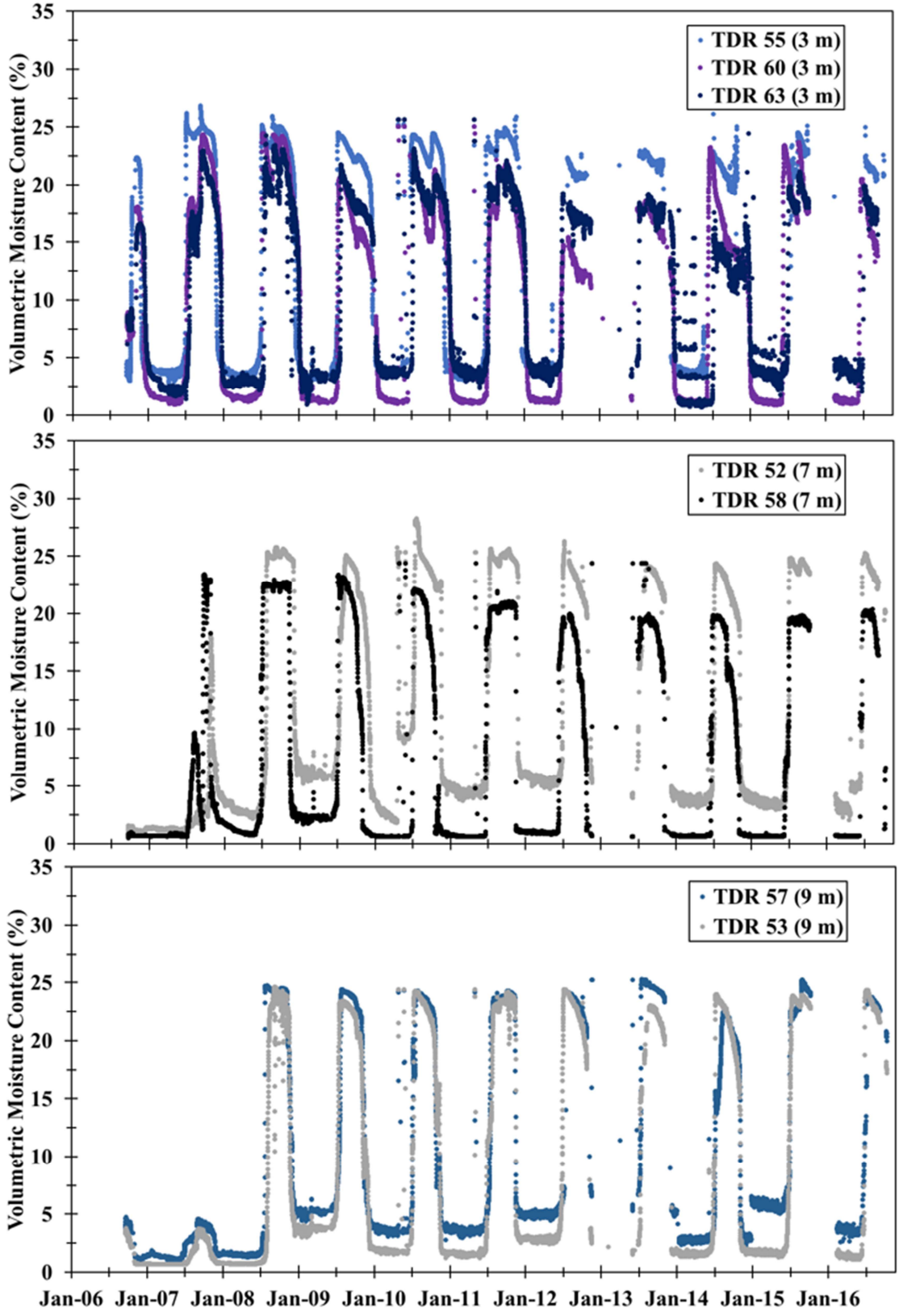

Figure 4.8. Volumetric moisture contents measured in the Type III test pile at 3, 7, and 9 m depth.

4.3.2.4 Basal drainage

The timing of basal drainage is dependent on the thermal regime. Although Figure 4.6C suggests the base of the test pile remains below 0°C throughout the year, heat trace in the base of the lysimeters may allow for flow to occur. Combined drainage from all BCLs is shown in Figure 4.9. BCL drainage begins as the test pile approaches its maximum thawed state around August. Flow ceases during freeze-up in October/November. No outflow from the BCLs was observed in 2015 or 2016, possibly indicating significant ice formation in the core of the pile.

Daily outflow volumes from the basal drains are shown in Figure 4.10. The average outflow from the test pile over the period of study was about 170 m^3. Most of the flow was from the South drain, which displayed relatively little variability year-to-year. Increased outflow from the North drain was observed from 2014-2015, decreasing in 2016, the cause of this variability is not understood. Approximately 74% of the total drainage from the pile is known to originate from snowmelt, this led to the conclusion that the hydrologic regime of the test pile is batter dominated, and the core -which only receives rainfall recharge- contributes relatively little to the overall water budget (Chapter 3).

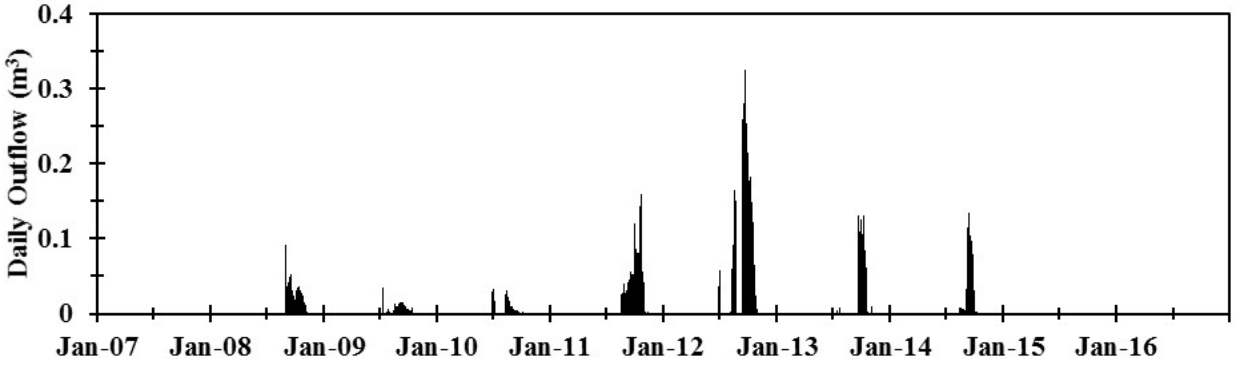

Figure 4.9. Total daily outflow from BCLs.

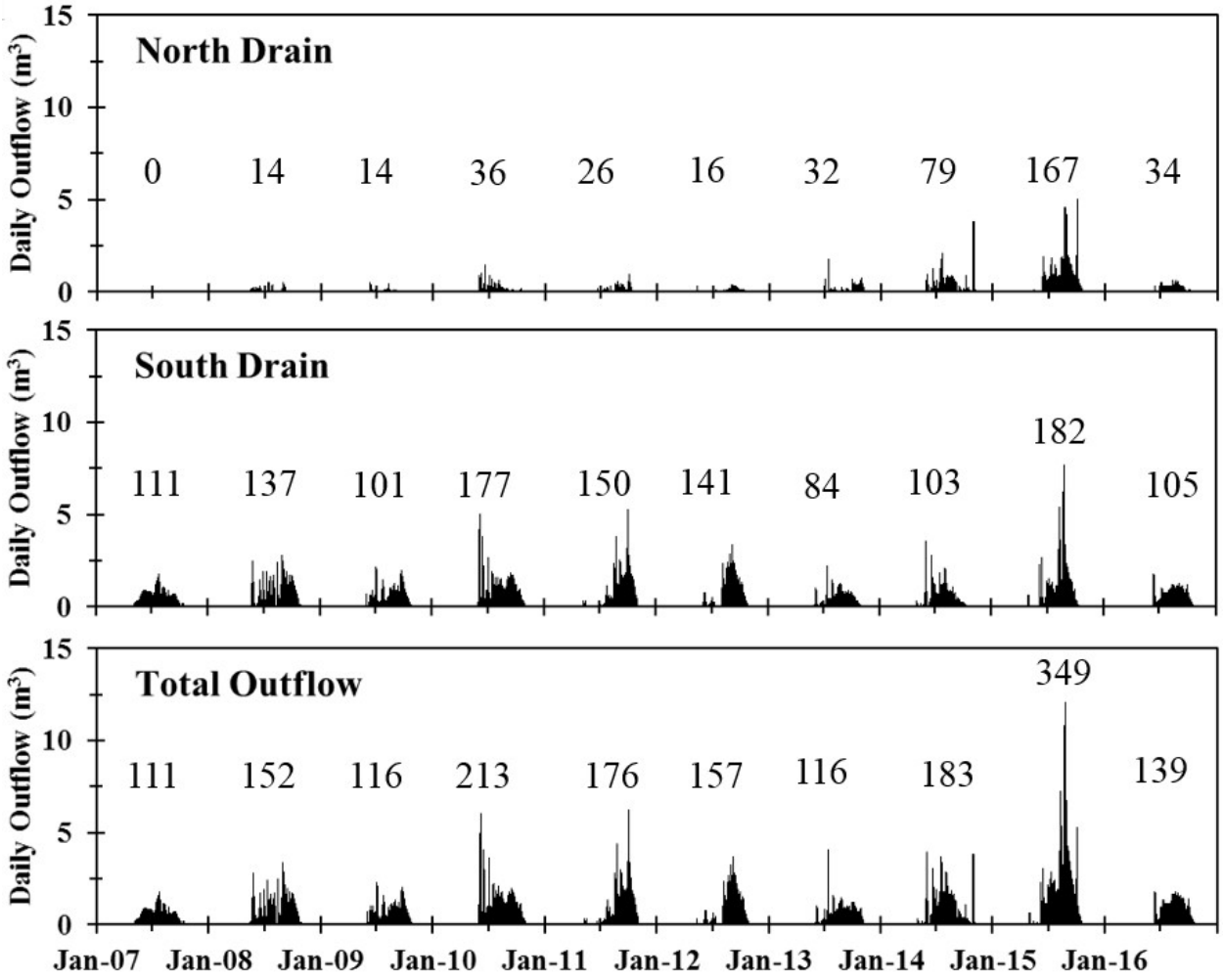

Figure 4.10. Total daily outflow from the North and South drains, as well as combined outflow volumes. Cumulative annual outflow (m^3) is indicated by text.

4.3.3 Movement of tracer

The results of the tracer test are primarily focused on bromide. Chloride and nitrate, would have been evenly distributed throughout the test pile due to blasting activity, complicating interpretations of the applied chloride mass. However, given that these solutes behave conservatively, concentrations and loadings of chloride and nitrate provide an additional method of evaluating solute transport in the test pile.

Transport of the tracers occurred when the test pile was in a thawed state. In order to accurately describe pore water velocities and residence times, time series have been thermally corrected, this is referred to as active or thawed time. Thermal corrections were completed separately for SWSS, BCLs and the basal drains. Temperature profiles from Pham (2013b) were used to identify periods when SWSS at a given depth were above freezing. For the BCLs and basal drains, active times were indicated by the number of days which flow from the lysimeters or drainage system occurred. The same active time scale was used for the North and South drains, opposed to separate active time scales for each.

4.3.3.1 Tracer concentrations in upper 9 m

Sinclair et al. (2015) showed the progression of bromide concentrations in the upper 9 m of the test pile from 2007-2012. This paper provides an update of this data, from 2007-2016. Figure 4.11 shows tracer concentrations measured from SWSS at various depths. Annual mean concentrations are connected by a dashed line on the plots, this line should not be used to interpolate concentrations between sampling events, but to give a sense of the migration of the tracer plume.

Elevated concentrations at 5-9 m depth in 2007 were a result of preferential flow induced during tracer application, velocities as high as 0.7 m/day were determined from these data (Krentz, 2014). Movement of the centre of tracer mass provides an indication of the pore water velocity. The centre of mass can be seen to be at 3-5 m depth in 2008, 5-7 m in 2009, and near 9 m in 2010. The movement of the centre of tracer mass in the range of SWSS yielded a pore water velocity of about 2-3 cm/day while thawed. Following the arrival of the centre of tracer mass,

tailing of concentrations was observed at all depths, a possible indication of the influence of an immobile domain on solute transport. Concentrations at 2 m depth during tailing are particularly elevated (about 100 mg/L) likely indicating the existence of a local low conductivity zone. Low conductivity zones likely exist elsewhere in the test pile, however it is difficult to assess the distribution with the limited number of SWSS locations.

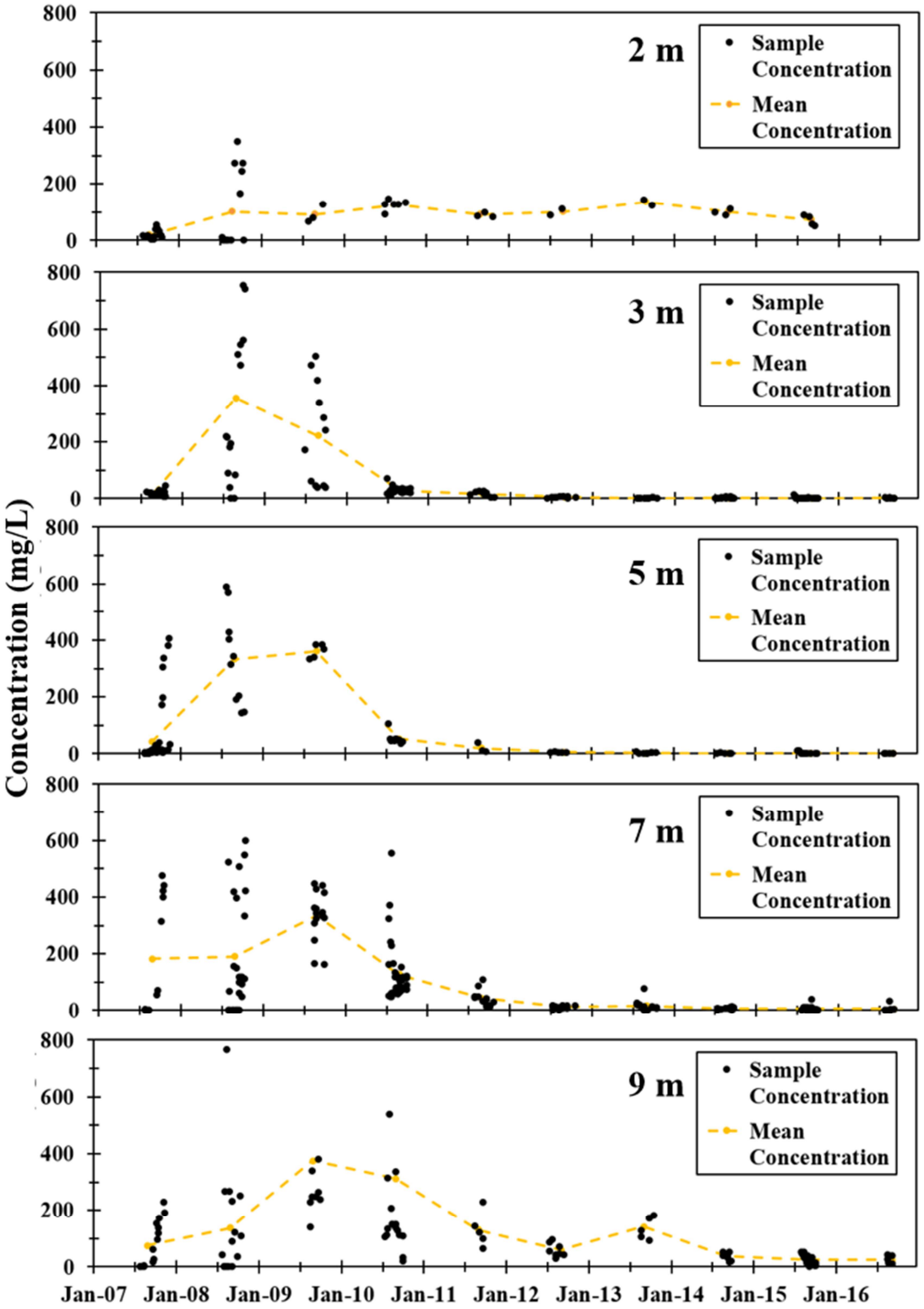

Figure 4.11. Bromide tracer concentrations from SWSS. Note that a measurement at 3 m of 1079 mg/L in October 2008, and at 9 m measurement of 1293 mg/L were truncated from the plots.

4.3.3.2 Tracer concentrations and mass loading to the basal drains

Bromide concentrations measured in the North and South basal drains of the Type III pile are shown in Figure 4.12. The concentrations between sampling events were linearly interpolated in order to calculate mass loading from the drains, shown in Figure 4.13. Concentrations and loadings in 2016 were particularly low, about 0-1 mg/L, corresponding to a total load of 0.08 kg, making these data not visible at the scales shown on the figures.

In terms of concentrations and loadings, the two drains displayed very different behaviour. The South drain experienced peak concentrations/loadings in 2011, indicating the arrival of the centre of tracer mass. Similar to SWSS, tailing of the BTC was observed following the arrival of the centre of mass, suggesting the possible influence of a low mobility domain. The North drain displayed irregular behaviour, minimal tracer arrival occurred from 2007-2013. There was not a well-defined centre of mass observable from the BTC. Loading from the drains was disproportionate, 2.8 kg was recovered from the North and 15.3 kg from the South, 6% and 34% of the applied mass respectively. In total, 18.1 kg was recovered from the basal drains of the 45 kg applied (40%).

The sensitivity of mass loading estimates to the interpolation of concentrations between sampling events was evaluated. The number of concentration measurements used in loading calculations was reduced by two-thirds, meaning a sampling frequency of approximately every nine days, opposed to every three days. This investigation yielded cumulative tracer loads of 2.9 kg and 15.1 kg from the North and South drains, respectively. These estimates are similar to those determined from the higher sampling frequency (2.8 kg and 15.3 kg), indicating the loading calculations completed are not sensitive to the interpolation of concentrations between sampling events.

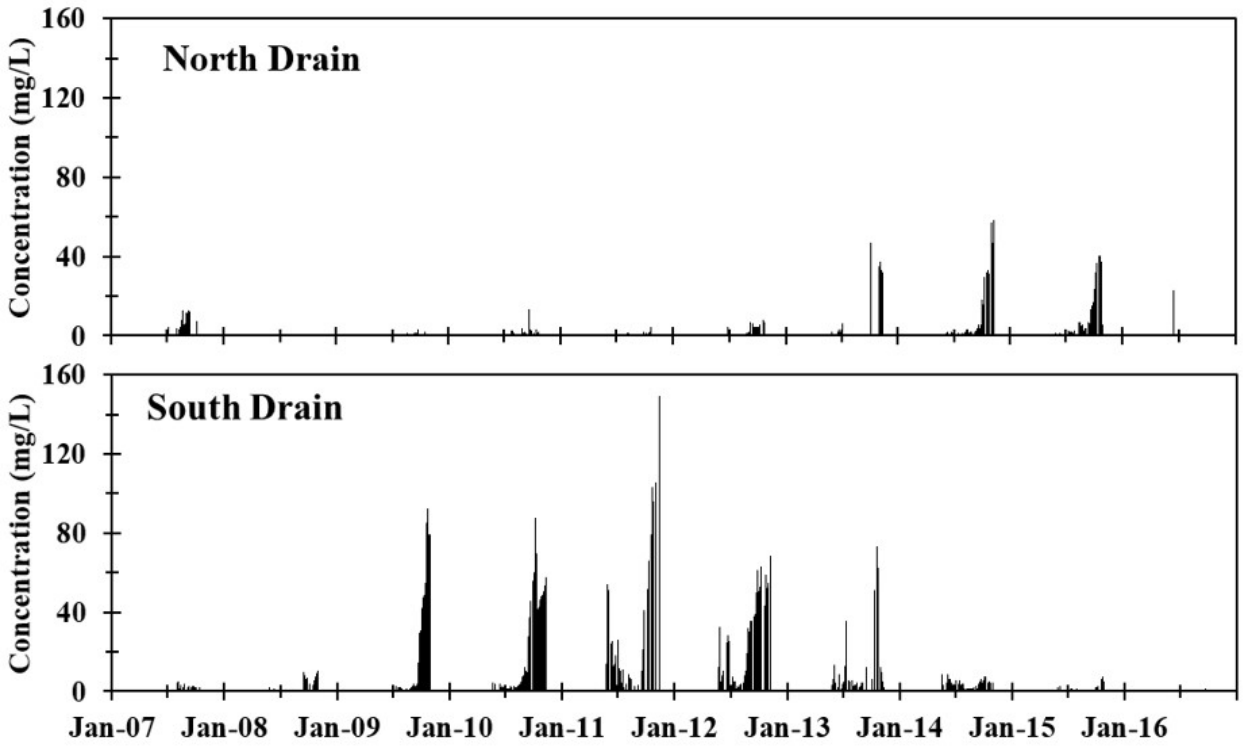

Figure 4.12. Concentrations of bromide measured in the North and South drains of the Type III test pile.

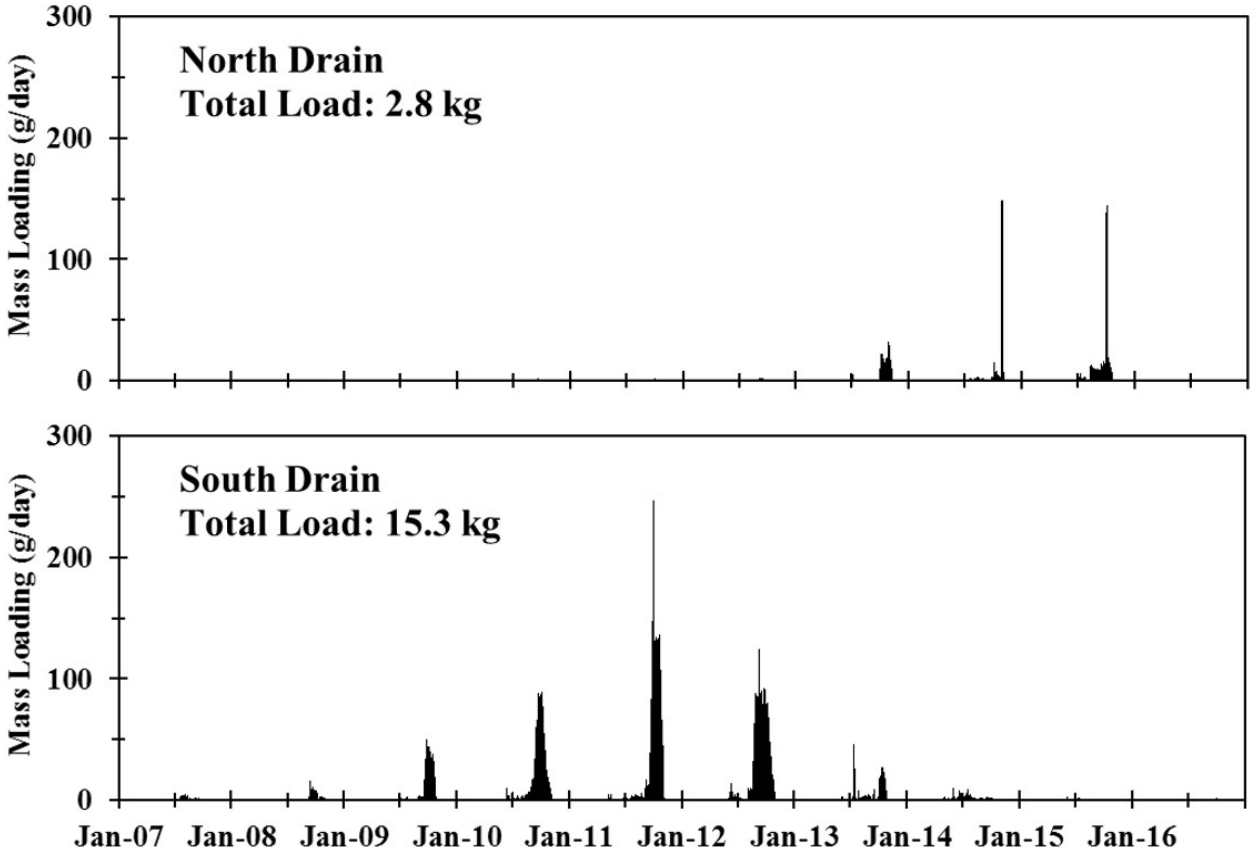

Figure 4.13. Mass loading of bromide from the North and South basal drains; concentrations have been interpolated between sampling events to determine loadings.

Loadings and volumetric flow from the North and South drains were used to determine the composite concentrations of bromide and blasting residuals chloride and nitrate (Figure 4.14). Composite concentrations represent the flow weighted average solute concentration of the discharge from the basal drains on the given day, as described by equation 4.1; where C represents the solute concentration measured in the North or South drain (mg/L), and Q represents the volumetric discharge from the respective drain (L/day) on the day of sampling.

Solute concentrations generally displayed two peaks through the year, an early season (June) and a larger late season peak (October/November). The late season peak signifies maximum

contributions to basal drainage from the core of the test pile. As the pile freezes from the batters inwards (Figure 4.6D), solutes become immobilized in the batters and concentrations in drainage rapidly decrease. Once thawing commences the spring (Figure 4.6B) solutes remaining from the previous flow season are flushed from the batters, signified by a peak of concentrations followed by lower concentrations. At this point, drainage is comprised entirely from batter waters since the core of the test pile remains frozen. As greater volumes of the pile thaw through the flow season, solute concentrations increase.

The general behaviour of concentrations of blasting residuals from the basal drains was similar to the concentrations of the applied bromide tracer. The arrival of the centre of mass for these solutes occurred in 2011, as indicated by peak concentrations. This suggests the applied and resident tracers have a similar transport velocity and residence time in the advective or mobile domain. These similarities were expected, despite the different distributions of tracer masses at time = 0, advective transport of blasting residuals would have been negligible until wet-up by artificial rainfall events had occurred. An average advective velocity of 2 cm/day and a transit or residence time of the mobile domain of 2.3 years when thawed were determined. Similar to SWSS, an extended period of tailing was observed following peak concentrations, possibly due to diffusion of solute between mobile and immobile domains.

$$Composite\ concentration = \frac{(C_{North}\ x\ Q_{North}) + (C_{South}\ x\ Q_{South})}{(Q_{North} + Q_{South})} \quad (4.1)$$

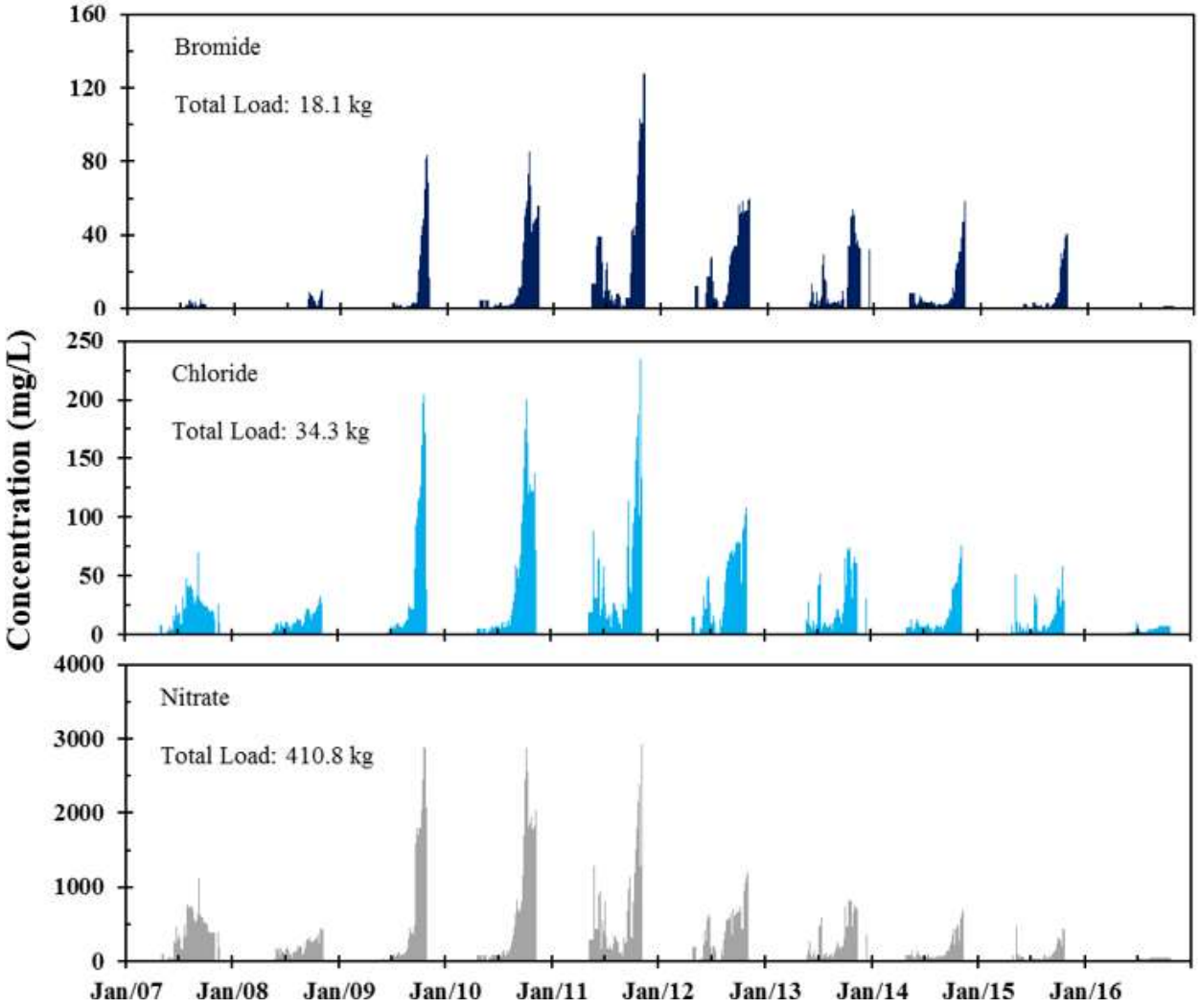

Figure 4.14. Flow weighted or composite concentrations of solutes and cumulative loads delivered through from basal drains- here concentrations have been interpolated between sampling events.

4.3.3.3 Tracer concentrations and mass loading to the BCLs

Concentrations and combined mass loading of bromide determined for two BCLs are shown in Figure 4.15; BCLs 3BNClys4E and 3BSClys4E were chosen since these lysimeters displayed the most consistent flow over time. Increased concentrations and solute loads observed in 2008 are attributed to preferential flow induced at the time of tracer application, a preferential flow

velocity of about 1 m/day when thawed was determined from these data; similar to the preferential flow velocity of 0.7 m/day determined from SWSS (Krentz, 2014). Peak concentrations coincided with peak loadings in 2011, representing the arrival of the centre of tracer mass. An average advective pore water velocity of 3 cm/day while thawed was determined from these data, consistent with the velocities determined from the SWSS and basal drains. Although loadings seem to show weak tailing on the BTC, concentrations did not follow a clear trend, this is not a surprise given the highly transient flow regime of the BCLs documented in Chapter 3. This irregular behaviour could be a result of the heterogeneous nature of the waste rock pile or possibly indicate the influence of ice on the transport of the tracer.

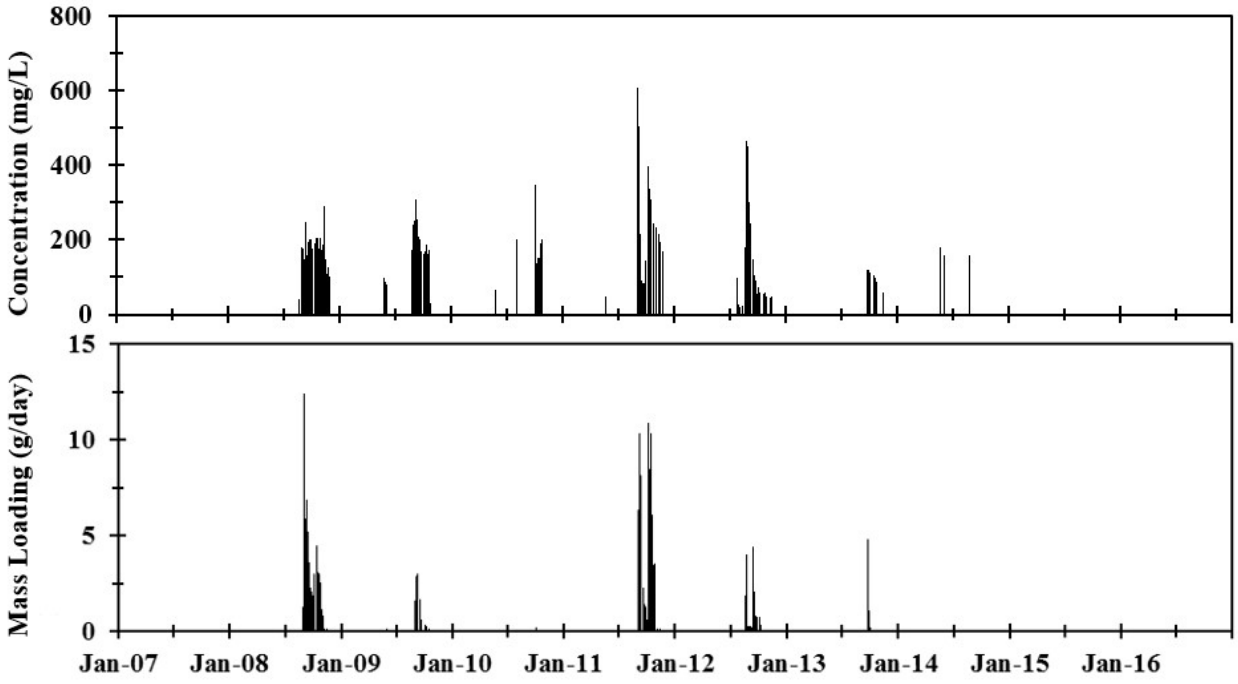

Figure 4.15. Bromide concentrations and mass loading to the BCLs 3BNClys4E and 3BSClys4E.

4.3.4 Cumulative tracer recovery

Annual recoveries of bromide from the BCLs and basal drains are shown in Figure 4.16. After ten years about 46% of the tracer had been recovered. Approximately 18.1 kg of bromide was recovered from the basal drains, representing 40% of the applied mass. Approximately 2.9 kg was recovered from the BCLs, about 6% of the applied mass.

Figure 4.17 shows cumulative recoveries from the drains and BCLs normalized to the amount of bromide applied at surface over the respective area; calculations assume the drains collect water from equal surface areas. These calculations indicate that the South drain recovered approximately 68% of the applied mass within the area from which it receives drainage. Normalized recoveries from combined basal drainage (North plus South) and the BCLs were similar, 47% and 36% respectively. Normalized recovery from the North drain was 18%. These results highlight the variability of tracer recovery from the North and South drains, and BCLs.

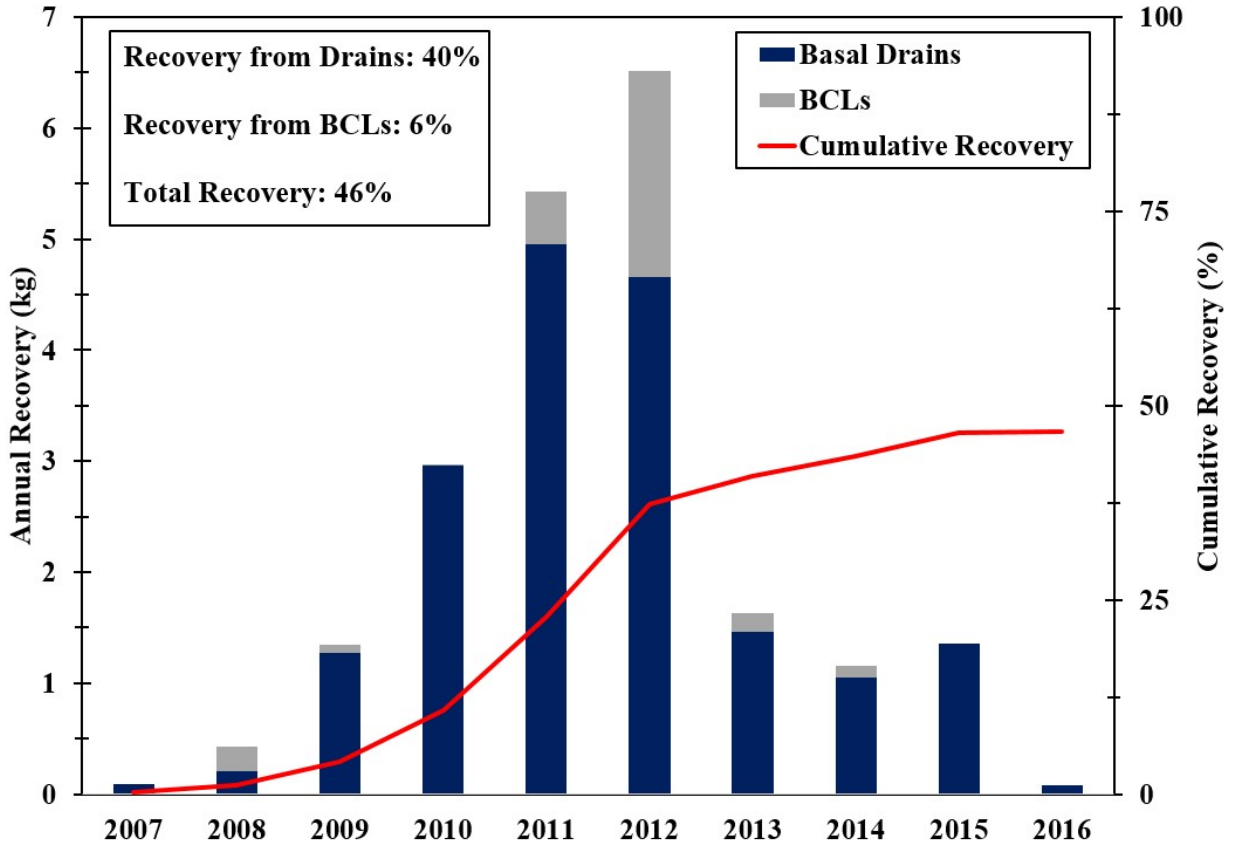

Figure 4.16. Annual and cumulative tracer recovery from BCLs and basal drains.

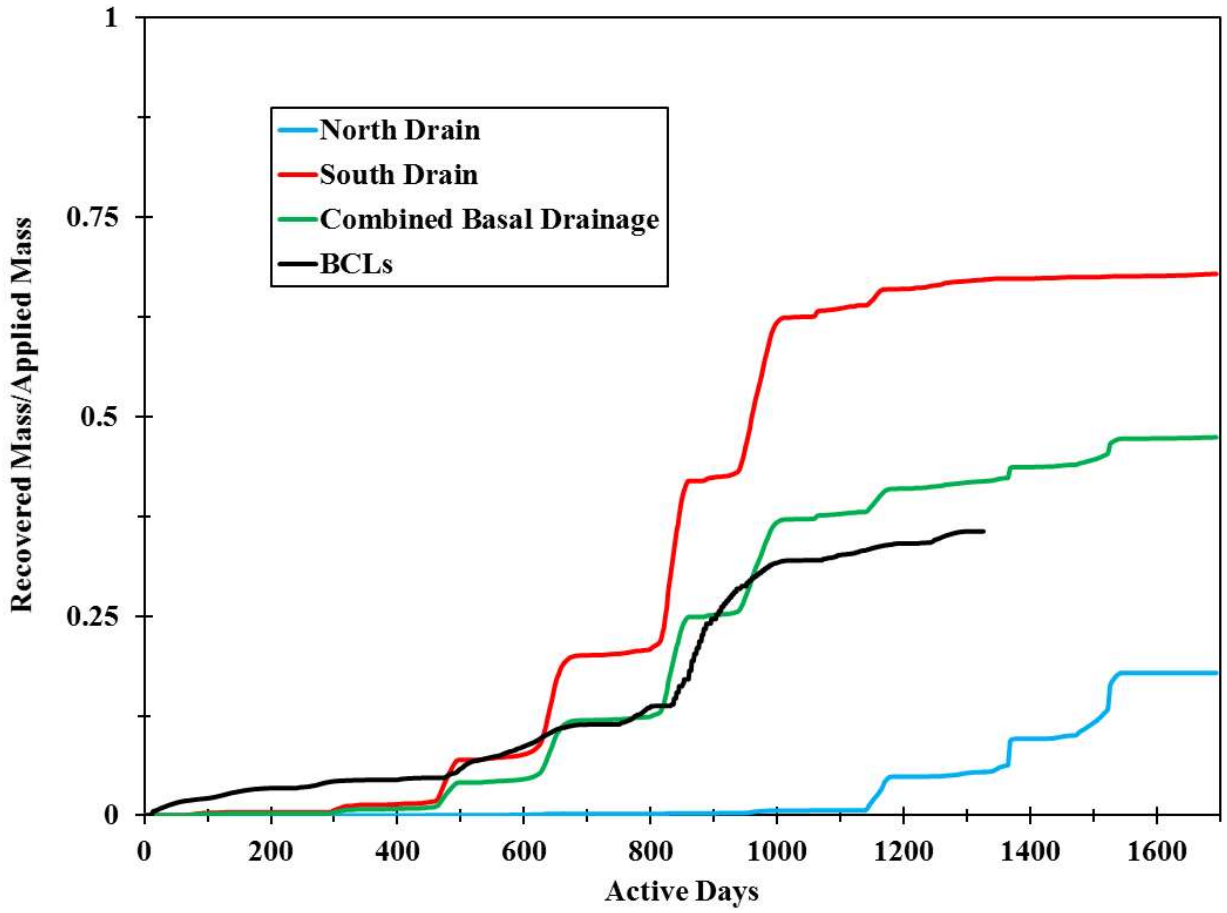

Figure 4.17. Cumulative tracer mass recovered normalized to the applied mass at surface.

4.4 Discussion

4.4.1 Unrecovered tracer

Following ten years of monitoring, approximately 46% of the applied tracer mass has been recovered. The interpretation of these results has direct implications for understanding processes controlling solute transport in waste rock at the field scale. This discussion considers the potential effects of multirate mass transfer and ice formation within the test pile to account for the unrecovered tracer mass. Without evidence provided by a calibrated transport model, which was out of the scope of this work, it is challenging to conclusively determine the significance of

any given process on the solute transport system. This discussion is aimed to develop hypotheses for characterizing solute transport in the test pile. The significance of multirate mass transfer to solute transport can be described quantitatively, however the influence of ice is best discussed conceptually. The approach taken here is to assess tracer concentrations in pore waters in the upper 9 m of the pile where influence ice formation is not anticipated (Chapter 2), with the objective of determining if multirate mass transfer is able to describe the evolution of late time concentrations. Once this has been investigated, late time solute concentrations from the basal drains are assessed. If multirate mass transfer is insufficient to describe the evolution of late time solute concentrations, the possibility of ice formation influencing solute transport is considered. The findings from the applied bromide tracer are compared to those of blasting residuals in order to better reconcile processes influencing solute transport.

4.4.1.1 Multirate mass transfer

The late time behaviour of BTCs has been used to investigate solute transport influenced by dual porosity and multirate mass transfer. Haggerty et al. (2001) completed a comprehensive assessment of the late time behaviour of pulse injection BTCs in a fractured rock aquifer. That study demonstrated that a conventional single rate dual porosity model should display power law behaviour during tailing, having a slope of 1.5 on a double log plot during late time (negative signs have been removed from slopes values for consistency with literature). The 1.5 slope is expected from the single rate dual porosity model given the asymptotic $t^{-1.5}$ dependence in the analytical solution (Tsang, 1995; Hadermann and Heer, 1996). Investigations of late time concentration slopes influenced by multirate mass transfer were observed to display power law slopes steeper (2-3) than those from the dual porosity model. Haggerty et al. (2001) showed that

late time power law slopes steeper than 1.5 are diagnostic of the multirate mass transfer. The caveat of this analysis being, late time behaviour must be caused by diffusion alone, which is a challenging statement to make with certainty (Becker and Shapiro, 2003). Regarding the implementation of this analysis in this paper, it is assumed that the late time BTC behaviour is caused by diffusion alone, the validity of this assumption is addressed later in this discussion. Interpretations are approached with caution since it is challenging to characterize late time behaviour to be caused entirely by diffusion, as well as positively confirm power law behaviour of late time concentrations from a limited time series.

Figure 4.18 shows double log plots of bromide, chloride, and nitrate concentrations obtained from SWSS at various depths over an active timescale (the same thermal correction of time as in section 4.3.3.1). On the y-axis, bromide concentrations have been normalized to the initial concentration of the tracer water. Chloride and nitrate concentrations have been normalized to the respective maximum concentrations observed in SWSS samples. In general SWSS at various depths displayed rising bromide concentrations at early time due to advection, followed by a sustained period of decreasing concentrations which appear to resemble power law behaviour through late time. Similar to bromide, chloride and nitrate displayed late time behaviour resembling power law with slopes consistent with multirate mass transfer. The measured slopes are summarized in Table 4-3, ranging from about 2-3, suggesting that multirate mass transfer may be a significant process involved in solute transport in the upper 9 m of the test pile.

For all solutes, late time slopes determined at 9 m depth were generally lower than those in the 3-7 m range, indicating the diffusion rate coefficient -which is dependent on the solute diffusivity and the diffusive path length- is lower at depth. The cause of this is not fully understood, it may be a result of material segregation with depth. A possibility is the diffusivity may decrease with

depth due to the thermal field. Diffusion coefficients for these solutes at various temperatures obtained from Li and Gregory (1974) are given in Table 4-4. The diffusivities are shown to increase by about 70% from 0ºC to 18ºC. Given the thermal field presented in Figure 4.6C, diffusion rates may decrease with depth. The observed decrease of late time concentration slopes could also be caused by a transport process unrelated to diffusion, such as low velocity pathways for example.

Unfortunately, in cases when the late time slope is less than 3 and power law behaviour is observed beyond the experimental observation time, it is not possible to estimate the characteristic residence time of the immobile zone or quantify transfer rates from these data alone. When the slope is less than 3, the harmonic mean diffusion rate coefficient is controlled by the minimum rate, which cannot be determined from the BTC, preventing the quantification of the residence time. Further investigation using numerical modeling is required to estimate a range of mass transfer rates (Haggerty et al., 2000). However, given these data, the residence time of the immobile zone must be greater than the length of the experiment, 3.2 years (thawed).

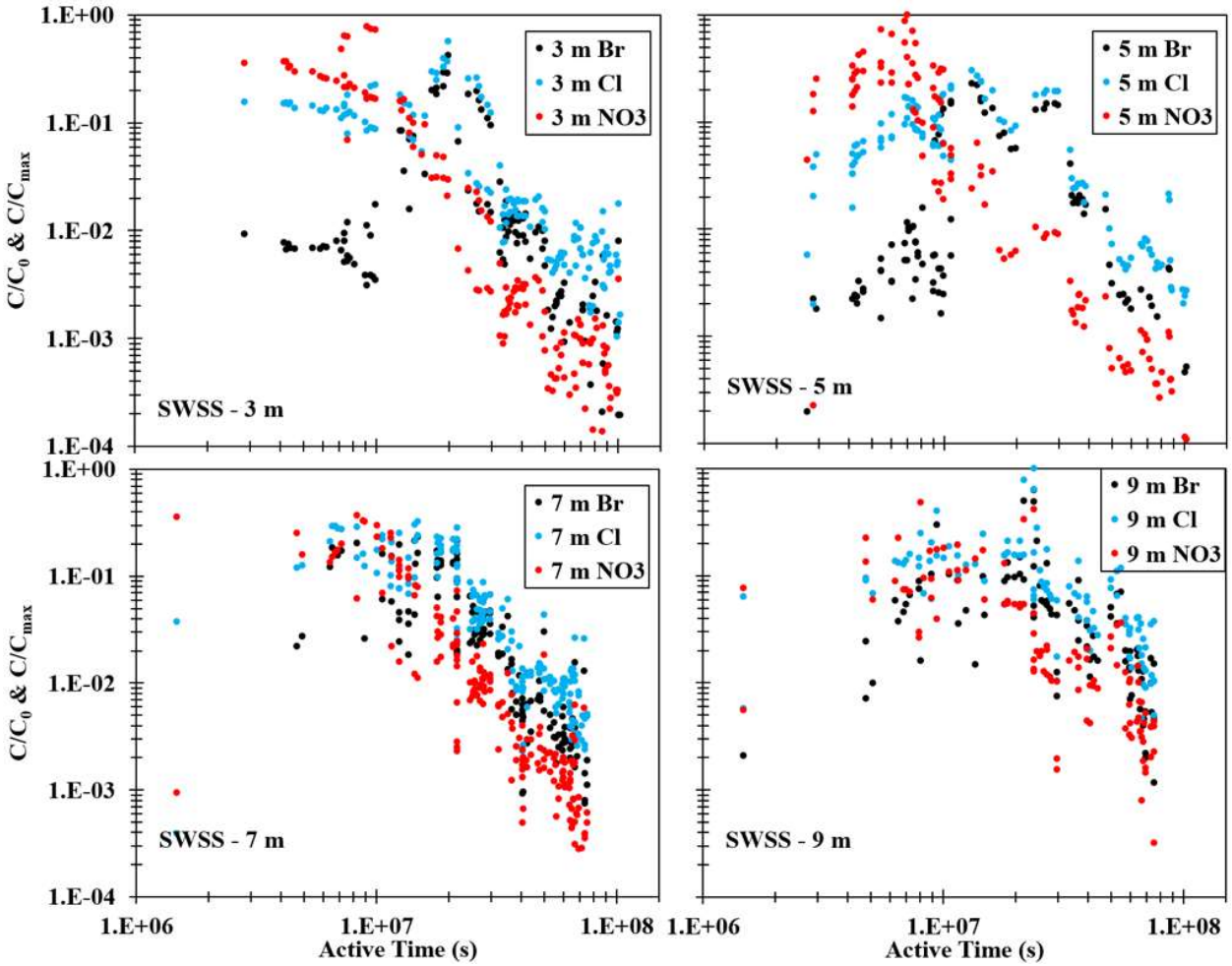

Figure 4.18. Bromide and blasting residual concentrations measured in SWSS, on a double log plot- time has been constrained to periods of above freezing temperatures at the given depth.

Table 4-3. Late time BTC slopes of solute concentrations measured in SWSS.

Depth (m)	Bromide	Chloride	Nitrate
3	2.5	1.3	2.0
5	3.1	2.0	1.9
7	2.9	2.2	2.6
9	2.0	1.5	1.4

Table 4-4. Diffusion coefficients in water at various temperatures (Li and Gregory, 1974).

Solute	Diffusion Coefficient (cm^2/day)	
	0°C	**18°C**
Cl^-	0.87	1.47
Br^-	0.91	1.52
NO_3^-	0.84	1.39

Tracer and blasting residual concentrations from the North, and South drains, and BCLs on double log plots are shown in Figure 4.19 and Figure 4.20. Interpretation of these data are more complicated than the SWSS plots. Concentrations measured from basal drains are influenced by regular freeze-thaw activity causing a variable amount of dilution of core derived waters containing tracer by recharge through the batters. These effects result in oscillating concentrations (Figure 4.14) which scatter the traditional signal for multirate mass transfer. However, it is suggested that late time concentrations measured over a long period of time are adequate to describe the slope of the BTC tail.

Data from the South drain indicates the arrival of the centre of bromide mass dominated by advection, followed by declining concentrations resembling power law behaviour with a slope of 4.3, steeper than slopes observed in SWSS data, however still consistent with multirate mass transfer. Nitrate and chloride concentrations also display behaviour resembling power law, with late time slopes of 4.4 and 3.7. Tracer and blasting residuals from BCLs (3BNClys4E and 3BSClys4E) do not display a well-defined centre of mass arrival, and do not show well-defined tailing according to power law behaviour; therefore, there is not sufficient evidence to suggest multirate mass transfer was the dominant process controlling the evolution of solute

concentrations observed from the BCLs. Similarly, concentrations from the North drain display irregular behavior, with no clear centre of mass arrival or tailing of applied and resident tracers. This suggests that multirate mass transfer is not the dominant process controlling the evolution of solute concentrations from North drain. For clarity, this does not rule out multirate mass transfer as a process influencing concentrations from the BCLs and North drain, rather, another factor has overprinted the multirate signature.

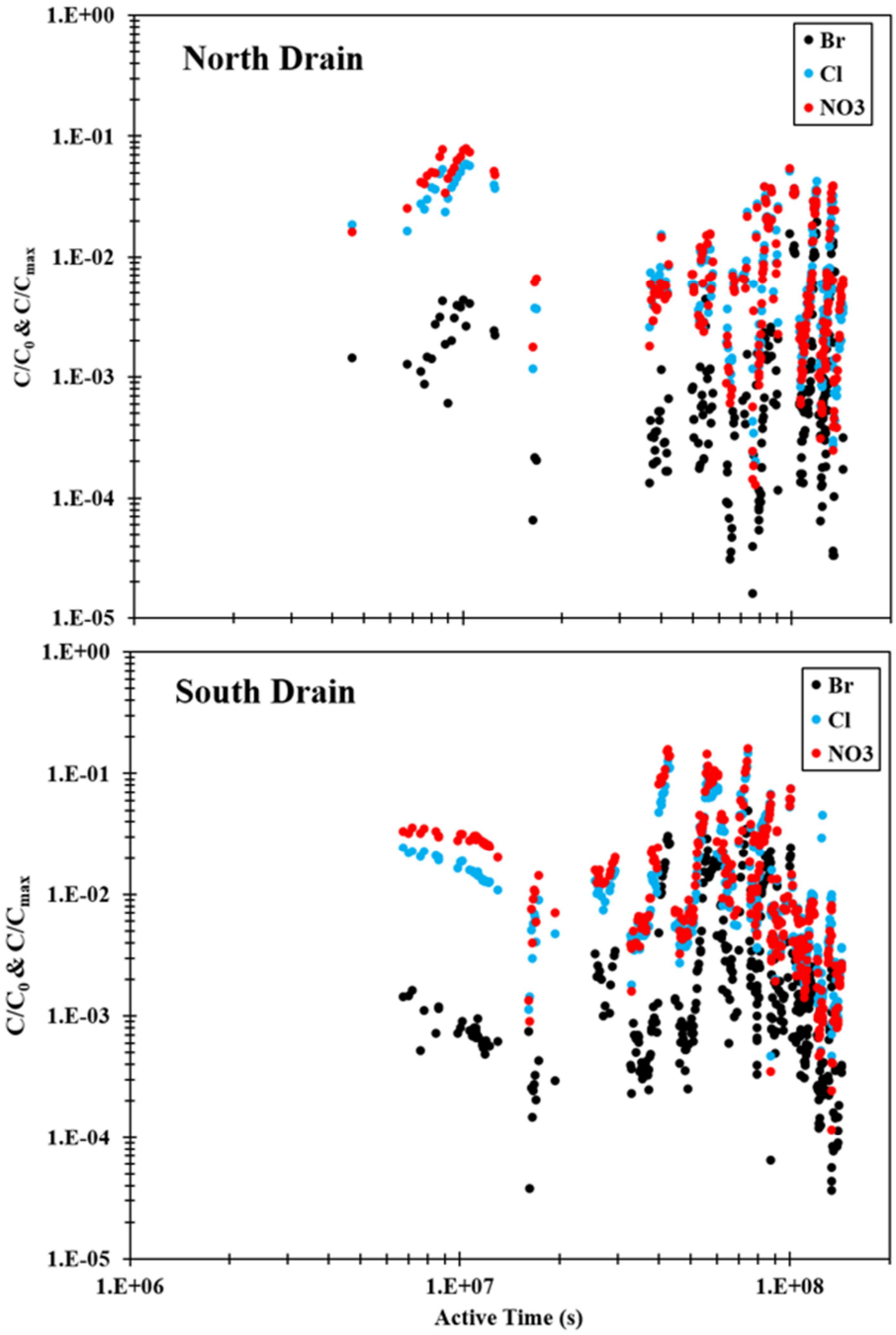

Figure 4.19. Bromide and blasting residual concentrations measured in North and South drains on double log plots- time has been constrained to periods of drainage from the basal drains.

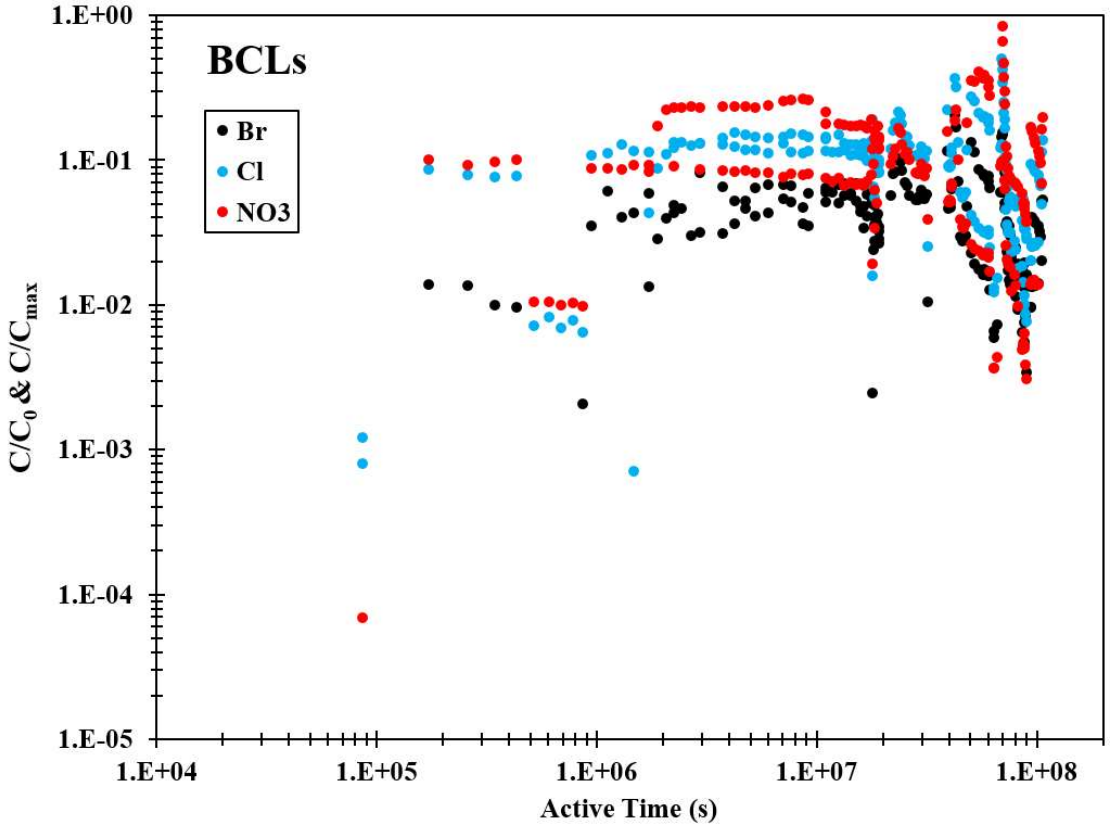

Figure 4.20. Bromide and blasting residual concentrations measured in the BCLs on double log plots- time has been constrained to periods of drainage from the BCLs.

Although the statistical significance has not been evaluated, in the cases where late time concentrations resembled power law behaviour (SWSS and South drain), chloride and nitrate displayed slopes which were generally slightly less than bromide, implying the resident tracers have lower diffusion rate coefficients. If the late time behaviour were strictly due to diffusion, the applied and resident tracers would have displayed near equal slopes given the similarity in the diffusivities (Table 4-4). Therefore, the evolution of late time concentrations cannot be accounted for entirely by the multirate mass transfer model. Considering the distribution of these solutes at time = 0, bromide in the mobile domain and blasting residuals mixed between the mobile and immobile domains; differences in late time behaviour may be partially influenced by

the flow regime, possibly low velocity pathways (heterogeneous advection or macrodispersion). Blasting residuals would display a greater influence from slower velocity pathways than the bromide due to the well mixed initial conditions, resulting in a decrease of late time slope. Without a flow model for the test pile, it is challenging to state that late time behaviour is entirely driven by diffusion.

Evidence for low conductivity regions is provided by the retention of high concentrations in samples collected from 2 m depth during late time. It is possible that these regions may be distributed throughout the pile resulting in a retention of some of the tracer mass. The high rate of tracer application (8 mm/hr) would have activated flow paths which are not normally activated by the low rainfall intensities experienced at Diavik. This could have led to the transport of tracer to low conductivity areas such as shadow zones beneath boulders. Since the existence of these zones is not be adequately represented by the limited number of SWSS, it is difficult to assess the influence on tracer recovery. Assuming low conductivity zones are equally distributed across the North and South halves of the pile, it does not seem reasonable these would have led to the large difference in tracer recovery from the North and South drains.

In order to evaluate if the unrecovered tracer mass (24 kg) can be accounted for by the mass retained in the matrix during tailing, bromide concentrations from SWSS (at 3, 5, 7, 9 m depth) shown in Figure 4.11 were used to approximate the mass of tracer remaining in the pile. Since solute concentrations determined from SWSS are partially dependent on the amount of suction applied, these calculations were completed using data from 2009 to demonstrate that the 45 kg of applied mass can be accounted for using this method. The calculations were completed again using data from 2016 to estimate the mass during late time. For these calculations, the matrix was assumed to occupy 18% of the bulk pile volume, having a porosity of 25% (Fretz, 2013).

Concentrations in 2009 in the upper 9 m were on average approximately 275 mg/L. VMC estimates from TDR show a range of 15-20% (Figure 4.8). These estimates yielded a mass of 40-53 kg bromide in the upper 9 m, 89-118% of the applied mass. For 2016 calculations, VMC measurements and bromide concentrations in the upper 9 m were assumed to represent the full thickness of the pile. An average concentration of 8 mg/L and a VMC range of 15-20% were used. These calculations yielded a mass of 2 kg remaining, about 4% of the applied tracer, which is not consistent with the amount of unrecovered tracer from the basal drains (24 kg). Addressing the error associated with these calculations: Water samples are preferentially collected from the higher mobility advective domain, as discussed by Harvey and Gorelick, (2000) who analyzed tracer test data for an aquifer in Mississippi. The principle presented in that paper, preferential sample collection from a higher mobility domain, would apply to sample collection from an unsaturated waste rock as well. In early time, water with a low concentration of tracer in the low mobility domain is not collected, resulting in an over estimation of concentrations. In contrast, late time concentrations are underestimated since water with low tracer concentrations is preferentially collected from the advective domain, resulting in dilution of mass collected from the diffusive domain. Conceding the error associated with these calculations, the mass of unrecovered tracer from the basal drains is significantly greater than the mass estimated using SWSS (24 kg vs 2 kg). This indicates that the majority of the remaining tracer is not able to be sampled by SWSS, possibly located near the base of the pile, suggesting an additional process is likely responsible for the majority of the unrecovered tracer mass.

4.4.1.2 Ice formation

Deconstruction of the Type I pile revealed significant ice accumulation in the batters. It is anticipated that this led to changes of flow paths within the pile by behaving similar to a barrier to flow (Chapter 2). Evidence for preferential ice formation in North batter of the Type III test pile was provided by the analysis of deuterium and oxygen-18 on drainage. Rainwater discharge from the basal drains was much less than infiltration determined from PM calculations, indicating a significant storage component in the water balance suggesting ice formation (Chapter 3).

The effects of ice formation on the transport of tracer in the Type III pile are difficult to constrain. Solute exclusion studied in the Type I pile was shown to cause concentrations of solutes in ice to be 1-2 orders of magnitude less than those in surrounding pore waters (Chapter 2). This means that in the event of ice formation, bromide would remain mobile, any influence of ice formation on tracer recovery would have resulted from an alteration of the hydrologic domain (disruption of flow paths). Analysis of deuterium excess (Chapter 3) indicated the drainage of waters influenced by repeated freeze-thaw cycles in 2014 and 2015; this was correlated with a period of increased flow from the North drain and interpreted as a significant internal melting event. During this period, increased concentrations of bromide were observed in drainage from the North. This suggests ice accumulation disrupted the flow path preventing water in the core of the pile from reaching the basal drain.

It is proposed that ice formation in the pile influenced the hydrologic regime, possibly by creating a stagnant or low flow region near the base of the pile not able to be sampled by SWSS, resulting in the incomplete recovery of the tracer mass. These effects are most noticeable in the North drain as well as in the BCLs, preventing the arrival of a well-defined centre mass and

tailing of concentrations. Although ice is believed to exist in the vicinity of the South drain, the effects on solute transport are not observable in the evolution of solute concentrations presented in Figure 4.19.

4.5 Conclusions

This paper describes solute transport of applied and resident tracers in waste rock located in a permafrost environment. After ten years of monitoring this tracer test, 54% of the applied mass remains unrecovered. The influences of multirate mass transfer and ice formation were explored to account for the unrecovered tracer mass. The most significant findings from this paper are summarized below:

1. After ten years, approximately 46% of the applied tracer mass (21 kg of 45 kg) was recovered from the waste rock test pile. BTCs from the BCLs, the North and South drains, and SWSS at various depths were variable relative to one another in terms of concentration profiles and cumulative mass recoveries. This variability demonstrates the heterogeneous nature of solute transport in the waste rock pile.

2. The cause of tailing of the BTCs remains inconclusive. Late time concentrations from SWSS and the South drain resembled power law behaviour with slopes indicative of multirate mass transfer, assuming tailing is a result of diffusion, a challenging assumption to justify. The comparison of late time slopes from applied and resident tracers suggests tailing may not be caused entirely by diffusion. The flow regime of the test pile, possibly low velocity pathways, may also influence tailing of the BTCs.

3. Well-defined tailing of BTCs from the North drain and BCLs was not observed. Low tracer recovery from these regions has been attributed to ice formation resulting in a significant influence on flow paths to this drain. Low recovery from the North drain is consistent with earlier interpretations of isotopic analysis stating there may be significant ice formation in the North batter.

4. Solute concentrations from the basal drains demonstrated two peaks annually, early and late flow season (June and October/November). The late season peak indicates maximum contributions from the core to basal drainage. As freezing commences from the base of the pile and batters inwards and high concentrations of solutes become immobilized in the batters. As thawing of the batters progresses the following year, solutes which were previously immobilized in this region become mobile resulting in a spike in concentrations.

5. The transit time (residence time) of the advective or mobile zone was determined to be 2.3 years when thawed. The characteristic residence time of the immobile zone was unable to be determined, however it must be beyond the current experimental timescale, 3.2 years thawed.

6. A general assessment of the behaviour of the applied bromide tracer versus resident tracers indicates similar behaviour of the solutes in the advective domain. The pore water velocity was constrained to 2-3 cm/day using concentrations/loadings from SWSS, BCLs, and basal drains.

7. Anomalously high tracer concentrations during late time in the upper 2 m of the pile indicates the existence of low conductivity zones in the pile. This may represent a lens of fine grained material or a shadow zone beneath boulders. The pervasiveness of these heterogeneities throughout the pile remains unknown.

The reliable prediction of late time concentrations discharged from waste rock piles is particularly important since management times are believed to extend indefinitely in many cases. It is challenging to determine the significance of diffusion to the BTCs presented here. Future modeling of solute transport at the field scale or larger at Diavik should investigate the influence of the flow regime on late time concentrations.

Chapter 5 Conclusions and recommendations

5.1 Conclusions

The intent of this research is to provide an improved hydrologic characterization of waste rock piles located in a permafrost environment. The investigations completed involved long-term datasets from two 14 m tall uncovered waste rock test piles. One of the test piles was deconstructed to better describe ice formation, variability in moisture contents, and internal flow fields. Isotopic analysis was completed to quantify snowmelt infiltration to the batters of one of the piles. Analysis of a tracer test provided insight towards processes influencing the long-term evolution of solute concentrations in drainage. A summary of the most significant conclusions is provided:

1. After ten years of monitoring a tracer test at the Type III pile, an estimated 46% of the applied mass was recovered. A pore water velocity of 2-3 cm/day was constrained. Breakthrough curves from the BCLs, and the North and South drains exhibited high variability relative to one another in terms of concentration profiles and mass loadings. This indicates the highly heterogeneous nature of the solute transport system in the waste rock pile.

2. Hypotheses were developed to explain tailing of solute breakthrough curves. Tailing of concentrations during late time from soil water solution samplers and the South drain appeared to resemble power law with slopes indicative of multirate mass transfer. The comparison of the applied tracer to blasting residuals suggests that tailing may not be

caused entirely by multirate mass transfer. Further work is required to determine the influence of low velocity pathways on late time concentrations.

3. An isotopic mass balance (δD and δ^{18}O) was used successfully to estimate an annual snowmelt infiltration value of about 77 mm to the batters of the Type III test pile. Snowmelt outflow was estimated to represent about 74% of the total annual outflow from the pile, indicating a batter dominated flow system. Early season flow was entirely snowmelt; as thawing of the pile progressed through the summer, larger portions of the pile contributed to drainage and the rainwater component in drainage increased. Peak outflow around September-October remained primarily snowmelt water. Outflow rapidly decreased as freezing progressed from the base and batters of the pile inwards.

4. Extensive ice was observed in the batters of the Type I test pile which experience temperatures above 0^{o}C during the summer months. In contrast, very little ice was observed in the core of the pile, where temperatures below freezing are sustained through the summers. This suggests that regions of ice formation cannot be simply identified by locating areas below 0^{o}C. The distribution of infiltration at surface also plays a significant role in the formation of ice throughout the pile.

5. Rainwater outflow from the basal drains of the Type III pile was significantly less than infiltration estimates, indicating an increase in storage in the pile. This has been interpreted to indicate ice formation, most significantly in the North side of the pile. Deuterium excess in drainage waters indicated the discharge of waters influenced by freeze-thaw cycles, further supporting the existence of ice in the pile.

6. The heterogeneous nature of flow in waste rock at the scale of 2-4 m was demonstrated by BCL water fluxes varying 1-2 orders of magnitude over space and time. Fluxes provided a poor representation of infiltration estimates. Additionally, years of increased infiltration did not always result in increased fluxes from the BCLs.

7. Moisture contents from TDR immediately prior to the deconstruction of the Type I pile were comparable to those observed during deconstruction. This places confidence in the history of moisture contents recorded in the Type I pile by TDR.

8. Preliminary investigation of the distribution of ice in the full scale pile revealed a 1-2 m thick layer located at about 5-10 m depth, continuous through the width of the excavation (>100 m). The nature of the ice appeared to be similar to ice in the batters of the Type I pile.

5.2 Recommendations for future work

This section outlines recommendations for future work to improve characterization of the hydrologic system at the test pile and full scales:

1. The influence of the heat trace system on the thermal regime of the Type III test pile is not understood. This makes it challenging to fully characterize solute transport and ice distribution in the test pile, given the North and South drains behave very differently. In order to better describe the influence of the heat trace on the thermal regime of the pile, the heat trace should be turned off for 1-2 years minimum to fully document any alterations to the thermal and hydrologic behaviour.

2. This thesis presents moisture contents determined from TDR in the Type I and Type III test piles, as well as mapped moisture contents from the Type I test pile. The two piles displayed very different behaviours of moisture, the cause of this is unclear and should be investigated. It is possible that the Type I test pile experienced increased potential evaporation due to a difference in surface material properties. Alternatively, it is possible that the applied rainfall events to the Type III pile created moisture conditions which are not achievable under natural conditions. Another possibility is that ice formation in the batters of the Type I pile effectively "dried" the soil, causing the matric potential to decrease, directing infiltration from beneath the crest outwards to batter regions bypassing TDR.

3. The next phase of the Diavik Waste Rock Project has proposed the installation of several boreholes on the full scale pile. This work should involve the analysis of oxygen and deuterium isotopes in pore waters and ice from drill cores, similar to Barbour et al. (2016). This is required to assess the importance of snowmelt recharge to the pile. Unlike the test piles, snowmelt is likely a more significant source of recharge to the crest of the full scale pile given the overall size.

4. Snowmelt likely is a major component of the water budget in the covered test pile. A similar investigation to the stable isotope work presented here (Chapter 3) should be completed on the covered test pile. Multiple years of spring snow pack measurements have been collected, this could be used to better quantify storage or possible ice

formation in the pile. Furthermore, isotopes in SWSS may provide an improved sense of the significance of rainwater evaporation occurring above the till layer.

5. An attempt was made to quantify the volume of snow on the batters of the Type III test pile using a LIDAR survey completed by the Diavik survey department. This survey yielded an unrealistic volume of snow. An effort should be made to accurately measure the snowpack on the pile to estimate the amount of snowmelt storage as ice in the batters of the pile.

6. Further investigation of the tracer test on the Type III test pile is recommended. In order to test hypotheses developed in this thesis, a calibrated transport model of the pile is required. Given the highly complicated solute loading patterns observed from the basal drains and BCLs. To simplify this model, the focus should be on reproducing tracer and blasting residual late time concentrations in SWSS. Modelling should consider the role of multirate mass transfer which assumes late time concentrations are a result of diffusion, and should also consider macrodispersion, which assumes there is no diffusion at all.

7. It is highly challenging to reconcile tracer tailing between influences from macrodispersion and multirate mass transfer. Future tracer experiments in waste rock material should consider the use of two or more tracers with very different diffusivities, this would be useful to better define the role of diffusion in solute transport.

References

Allison, G.B., 1982. The relationship between 18O and deuterium in water in sand columns undergoing evaporation. J. Hydrol. 55, 163– 169.

Amos, R.T., Blowes, D.W., Bailey, B.L., Sego, D.C., Smith, L., Ritchie, A.I.M. 2014. Waste-rock hydrogeology and geochemistry. Applied geochemistry, vol 57, pp. 140-156.

Amos, R.T., Blowes, D.W., Smith, L., Sego, D.C. 2009. Measurement of wind-induced pressure gradients in a waste rock pile. *Vadose Zone Journal*. v. 8, No. 4, pp. 953-962.

Andrina, J. 2009. Physical and geochemical behaviour of mine rock stockpiles in high rainfall environments. Ph.D. Thesis, University of British Columbia, Department of Mining Engineering.

Atherton, C. 2017. An investigation of heterogenity and the impact of acidic regions on bulk effluent from a deconstructed low sulfide waste-rock pile. M.Sc. Thesis, Department of Earth Sciences, University of Waterloo. 2017.

Bailey, B.L., Blowes, D.W., Smith, L., Sego, D.C. 2015. The Diavik Waste Rock Project: Geochemical and microbial characterization of drainage from low-sulfide waste rock: Active zone field experiments. Applied geochemistry. Vol 62, pp. 18-34.

Bailey, B.L., Smith, L.J.D., Blowes, D.W., Ptacek, C.J., Smith, L., Sego, D.C. 2013. The Diavik Waste Rock Project: Persistence of contaminants from blasting agents in waste rock effluent. Applied geochemistry. Vol 36, pp. 256-270.

Barbour, S.L., Hendry, J.M., Carey, S.K. 2016. High-resolution profiling of the stable isotopes of water in unsaturated coal waste rock. Journal of hydrology. vol 534, pp. 616-629.

Barsi, D. 2017. Spatial variability of particles in waste rock piles. Masters Thesis, University of Alberta, Department of geoenvironmental engineering.

Becker, M.W., and Shapiro, A.D. 2003. Interpreting tracr breakthrough tailing from different forced-gradient tracer experiment configurations in fractured bedrock. Water Resour. Res. Vol 39(1). 1024, doi:10.1029/2001WR001190.

Blackmore, S. 2015. The role of hydrology, geochemistry, and microbiology in flow and solute transport through highly heterogeneous, unsaturated waste rock at various test scales. PhD Thesis, The University of British Columbia, Department of earth, ocean, and atmospheric sciences.

Blackmore, S., Smith, L., Mayer, K.U., Beckie, R.D. 2014. Comparison of unsaturated flow and solute transport through waste rock at two experimental scales using temporal moments and numerical modeling. Journal of contaminant hydrology. Vol. 171, pp. 49-65.

Blowes, D.W., Ptacek, C.J., Jambor, J.L., Weisener, C.G., 2003. The geochemistry of acid mine drainage. In: Holland, H.D., Turekian, K.K. (Eds.), Treatise on Geochemistry. Pergamon, Oxford, pp. 149–204.

Chi, X., Amos, R.T., Stastna, M., Blowes, D.W., Sego, D.C., Smith, L. 2013. The Diavik Waste Rock Project: implications of wind-induced gas transport. Applied geochemistry. Vol 36, pp. 246-255.

Cidu, R., 2011. Mobility of aqueous contaminants at abandoned mine sites: insights from case studies in Sardinia with implications for remediation. Environ. Earth Sci. 64, 503–512.

Clark, I.D., and Fritz, P., 1997. Environmental isotopes in hydrogeology: New York, Lewis Publishers.

Connaughton, D.F., Stedinger, J.R., Lion L.W., Shufer, M.L. 1993. Description of time-varying desorption kinetics: Release of naphthalene from contaminated soils. Environ. Sci. Technol., Vol 27, pp. 2397-2403.

Craig, H., 1961. Isotopic variations in meteoric waters. Science Vol. 133, pp. 1702–1703.

Crawford, J., Hughes, C.E., Lykoudis. 2014. Alternative least squares methods for determining the meteoric water line, demonstrated using GNIP data. Journal of Hydrology, vol 519, part B, pp 2331-2340.

Diodato, D.M., Parizek, R.R. 1994. Unsaturated hydrogeolgic properties of reclaimed coal strip mines. Ground water. Vol. 32(1), pp. 108-118.

Environment Canada, 2012. Monthly Data Report for Ekati A, Northwest Territories. 2013. <http://climate.weatheroffice.ec.gc.ca/climateData/canada_e.html>.

Eriksson, N., Gupta, A., Destouni, G. 1997. Comparative analysis of laboratory and field tracer tests for investigating preferential flow and transport in mining waste rock. Journal of hydrology. Vol 194, pp. 143-163.

Fala, O., Molson, J., Bussiere, B. 2005. Numerical modelling of flow and capillary barrier effects in unsaturated waste rock piles. Mine water and the environment. Vol 24, pp. 172-185. 2005.

Fretz, N. 2013 Multi year hydrologic response of experimental waste rock piles in a cold climate: active zone development, net infiltration, and fluid flow." Master's Thesis, University of British Columbia, Earth Ocean and Atmospheric Sciences.

Friedman, I., Machta, L., Soller, R. 1962. Water-vapor exchange between a water droplet and its environment. Journal of geophysical research, vol 67, No. 7, pp. 2761-2766.

Froehlich, K., Gibson, J.J., and Aggarwal, P. 2002. Deuterium excess in precipitation and its climatological significance: study of environmental change using isotope techniques: Vienna, Austria, International Atomic Energy Agency C&S Papers Series 13/P, p. 54–65.

Gammons, C.H., Poulson, S.R., Pellicori, D.A., Reed, P.J., Roesler, A.J., Petrescu, E.M. 2005. The hydrogen and oxygen isotopic composition of precipitation, evaporated mine water, and river water in Montana, USA. Journal of hydrology. Vol 328, pp. 319-330.

Golder Associates, 2008. Report on 2007 review of baseline climate and surface water hydrology for the Diavik Diamond Mine, prepared by Golder Associates, Burnaby, BC.

Hadermann, J., and Heer, w. 1996. The Grimsel (Switzerland) migration experiment: integrating field experiments, laboratory investigations and modelling. Journal of Contaminant Hydrology. Vol 21, pp. 87-100.

Haggerty R,. S . M. Gorelick. 1998. Modeling mass transfer processes in soil columns with pore-scale heterogeneity. Soil Science. Society. Vol 62(1), pp. 62-74.

Haggerty, R., Fleming, S.W., Meigs, L.C., McKenna, S.A. 2001. Tracer tests in a fractured dolomite 2. Analysis of mass transfer in single-well injection-withdrawal tests. Water resources research. Vol 37(5), pp. 1129-1142.

Haggerty, R., Gorelick, S.M. 1995. Multiple-rate mass transfer for modeling diffusion and surface reactions in media with pore-scale heterogeneity. Water resources research. Vol 31(10), pp. 2383-2400.

Haggerty, R., Harvey, C.F., von Schwerin, C.F., Meigs, L.C. 2004. What controls the apparent timescale of solute mass transfer in aquifers and soils? A comparison of experimental results. Water Resour. Res. Vol. 40 WO1510.

Haggerty, R., S. A. McKenna, L. C. Meigs. 2000. On the late-time behavior of tracer test breakthrough curves, Water Resource. Research. Vol 36(12), pp. 3467-3479.

Hallet, B. 1978**.** Solute redistribution in freezing ground. third international Conference on Permafrost, Edmonton, Alberta, pp: 86-9 1.

Harvey, F.E. 2001. Use of NADP archive samples to determine the isotope composition of precipitation: Characterizing the meteoric input function for use in ground water studies. Ground water, vol 39, No. 3, pp 380-390.

Harvey, F.E., 2005. Stable hydrogen and oxygen isotope composition of precipitation in Northeastern Colorado. Journal of the American Water Resources Association 41, 447–459.

Harvey, F.E., Welker, J.M. 2000. Stable isotopic composition of precipitation on the semi-arid north-central portion of the US Great Plains. Journal of hydrology. Vol 238, pp. 90-109.

Hughes, C.E., Crawford, J. 2012. A new precipitation weighted method for determining the meteoric water line for hydrological applications demonstrated using Australian and global GNIP data. Journal of Hydrology, vol 464-465, pp. 344-351.

Konrad, J.M.m McCammon, A.W. 1990. Solute partitioning in freezing soils. Canadian Geotechnical Journal. Vol. 67, pp. 726-736.

Krentz, A. 2014. The hydrologic behaviour of waste rock piles in the Canadian Arctic. M.Sc. Thesis, Earth Ocean and Atmospheric Sciences, The University of British Columbia.

Lewkowicz, A G., and French, H.M.1982. Downward water movement and solute concentrations in the active layer. Fourth Canadian Permafrost Conference, Calgary, Alberta, pp: 163- 172.

Li, Y.H., Gregory, S. 1974. Diffusion of ions in sea water and in deep sea sediments. Geochemica et cosmmochimica Acta. Vol. 38, pp. 714.

Lorden, S.W., Chen, W., Lion, L.W. 1998. Experiments and modeling of the transport of trichloroethene vapor in unsaturated aquifer material, Eviron. Sci. Techno. Vol 32(13), pp. 2009-2017.

Ma, R., Zheng, C., Prommer, H., Greskowiak, J., Liu, C., Zachara, J., Rockhold, M. 2010. A field-scale reactive transport model for U(VI) migration influenced by coupled multirate mass transfer and surface complexation reactions. Water Resour. Res. Vol. 46, W05509.

Marcoline, J.R. 2008. Investigations of water and tracer movement in covered and uncovered unsaturated waste rock. PhD thesis, The University of British Columbia, Department of Earth and Ocean Sciences.

McCarter, M.K. 1990. Design and operating considerations for mine waste embankments. Society of mining engineers of AIME, pp. 1-10.

Merlivat, L., Jouzel, J. 1979. Global climate interpretation of the deuterium-oxygen 18 relationship for precipitation. Journal of geophysical research, vol 84, pp. 5029-5033.

Momeyer, S.A. 2014. Hydrologic processes in unsaturated waste rock piles in the Canadian subarctic. MSc Thesis, The University of British Columbia, Department of Earth Ocean and Atmospheric Sciences.

Neuner, M. 2009. Water flow through unsaturated mine waste rock in a region of permafrost. Master's Thesis. The University of British Columbia, Earth and Ocean Science.

Neuner, M., Smith, L., Blowes, D.W., Sego, D.C., Smith, L.J.D., Fretz, N., Gupton, M. 2013. The Diavik waste rock project: Water flow through mine waste rock in a permafrost terrain. Applied geochemistry. Vol 36, pp. 222-233.

Nichol, C.F., Beckie, R., Smith, L., 2002. Evaluation of uncoated and coated time domain reflectometry probes for high electrical conductivity systems. Soil Sci. Soc. Am. J. 66, 1454–1465.

Nichol, C.F., Smith, L., Beckie, R. 2003 Time domain reflectometry measurements of water content in coarse waste rock. Candian geotechnical journal. Vol. 40, pp. 137-148.

Nichol, C.F., Smith, L., Beckie, R., 2005. Field scale experiments of unsaturated flow and solute transport in a heterogeneous porous medium. Water Resour. Res. 41, 1–11.

O'Kane, M., Wilson, G.W., Barbour, S.L. 1998. Instrumentation and monitoring of an engineered soil cover system for mine waste rock. Can. J. Geotech. J., vol 35, pp. 828-846.

Orlando, B.A., Ladanyi, B. 1994. Frozen ground engineering. John Wiley & Sons, Inc.

Overduin, P.P. 1997. Soil moisture and soil water solutes during freeze-back at Lake Levinson-Lessing, Taymyr Peninsula, Siberia. M.Sc. Thesis, York University, Department of geography.

Penman, H.L. 1948. Natural evapotranspiration from open water, bare soil, and grass. Proceedings of the Royal Society of London, Series A, No. 193, pp. 120–145.

Pham, N.H. 2013a. Heat transfer in waste-rock piles constructed in a continuous permafrost region. PhD Thesis, University of Alberta, Department of civil and environmental engineering. 2013.

Pham, N.H. 2013b. Personal communication. Research group memo.

Pham, N.H., Sego, D.C., Arenson, L.U., Blowes, D.W, Amos, R.T., Smith, L. 2013. The Diavik Waste Rock Project: Measurement of the thermal regime of waste-rock test pile in a permafrost environment. Applied geochemistry. Vol 36, pp. 234-245.

Rasmussen T.C., Baldwin Jr., R.H., Dowd, J.F., Williams, A.G., 2000. Tracer vs. pressure wave velocities through unsaturated saprolite, Soil Sci. Soc. of Am. J., v. 64(1) pp. 75-85.

Richards, L.A. 1931. Capillary conduction of liquids through porous mediums. Journal of Applied Physics 1, 318–333.

Sinclair, S.A. 2014. Influence of freeze-thaw dynamics and spatial contributions on geochemical loading from a low sulphide waste-rock pile. M.Sc thesis. University of Waterloo, Department of Earth Sciences.

Sinclair, S.A., Pham, N., Amos, R.T., Sego, D.C., Smith, L., Blowes, D.W. 2015. Influence of freeze-thaw dynamics in internal geochemical evolution of low sulfide waste rock. Applied geochemistry. Vol. 61, pp. 160-174.

Smith, L., Lopez, D.L., Beckie, R., Morin, K., Dawson, R., Price, W.A. 1995. Hydrogeology of Waste Rock Dumps, British Columbia Acid Mine Drainage Task Force.

Smith, L.J.D., Bailey, B.L., Blowes, D.W., Jambor, J.L., Smith, L., Sego, D.C., 2013a. The Diavik Waste Rock Project: initial geochemical response from a low sulfide waste rock pile. Appl. Geochem. 36, 210–221.

Smith, L.J.D., Moncur, M.C., Neuner, M., Gupton, M., Blowes, D.W., Smith, L., Sego, D.C., 2013b. The Diavik waste rock project: design, construction and instrumentation of field-scale experimental waste rock piles. Appl. Geochem 187–199.

Sracek, O., Choquette. M., Ge´linas, P., Lefebvre, R., Nicholson, R.V. Geochemical characterization of acid mine drainage from a waste rock pile, Mine Doyon, Quebec, Canada. 2004. Journal of contaminant hydrology. v. 69, pp. 45-71.

Stager, M.P., and Perram, G.P. 1999. Long-term desporption of trichloroethylene from fine clay using multiplexed optical detection. Environ. Poll. Vol 104(3), pp. 347-400.

Steig RJ, Fitzpatrick JJ, Porter N Jr, Clark DH. 1998. The geochemical record in rock glaciers. Geografiska Annaler 80A: 277–286.

Taylor, J.R., 1997. An introduction to error analysis: The study of uncertainties in physical measurements, 2d ed.: Sausalito, Calif., University Science Books, pp. 327.

Tsang, Y.W. 1995. Study of alternative tracer test in characterizing transport in fractured rocks. Geophysical research letters, Vol. 22, No. 11, pp. 1421-1424.

Wagner, K., Smith, L., Beckie, R., 2006. Hydrogeochemical characterization of effluent from mine waste rock, Cluff Lake, Saskatchewan. In: Proceedings of the7th International Conference on Acid Rock Drainage, St. Louis, MO, USA.

Welker, J.M. 2000. Isotopic (d18O) characteristics of weekly precipitation collected across the USA: an initial analysis with application to water source studies. Hydrol. Processes. Vol 14, pp. 1449-1464.

Williams, M.W., Knauf, M., Caine, N., Liu, F., Verplanck., P.L. 2006. Geochemistry and source waters of rock glacier outflow, Colorado Front Range. Permafrost and periglac. Process. Vol 17, pp. 13-33.

Appendix A Type III BCL Temperatures

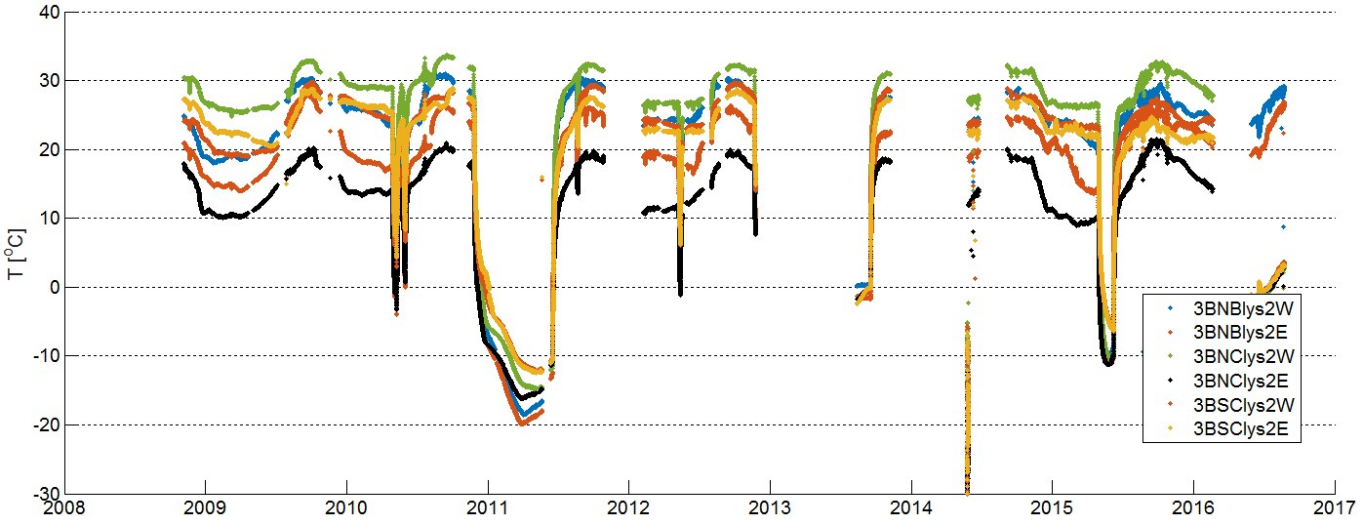

Figure A.1. Temperature history of Type III BCLs with functional heat trace.

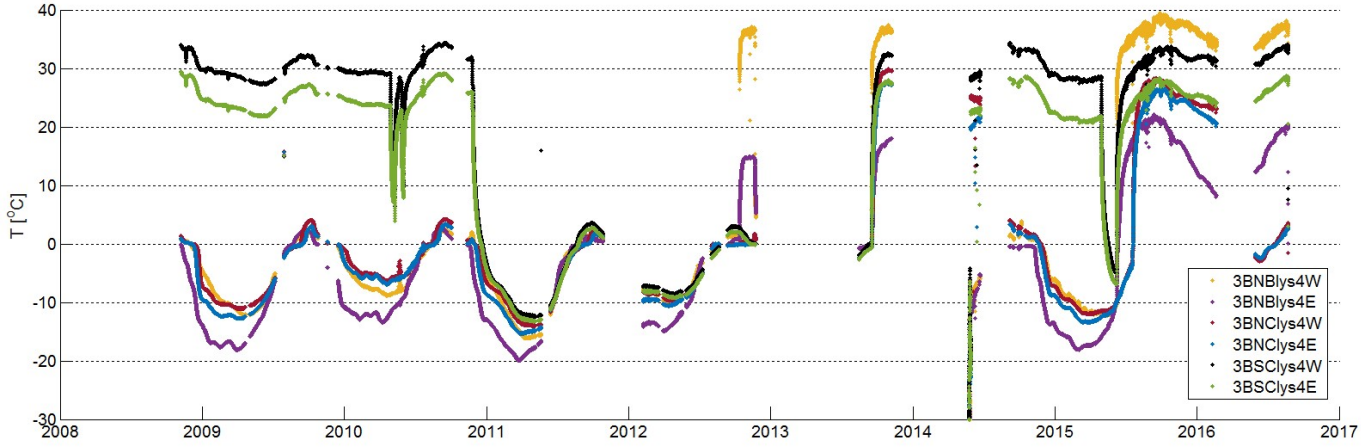

Figure A.2. Temperature history of Type III BCLs with unreliable heat trace.

Appendix B Hydrology Dataset

B.1 Type III pile

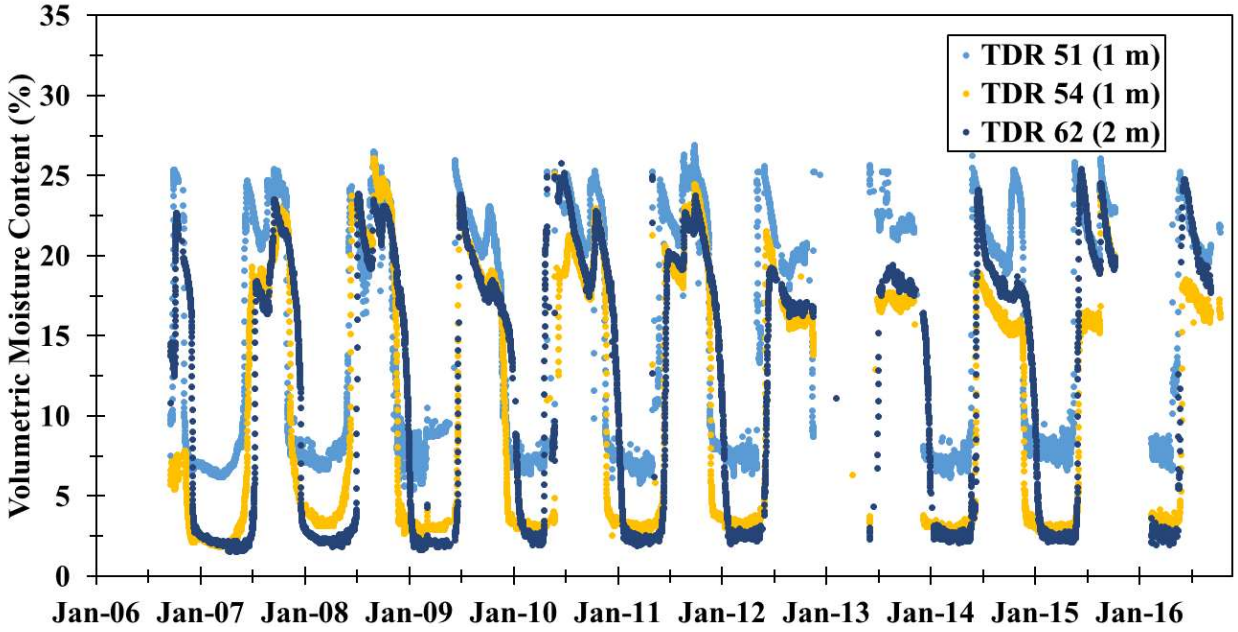

Figure B.1. TDR in the Type III test pile, 1 m depth.

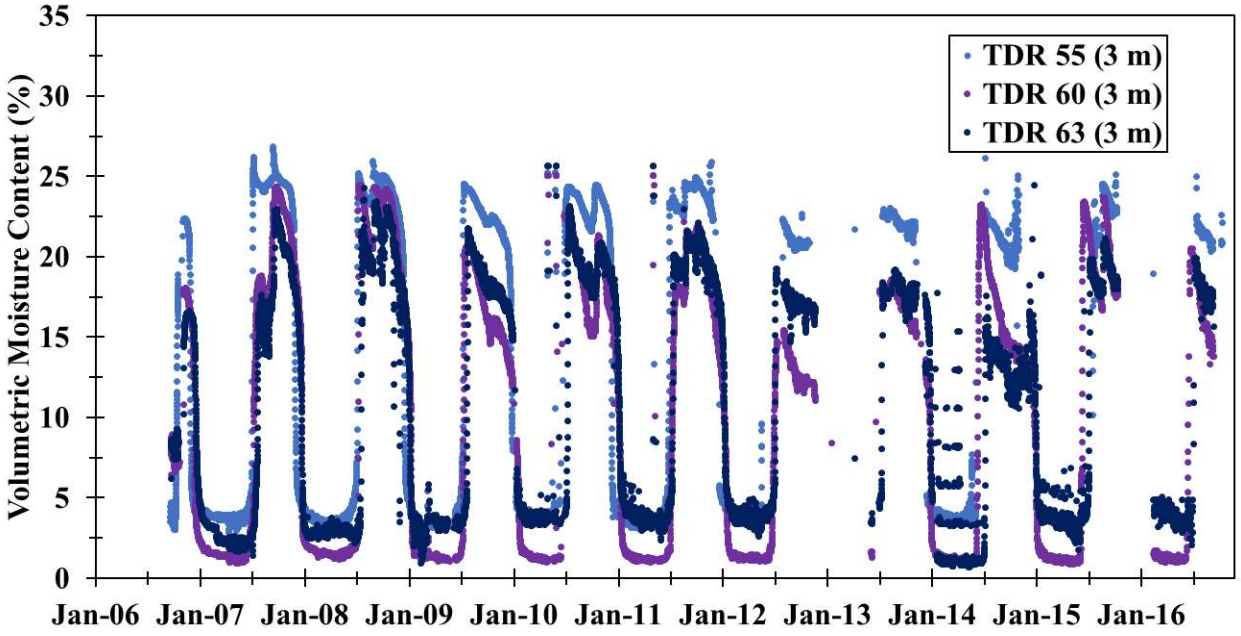

Figure B.2. TDR in the Type III test pile, 3 m depth.

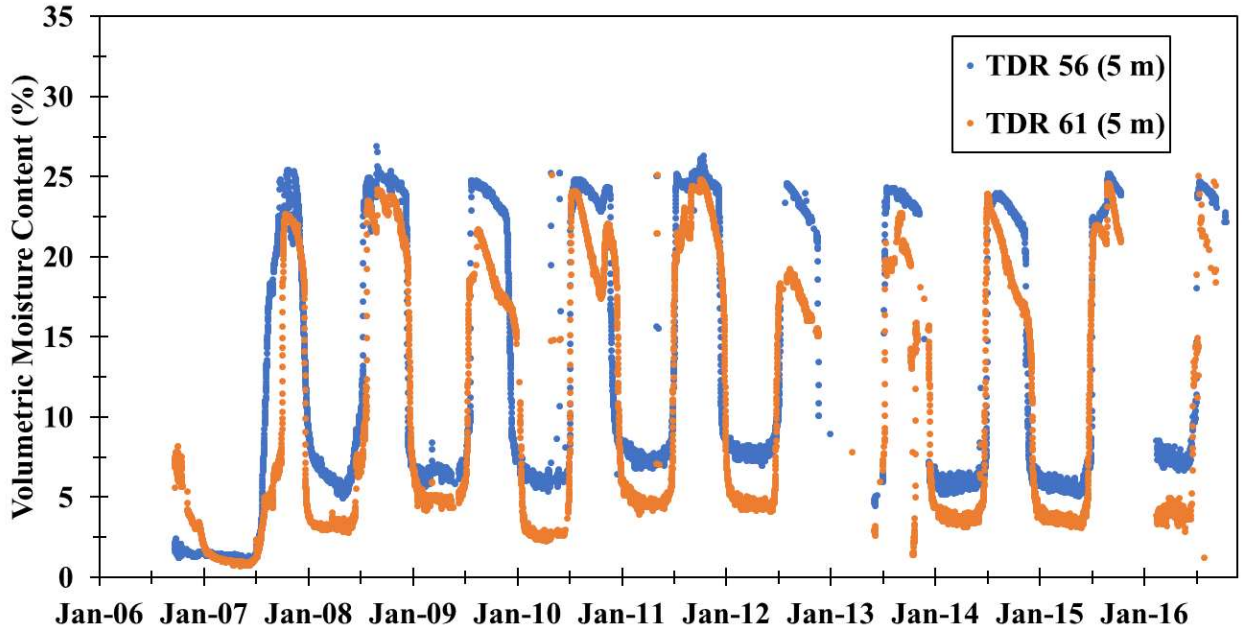

Figure B.3. TDR in the Type III test pile, 5 m depth.

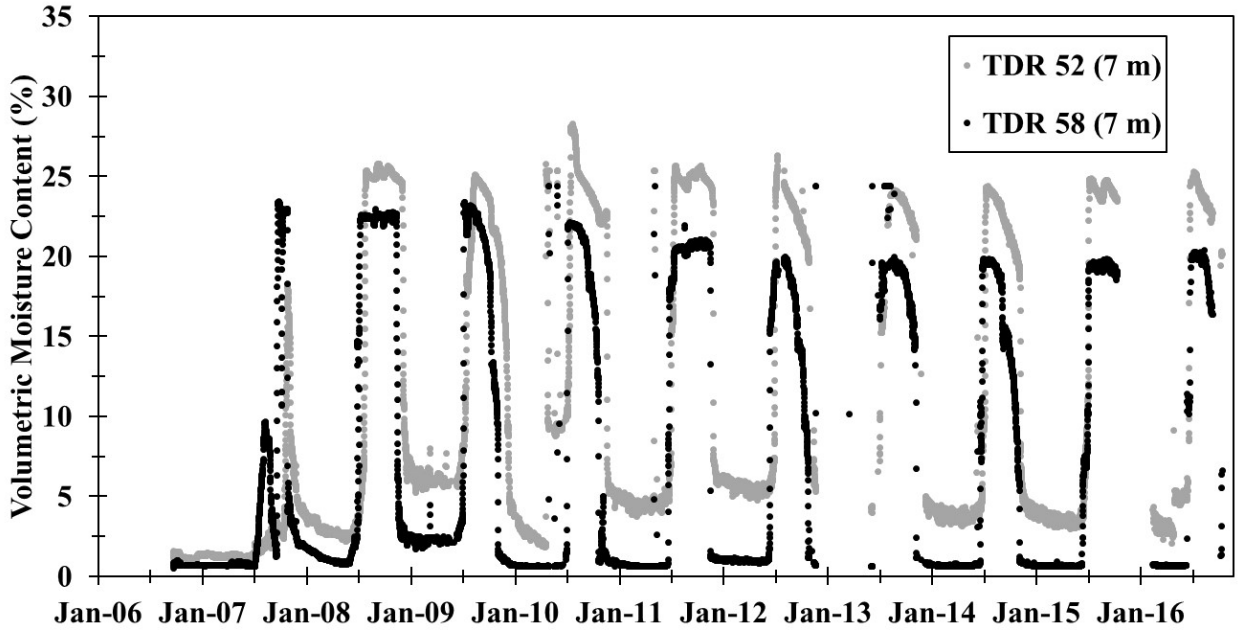

Figure B.4. TDR in the Type III test pile, 7 m depth.

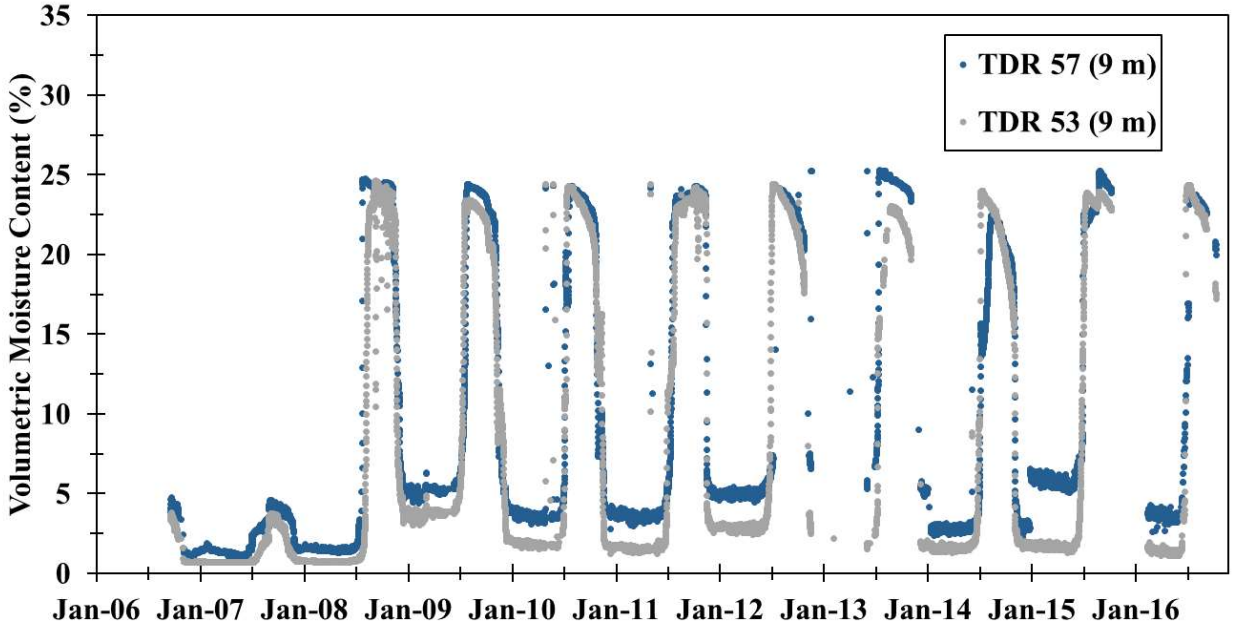

Figure B.5. TDR in the Type III test pile, 9 m depth.

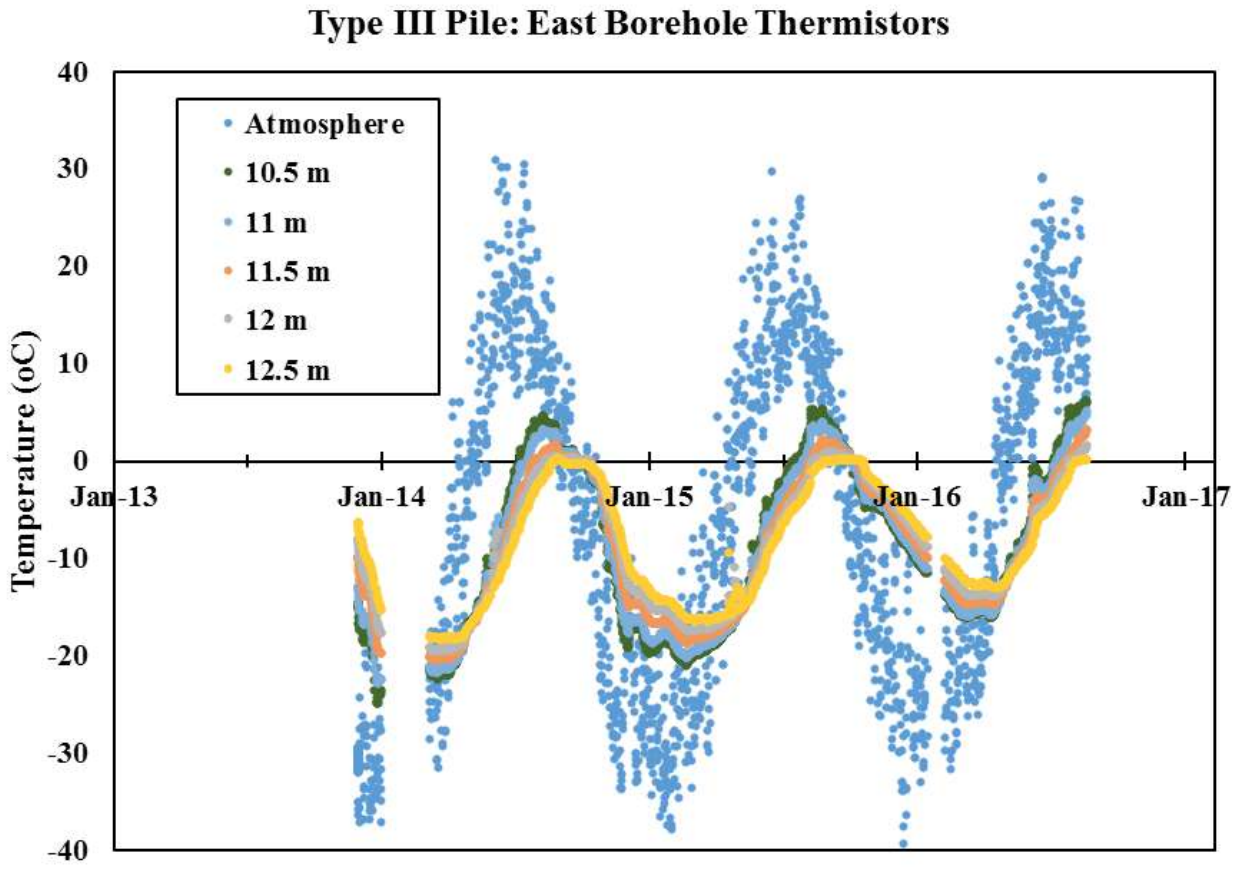

Figure B.6. East borehole thermistor readings near the base of the Type II test pile.

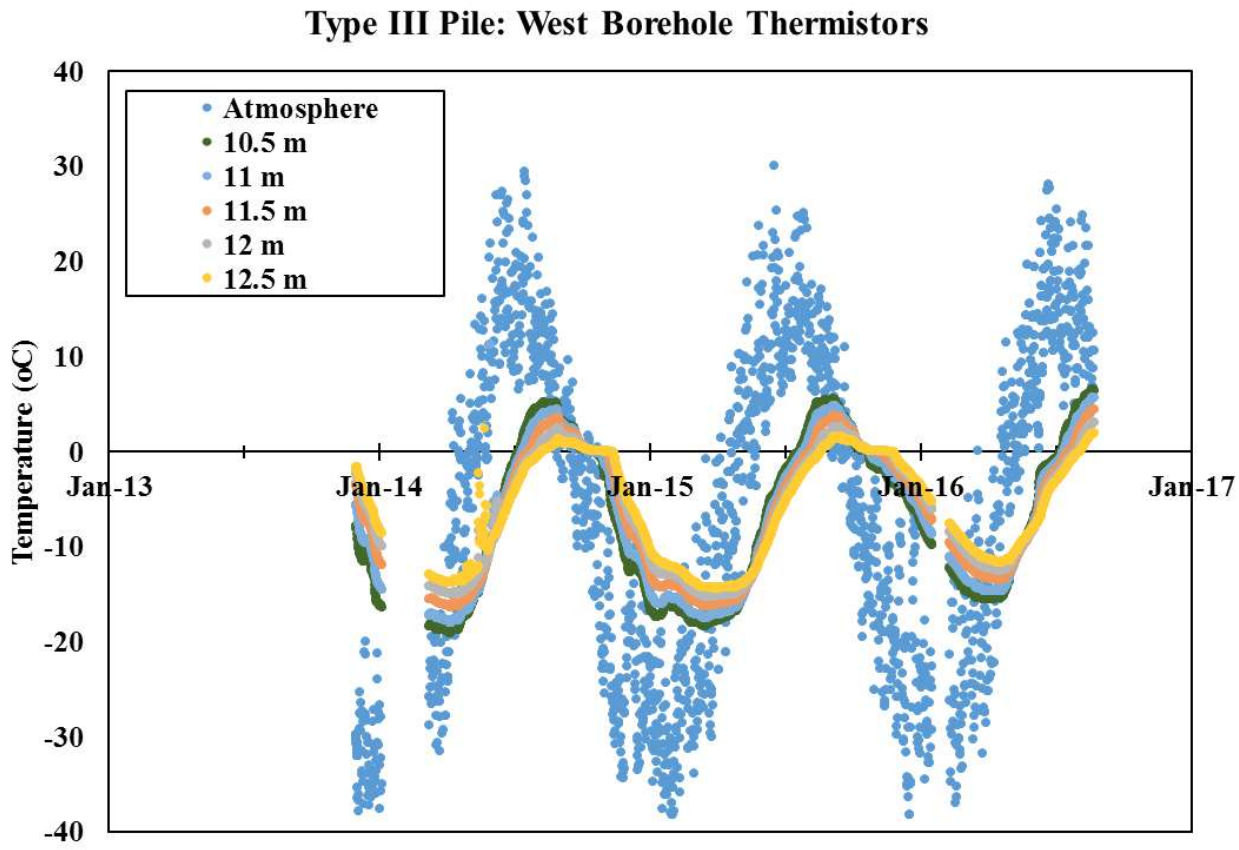

Figure B.7 West borehole thermistor readings near the base of the Type II test pile.

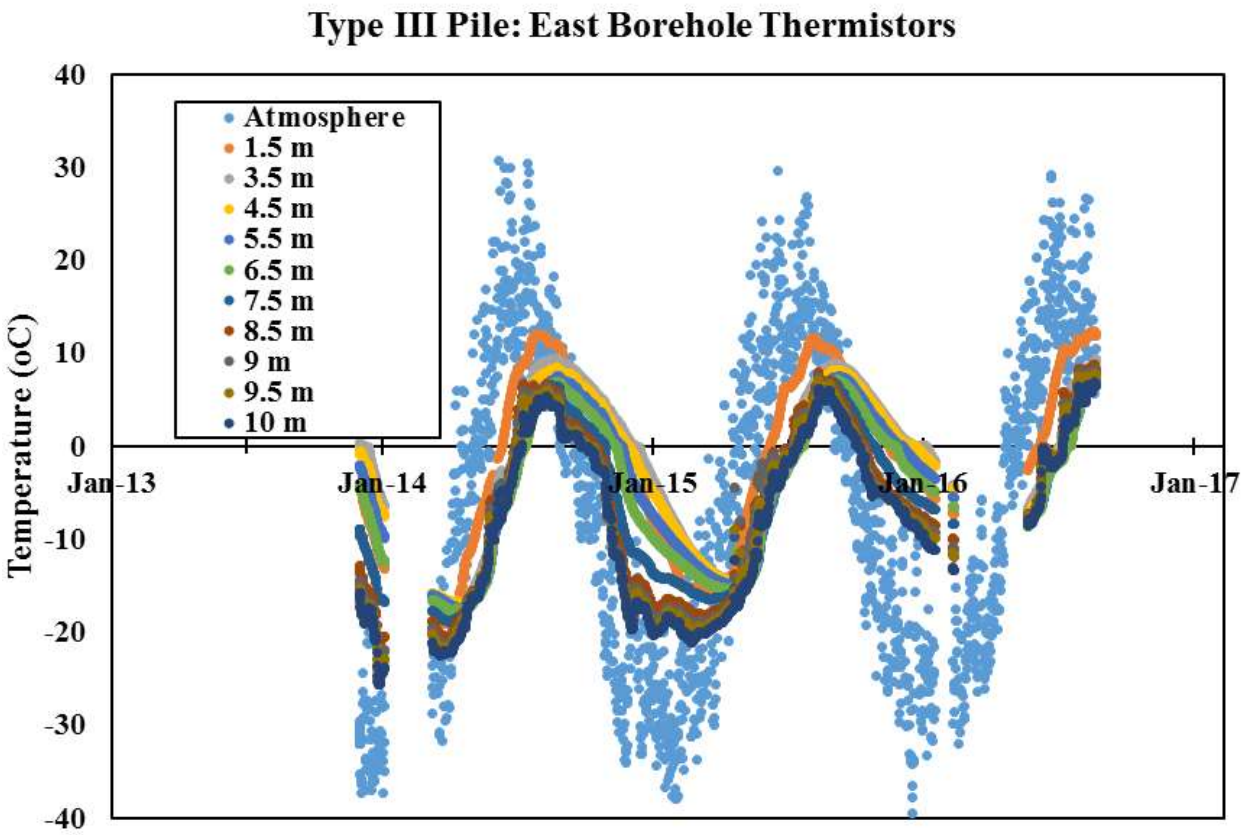

Figure B.8. East borehole thermistors readings in Type II test pile.

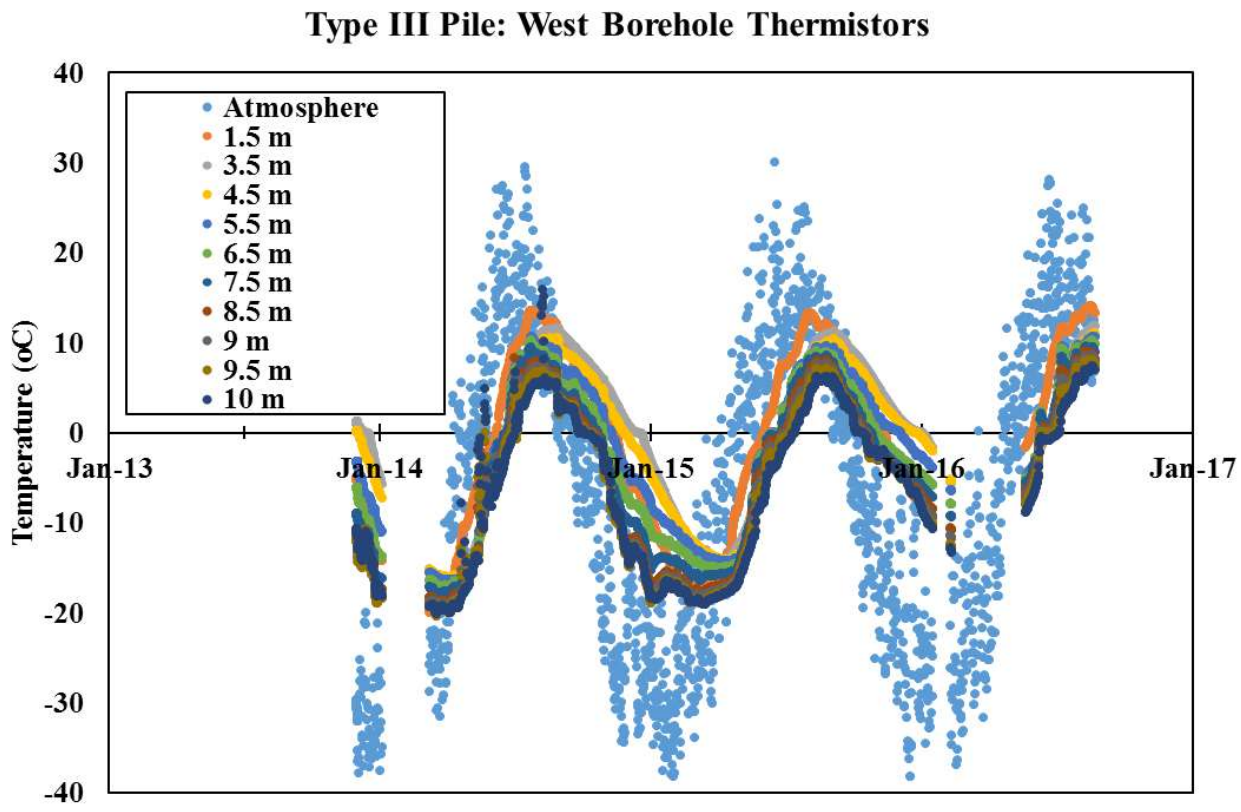

Figure B.9. West borehole thermistors readings in Type II test pile

B.2 Covered pile

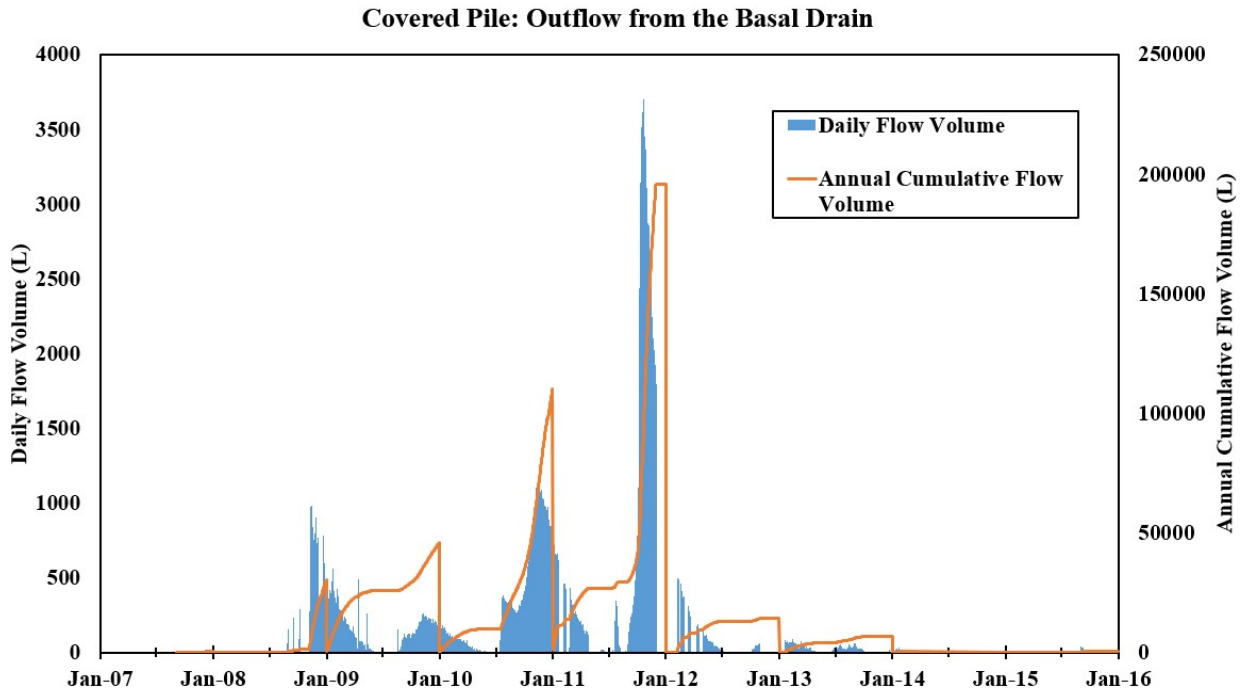

Figure B.10. Daily outflow and cumulative outflow from the covered pile basal drain.

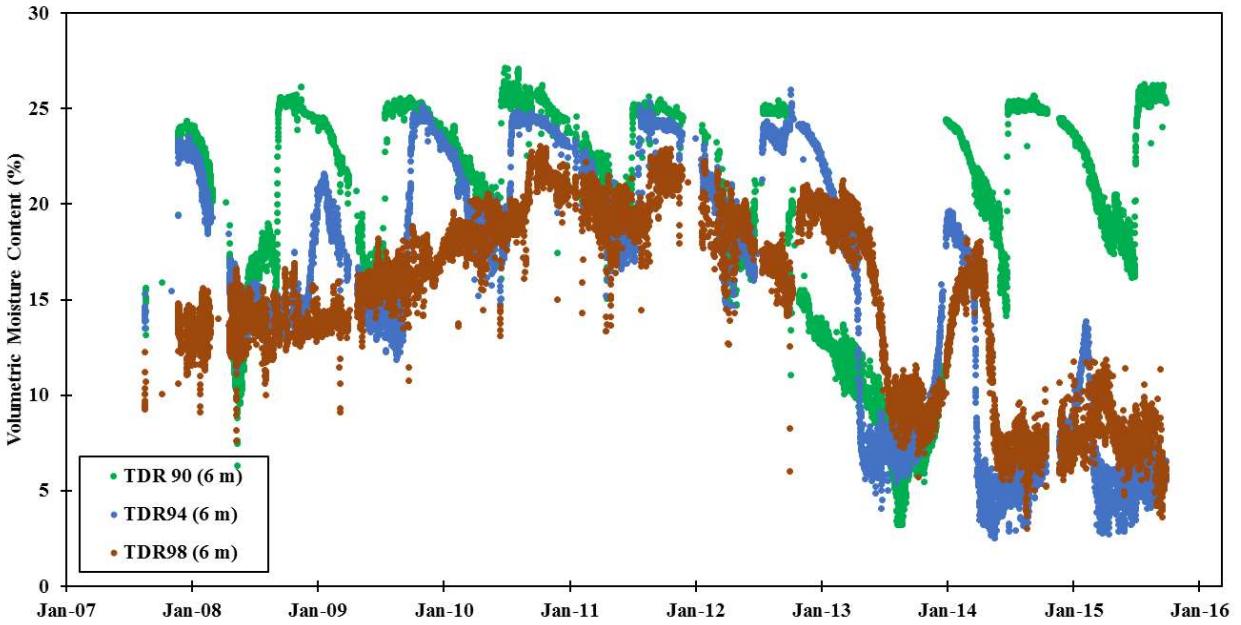

Figure B.11. TDR in the covered test pile, 6 m depth.

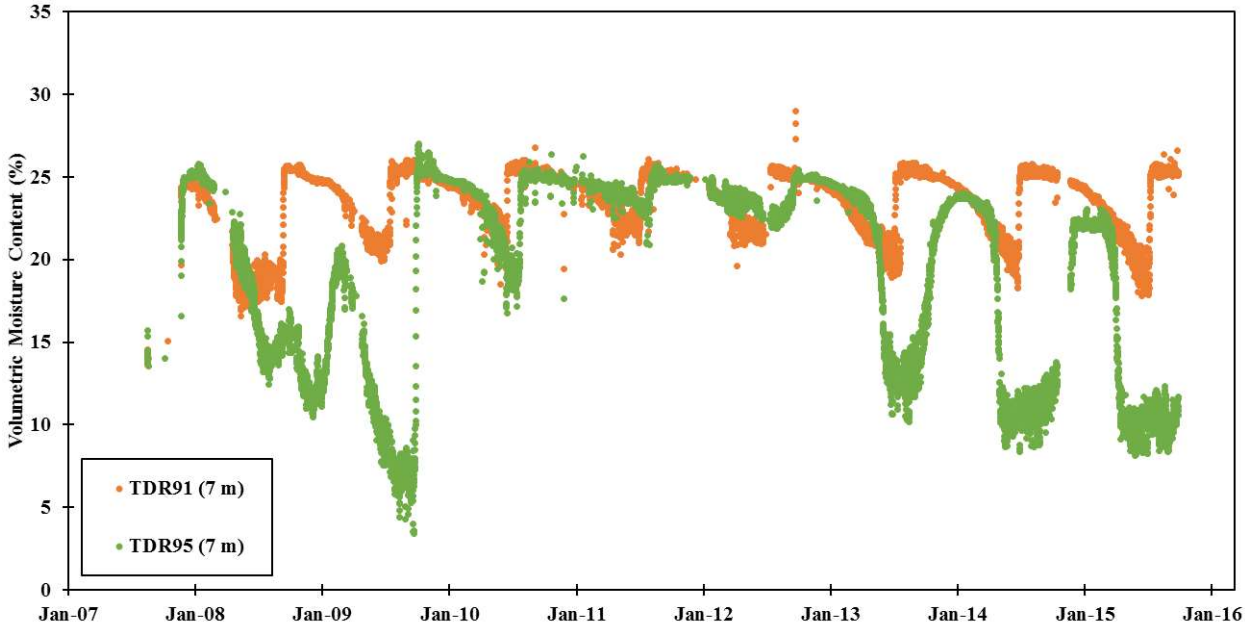

Figure B.12. TDR in the covered test pile, 7 m depth.

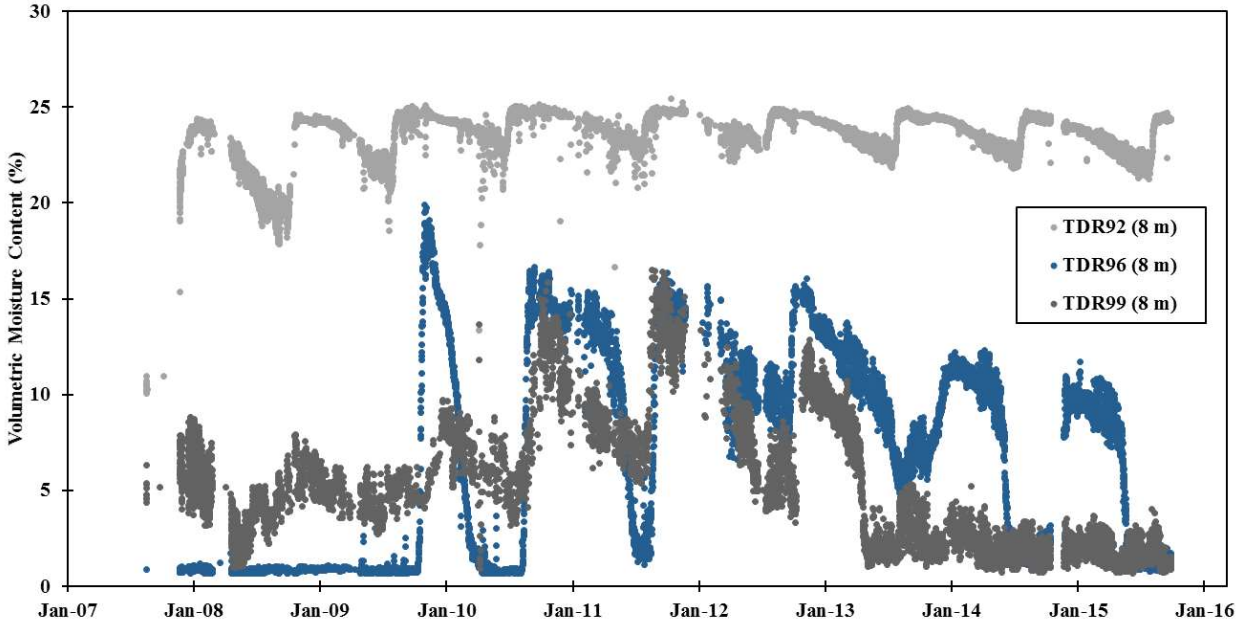

Figure B.13. TDR in the covered test pile, 8-9 m depth.

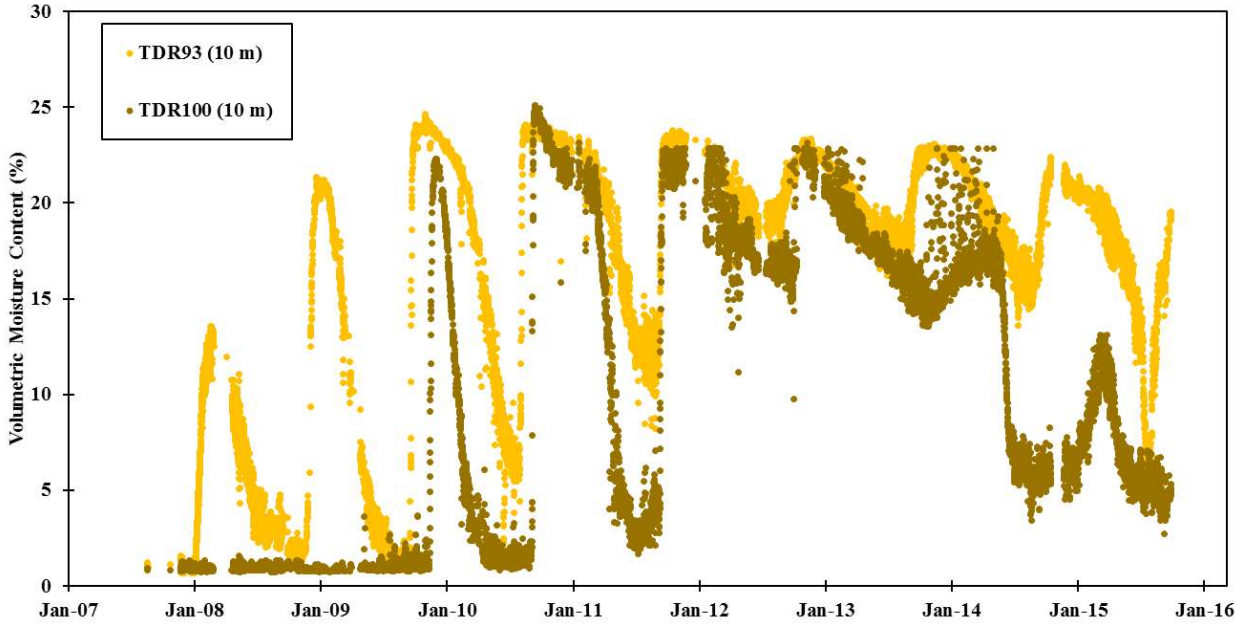

Figure B.14. TDR in the covered test pile, 10 m depth.

B.3 Active zone lysimeters

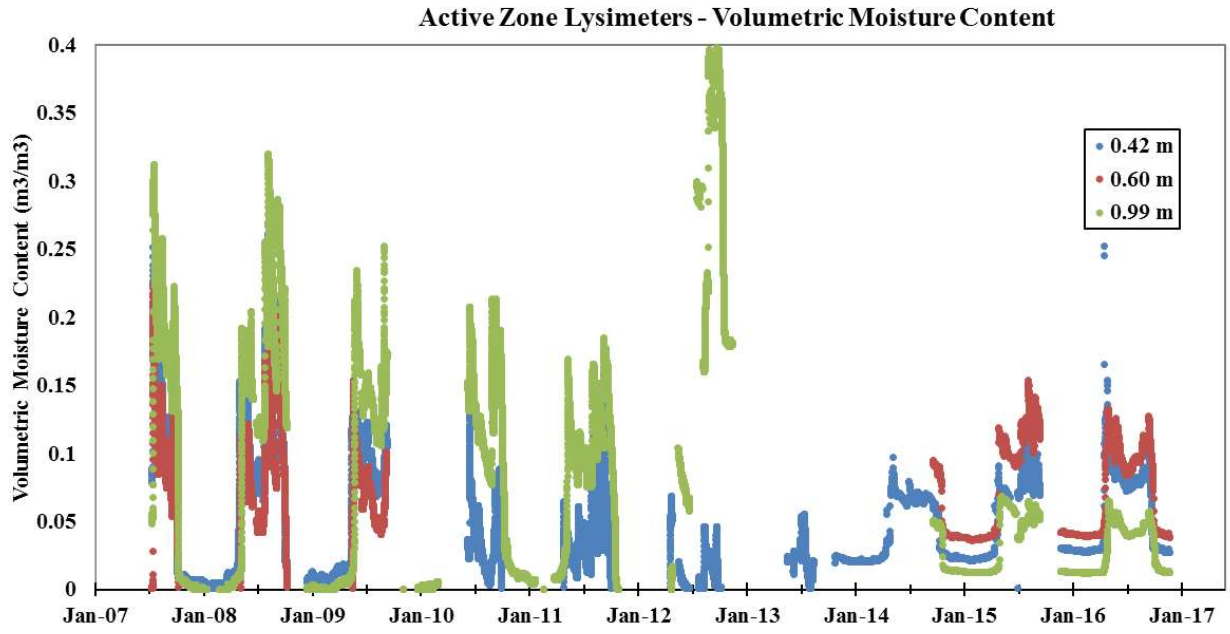

Figure B.15. Volumtric moistire contents at the AZLs, from ECH2O probes.

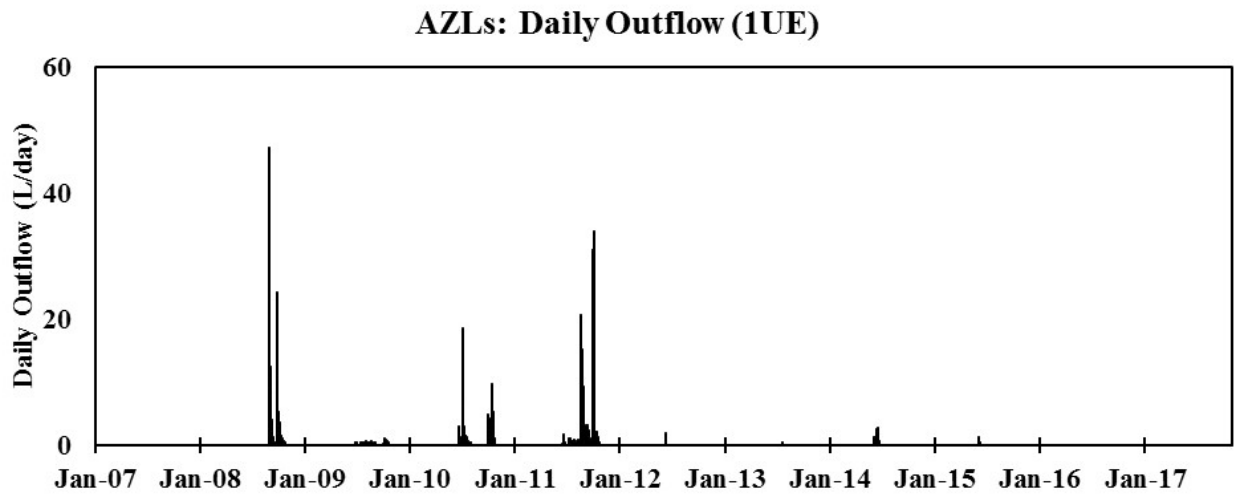

Figure B.16. Daily outflow from AZL 1UE.

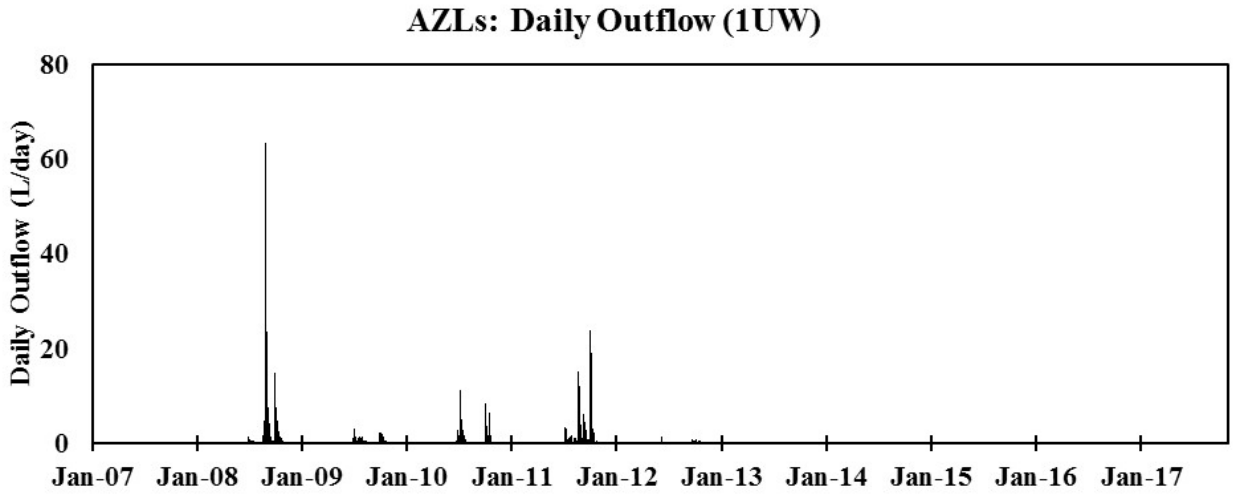

Figure B.17. Daily outflow from AZL 1UW.

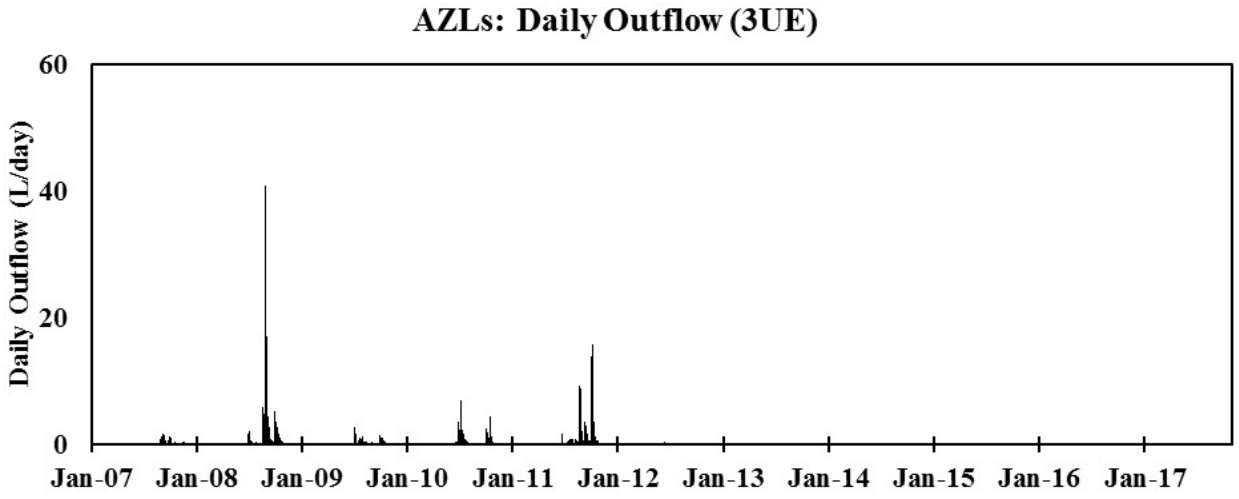

Figure B.18. Daily outflow from AZL 3UE.

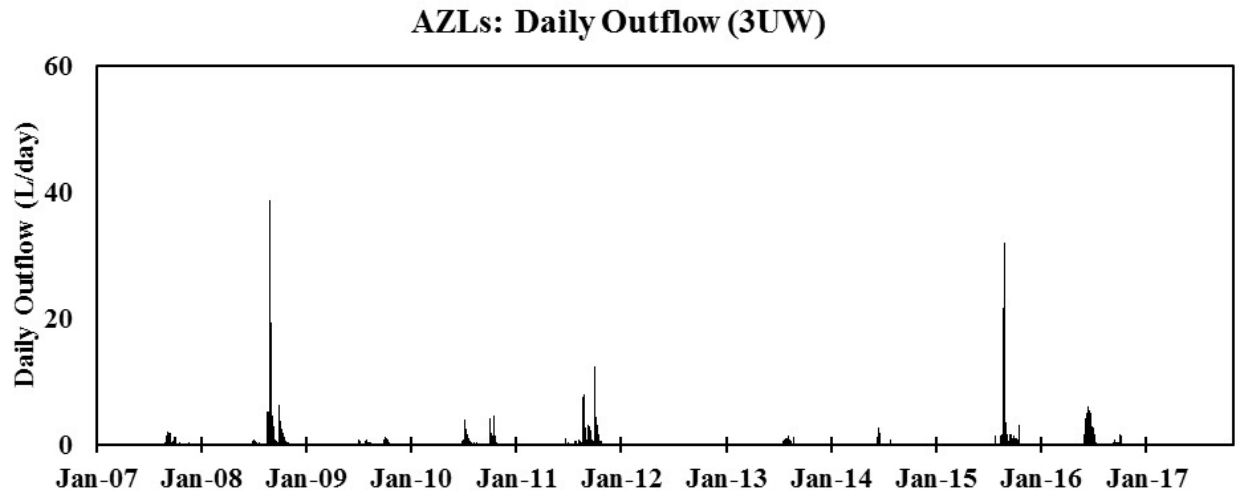

Figure B.19. Daily outflow from AZL 3UW.

B.4 Full scale pile

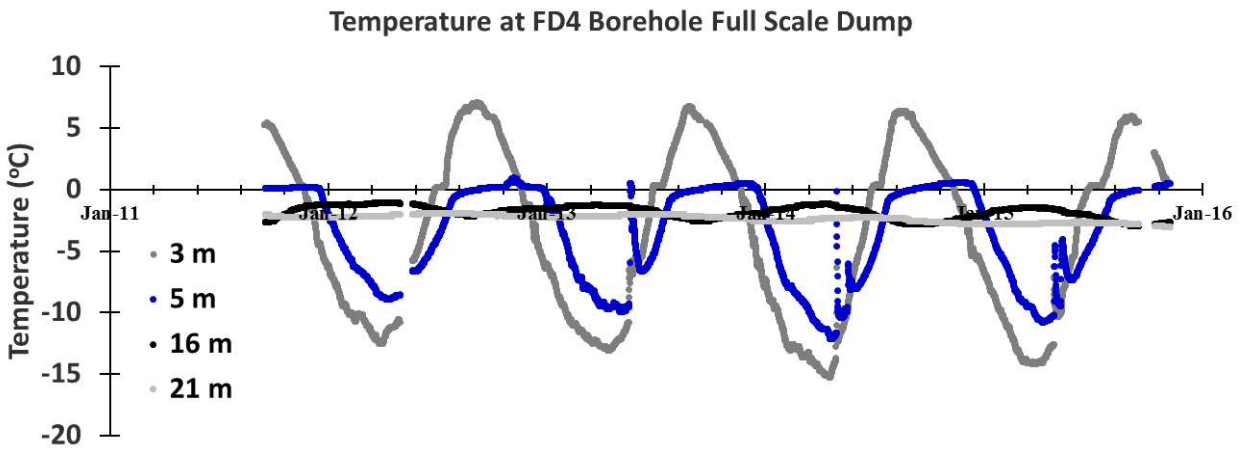

Figure B.20. Temperatures obtained from an ECH2O probe in borehole FD4 located on the full scale pile.

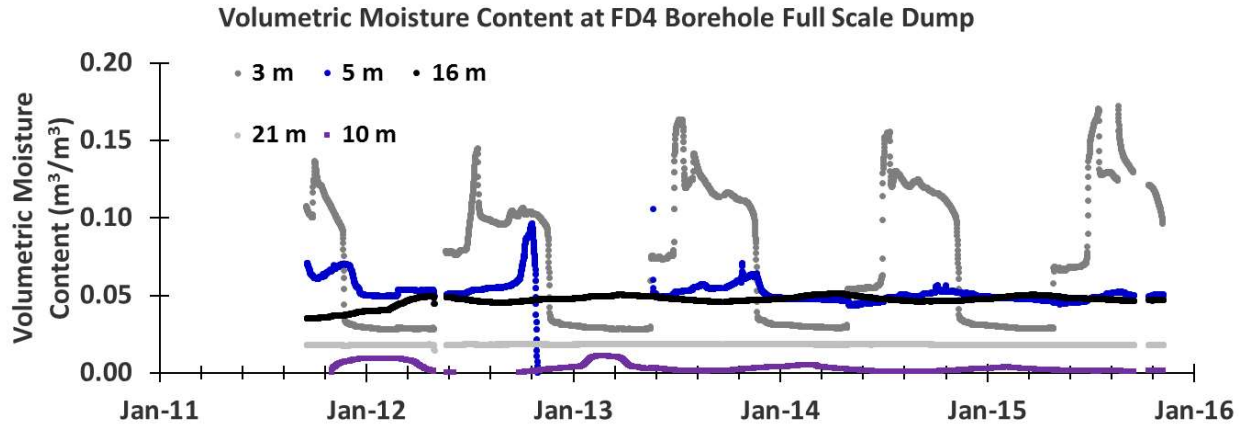

Figure B.21. Volumetric moisture contents obtained from an ECH2O probe in borehole FD4 located on the full scale pile.

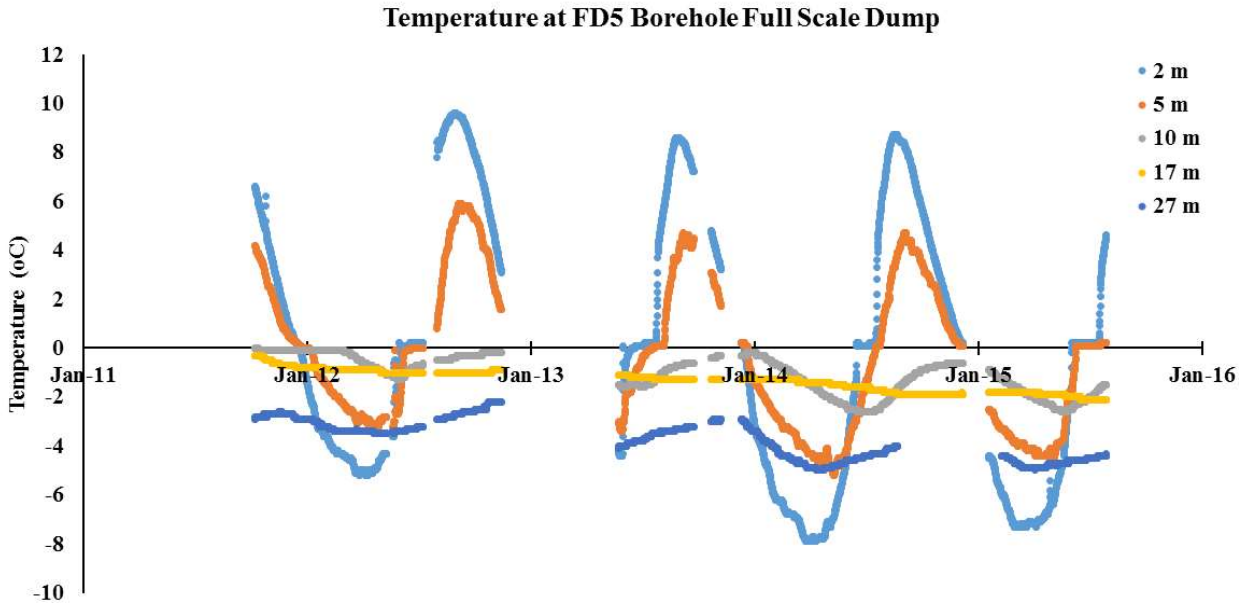

Figure B.22. Temperatures obtained from an ECH2O probe in borehole FD5 located on the full scale pile.

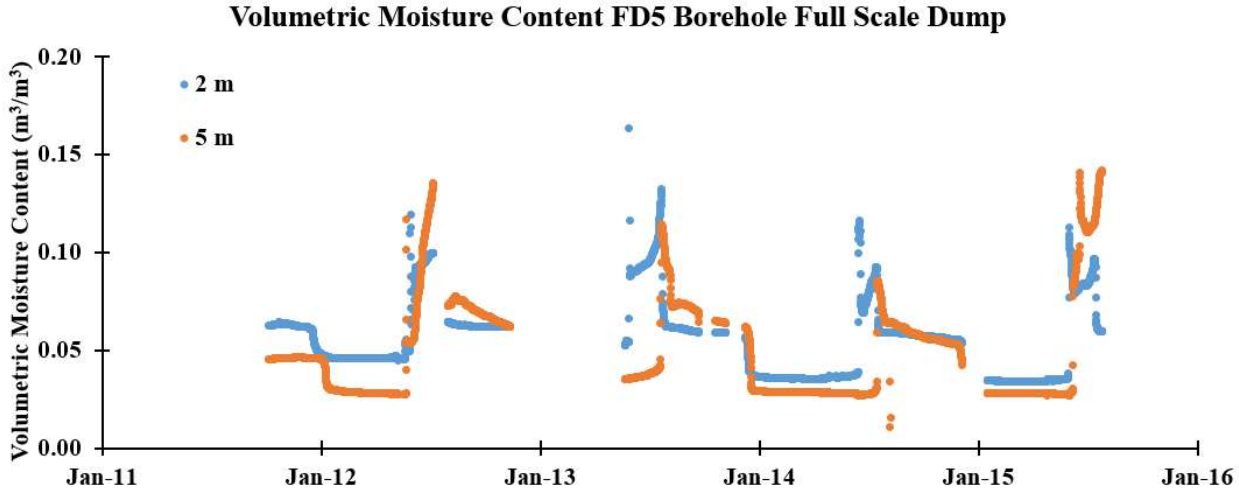

Figure B.23. Volumetric moisture contents obtained from an ECH2O probe in borehole FD5 located on the full scale pile.

Appendix C Penman Monteith infiltration calculation

The purpose of this section is to give an understanding of the modified Penman Monteith (PM) calculation used in this thesis to estimate rainfall infiltration to the crest of the test piles. These modified PM equations were also used by Fretz (2013) and Krentz (2014) to determine infiltration to the test piles at Diavik.

The PM method is used to calculate evaporation (E_a) over time. This is completed by first determining a value for reference evapotranspiration (ET_o) using meteorological data obtained from the Diavik Environment Department. ET_o is a measurement of the amount of evaporation which would occur from the surface of a reference material, if not limited by water availability. The calculation of ET_o is summarized in equation C.1; where ET_o is given in mm/hr, R_n is net radiation at the soil surface (MJ/m^{2}hr), G is the soil heat flux density (MJ/m^{2}hr), T_{hr} is the mean hourly air temperature (^{o}C), Δ is the saturation slope vapour pressure curve at T_{hr} (kPa/^{o}C), γ is the psychrometric constant (kPa/^{o}C), $e^o(T_{hr})$ is the saturation vapour pressure at T_{hr} (kPa), u_2 is the average hourly wind speed (m/s). Over the course of each year, ET_o was calculated on an hourly basis, then summed to produce daily estimates.

$$\mathrm{ET_o}(t) = \frac{0.408\Delta(R_n - G) + \gamma\left(\frac{37}{T_{hr}+273}\right)u_2(e^o(T_{hr}) - e_a)}{\Delta + \gamma(1 + 0.34u_2)} \qquad \text{(C.1)}$$

The value obtained for ET_o is used to estimate Ea (mm/day) using a dual crop coefficient, shown in equation C.2; where k_f is the frozen soil coefficient and K_e is the soil evaporation coefficient. K_f is either 0 or 1, representing frozen or unfrozen surface conditions. The purpose of K_e is to reduce evaporation as the availability of water decreases near the soil surface, the determination of this parameter is explained by Fretz, (2013).

$$E_a(t) = K_f K_e ET_o \quad \text{(C.2)}$$

Infiltration occurs once the moisture content in the evaporation layer reaches field capacity. Infiltration or deep percolation ($DP_{e,i}$ (mm)) was determined on a daily basis, using equation C.3; where P is precipitation (mm) occurring on the given day, and RO is runoff, $D_{e,i-1}$ is the cumulative depth of evaporation from the evaporative layer at the end of the day i-1 (mm). Runoff is known to not occur from the surface of the test piles, therefore, this value has been set to 0. The sum of $DP_{e,i}$ values over the course of the year gives the annual net infiltration. Further information regarding these calculations and the limitations of the PM method is provided by Fretz, (2013).

$$DP_{e,i} = (P_i - RO_i) - D_{e,i-1} \geq 0 \quad \text{(C.3)}$$

Appendix D Covered pile snow survey data

Table 5-1. Raw snow survey data collected April 29, 2015 on the covered pile.

Date:				**Crew:**			
29-Apr-15				**Jordan Zak**			
				David Barsi	**Long Core empty (cm H2O)**		
Location	**Easting (m)**	**Northing (m)**	**Depth of Snow**	**Length of Snow Core (cm)**	**Snow + Tube weight (SWE)**	**Corrected cm of water**	**Density (cm water/cm snow)**
B2891C	533419.588	7150958.935	5	9	52	14	1.56
B28921	533419.588	7150932.957	20	19	51	13	0.68
B28922	533419.441	7150946.024	28	27	55	17	0.63
B28923	533419.588	7150919.654	29	27	45	7	0.26
B2892E	533419.588	7150903.068	40	39	50	12	0.31
B2894C	533439.588	7150946.417	0	0	0		
B2894D	533439.588	7150932.957	8	8	42	4	0.50
B2894E	533439.588	7150919.112	0	0	0		
B2894F	533439.588	7150903.068	32	20	60	22	1.10
B28950	533459.588	7150903.068	130	135	88	50	0.37
B28951	533459.588	7150918.237	25	23	49	11	0.48
B28952	533399.588	7150919.012	92	90	75	37	0.41
B28953	533399.588	7150947.336	0	0	0		
B28955	533399.588	7150932.743	79	70	61	23	0.33
B28956	533379.588	7150919.266	40	36	55	17	0.47
B28957	533379.588	7150903.939	113	105	81	43	0.41
B2895A	533399.588	7150903.883	35	33	54	16	0.48
B2896B	533407.765	7150960.14	18	20	48	10	0.50
B2896C	533393.824	7150959.88	10	9	44	6	0.67
B2896D	533380.811	7150959.88	22	22	50	12	0.55
B2896E	533367.917	7150959.88	54	54	63	25	0.46
B2896F	533355.962	7150959.173	100	96	72	34	0.35
B28970	533434.451	7150959.88	7	7	40	2	0.29
B28971	533445.939	7150959.88	33	30	50	12	0.40
B28975	533481.175	7150959.88	35	31	42	4	0.13
B28976	533473.269	7150959.88	25	16	47	9	0.56

Location	Easting (m)	Northing (m)	Depth of Snow	Length of Snow Core (cm)	Snow + Tube weight (SWE)	Corrected cm of water	Density (cm water/cm snow)
B28977	533447.386	7150979.88	26	25	43	5	0.20
B28978	533434.254	7150979.88	0	0	0		
B28979	533461.977	7150979.835	17	14	44	6	0.43
B2897A	533475.806	7150979.746	35	29	50	12	0.41
B2897B	533435.626	7151000.116	0	0	0		
B2897C	533449.867	7150999.88	17	17	44	6	0.35
B2897D	533463.59	7150999.88	29	29	41	3	0.10
B2897E	533405.064	7150979.456	8	8	45	7	0.88
B2897F	533392.195	7150979.406	28	26	49	11	0.42
B28980	533380.032	7150979.88	25	25	50	12	0.48
B28981	533388.543	7150999.88	15	13	45	7	0.54
B28982	533354.871	7150999.88	56	40	53	15	0.38
B28983	533383.181	7150939.559	9	8	43	5	0.63
B28984	533368.026	7150939.88	27	25	50	12	0.48
B28986	533355.469	7150939.88	135	125	86	48	0.38
B28987	533352.094	7150919.88	46	46	58	20	0.43
B28988	533479.588	7150919.88	47	49	58	20	0.41
B28989	533457.162	7150939.88	0	0	0		
B2898A	533472.274	7150939.88	33	32	50	12	0.38
B2898B	533480.562	7150939.88	111	106	85	47	0.44
B2898C	533401.852	7150999.88	11	9	50	12	1.33
B28969	533359.588	7150903.068	52	51	55	17	0.33
B2896A	533479.588	7150903.068	75	40	61	23	0.58
B289BA	533458.237	7150959.88	23	19	42	4	0.21

Table 5-2. Raw snow survey data collected April 25, 2016 on the covered pile.

Date:				**Crew**			
25-Apr-16				**Jordan Zak**	**Small core empty (cm H2O)**		
				Carly Kemp	**Long core empty (cm H2O)**	**40**	
Location	**Easting (m)**	**Northing (m)**	**Depth of Snow (cm)**	**Length of Snow core (cm)**	**Equivalent cm of water**	**Corrected cm of water**	**Density (cm water/cm snow)**
B2892E	533419.588	7150903.07	33	12	43	3	0.25
B2894F	533439.588	7150903.07	30	11	43	3	0.27
B28950	533459.588	7150903.07	83	83	60	20	0.24
B28969	533359.588	7150903.07					
B2896A	533479.588	7150903.07					
B2895A	533399.588	7150903.88	50	41	51	11	0.27
B28957	533379.588	7150903.94	84	83	63	23	0.28
B28951	533459.588	7150918.24					
B28952	533399.588	7150919.01	35	27	50	10	0.37
B2894E	533439.588	7150919.11	5				
B28956	533379.588	7150919.27	32	24	52	12	0.50
B28923	533419.588	7150919.65	30	14			0.00
B28987	533352.094	7150919.88					
B28988	533479.588	7150919.88					
B28955	533399.588	7150932.74	55	53			
B28921	533419.588	7150932.96	24	20	43	3	0.15
B2894D	533439.588	7150932.96	20	17	46	6	0.35
B28983	533383.181	7150939.56	23	20	40	0	0.00
B28984	533368.026	7150939.88	155	152	77	37	0.24
B28986	533355.469	7150939.88	165	145	85	45	0.31
B28989	533457.2	7150939.9	30	29	46	6	0.21
B2898A	533472.3	7150939.9					
B2898B	533480.6	7150939.9	110	105	67	27	0.26
B28922	533419.4	7150946.0	10	10	42	2	0.20
B2894C	533439.6	7150946.4	2				
B28953	533399.6	7150947.3	2	2	40	0	0.00

Location	Easting (m)	Northing (m)	Depth of Snow (cm)	Length of Snow core (cm)	Equivalent cm of water	Corrected cm of water	Density (cm water/cm snow)
B2891C	533419.6	7150958.9					
B2896F	533356.0	7150959.2	132	125	81	41	0.33
B2896C	533393.8	7150959.9	85	79	71	31	0.39
B2896D	533380.8	7150959.9	108	108	70	30	0.28
B2896E	533367.9	7150959.9	97	96	74	34	0.35
B28970	533434.5	7150959.9	2				
B28971	533445.9	7150959.9	13	13	44	4	0.31
B28975	533481.2	7150959.9	63	53	56	16	0.30
B28976	533473.3	7150959.9	7				
B289BA	533458.2	7150959.9	1				
B2896B	533407.8	7150960.1	0	0			
B2897F	533392.2	7150979.4	121	120	75	35	0.29
B2897E	533405.1	7150979.5	0	0			
B2897A	533475.8	7150979.7	50	37	47	7	0.19
B28979	533462.0	7150979.8	2				
B28977	533447.4	7150979.9	37	28	45	5	0.18
B28978	533434.3	7150979.9	0	0			
B28980	533380.0	7150979.9	137	121	76	36	0.30
B2897C	533449.9	7150999.9	15	15	48	8	0.53
B2897D	533463.6	7150999.9	16	16	42	2	0.13
B28981	533388.5	7150999.9	165	90	70	30	0.33
B28982	533354.9	7150999.9					
B2898C	533401.9	7150999.9	0	0			
B2897B	533435.6	7151000.1	0	0			

Appendix E Active zone lysimeters – Tracer test

Irrigation events were applied to the active zone lysimeters and tensiometer nest during the late summer and early fall of 2015. Events were applied using oscillating sprinklers (Figure E.1) at a rates of about 65 mm/hr. A total of 25 events were applied, at a frequency of about every other day. An initial wet-up event of 15 mm labeled with bromide (about 3000 mg/L) was applied first. Four 7 mm events were applied with chloride (about 3000 mg/L), followed by eighteen 12 mm events (about 3000 mg/L). Two 12 mm events without any tracer were applied at the end of the experiment. A complete history of the events is given in Table 5-3.

Part way through the experiment, it was discovered using a borehole camera that the drain lines of lysimeters 1UW and 3UE were severely damaged. Following this point in time, irrigation events were not applied to these lysimeters. A complete history of the applied rainfall events is given in Table 5-3. Samples of the tracer water were collected during each event, the concentrations have not been listed here, although they are reflected Table E.5-4 which gives the cumulative mass of the tracers applied to each lysimeter.

Figure E.1. Oscillating sprinkler applying a tracer event to an AZL.

Table 5-3. List of applied rainfall events to the active zone lysimeters

Event Number	Location	Date	Magnitude (mm)
1	1UE	25-Jul	3
	1UW	25-Jul	3
	3UE	25-Jul	16
	3UW	25-Jul	12
	Tensio	25-Jul	15
2	1UE	27-Jul	16
	1UW	27-Jul	7
	3UE	27-Jul	33
	3UW	27-Jul	20
	Tensio	27-Jul	23
3	1UE	29-Jul	9
	1UW	29-Jul	8
	3UE	29-Jul	15
	3UW	29-Jul	9
	Tensio	29-Jul	12
4	1UE	31-Jul	9
	1UW	31-Jul	20
	3UE	31-Jul	16
	3UW	31-Jul	29
	Tensio	31-Jul	13
5	1UE	2-Aug	5
	1UW	2-Aug	4
	3UE	2-Aug	7
	3UW	2-Aug	14
	Tensio	2-Aug	15
6	1UE	5-Aug	13
	1UW	5-Aug	16
	3UE	5-Aug	15
	3UW	5-Aug	15
	Tensio	5-Aug	14
7	1UE	7-Aug	16
	1UW	7-Aug	20
	3UE	7-Aug	14
	3UW	7-Aug	13
	Tensio	7-Aug	14

Event Number	Location	Date	Magnitude (mm)
8	1UE	9-Aug	13
	1UW	9-Aug	12
	3UE	9-Aug	15
	3UW	9-Aug	14
	Tensio	9-Aug	13
9	1UE	12-Aug	13
	1UW	12-Aug	15
	3UE	12-Aug	16
	3UW	12-Aug	13
	Tensio	12-Aug	15
10	1UE	14-Aug	14
	1UW	14-Aug	14
	3UE	14-Aug	14
	3UW	14-Aug	14
	Tensio	14-Aug	13
11	1UE	16-Aug	16
	1UW	16-Aug	13
	3UE	16-Aug	14
	3UW	16-Aug	13
	Tensio	16-Aug	15
12	1UE	19-Aug	13
	1UW	19-Aug	14
	3UE	19-Aug	16
	3UW	19-Aug	17
	Tensio	19-Aug	15
13	1UE	23-Aug	13
	1UW	23-Aug	15
	3UE	23-Aug	11
	3UW	23-Aug	14
	Tensio	24-Aug	15
14	1UE	26-Aug	6
	1UW	26-Aug	6
	3UE	26-Aug	6
	3UW	26-Aug	4
	Tensio	26-Aug	11

Event Number	Location	Date	Magnitude (mm)
15	1UE	28-Aug	14
	1UW	28-Aug	12
	3UE	28-Aug	15
	3UW	28-Aug	18
	Tensio	28-Aug	17
16	1UE	30-Aug	17
	1UW	30-Aug	20
	3UE	30-Aug	18
	3UW	30-Aug	17
	Tensio	30-Aug	10
17	1UE	1-Sep	11
	1UW	1-Sep	13
	3UE	1-Sep	14
	3UW	1-Sep	15
	Tensio	1-Sep	21
18	1UE	9-Sep	13
	1UW	9-Sep	13
	3UE	9-Sep	13
	3UW	9-Sep	12
	Tensio	9-Sep	12
19	1UE	11-Sep	11
	1UW	11-Sep	14
	3UE	11-Sep	12
	3UW	11-Sep	13
	Tensio	11-Sep	14
20	1UE	13-Sep	13
	3UW	13-Sep	14
	Tensio	13-Sep	16
21	1UE	15-Sep	15
	3UW	15-Sep	16
	Tensio	15-Sep	15
22	1UE	17-Sep	15
	3UW	17-Sep	11
	Tensio	17-Sep	13
23	1UE	21-Sep	11
	3UW	21-Sep	20
	Tensio	21-Sep	18

Event Number	Location	Date	Magnitude (mm)
24	1UE	30-Sep	22
	3UW	30-Sep	17
	Tensio	30-Sep	16
25	1UE	4-Oct	19
	3UW	4-Oct	19

Table E.5-4. Mass of tracers applied to active zone lysimeters during the irrigation experiment.

Lysimeter	Bromide (g)	Chloride (g)
1UE	34	2634
1UW	35	2356
3UE	102	1291
3UW	69	3022